Materials for transfer of heat from solar panels

Materialer for overføring av varme fra solcellepaneler

Ali Haider Raja

Bachelor Thesis

Project Number: IMA-B-09-2019

Unclassified (open) project

May 31st, 2019

Norwegian University of Science and Technology

Department of Materials Science and Engineering

In association with SINTEF, Norway

Internal supervisor: Kjersti Kleveland

External supervisor: Martin Bellman

Preface

This report was written in spring 2019 as part of the bachelor thesis in Materials Science and Engineering, NTNU, Trondheim. The task of this report is part of SINTEF project in association with PVadapt, a European Union project. The purpose of this report is to investigate the best thermal interface materials in a photovoltaic/thermal system. All report related tasks including the research and experimentation were carried out at Realfagbygget and SINTEF byggforsk, NTNU Gløshaugen, Trondheim. This investigation is also presented in the form of a popular science article and is attached as attachment 1 in appendix.

This thesis spanned for 5 months under constant and reliable supervision of professors and engineers. I would like to extend my gratitude to Kjersti Kleveland, my professor and supervisor from NTNU. Without her guidance and encouragement, the task of this thesis would not have been accomplished. I would also like to thank Martin Bellman, my supervisor from SINTEF, of his invaluable insight and assistance throughout the course of this task.

I want to thank Pål Tetlie and Per Christian for their help in the experimental part of this task. Without their ceaseless cooperation, it would have been very difficult to bring this project to completion.

Lastly, I would like to thank my family and friends for their undying support throughout the extensive months of spring 2019.

Abstract

An innovative method of enhancing photovoltaic (PV) solar cell's efficiency upon increased ambient temperature is by utilizing a photovoltaic/thermal (PV/T) system. This is a hybrid structure which has a PV system adhered to a multi-functional solar collector. Consequently, PV/T system offers a cooling mechanism for the PV module by exploiting its excess heat for space or water heating. This research attempted to propose a thermal interface material (TIM) which offers maximum heat transfer from the PV module onto the heat mat. Two scenarios for a sandwich structure of a PV/T system are investigated in this report where the heat mat is mimicked by an aluminium plate. Scenario A aimed at inserting a TIM between a glass/glass PV module and the aluminium plate. Scenario B aimed at replacing the rear glass of the PV module with a TIM. This investigation was conducted in two parts. Firstly, experimentation using SINTEF's custom-built heat flow apparatus was done for both scenarios. Secondly, a desk study on scenario B for TIMs available in the market was conducted; furthermore, to find a theoretically suited TIM, Edu Pack modelling on composites was done.

Incorrect use of the heat flow apparatus resulted in the error in the experimental results. Thus, the greatest heat transfer between the PV module and the aluminium plate could not be determined. However, the in-built apparatus' monitors revealed that copper tape as TIM for scenario A offered the greatest heat flux, 96.9 W/m^2, and the lowest thermal insulance, 0.14 m^2K/W, through its sandwich structure. PVC pad as TIM for scenario B offered the lowest heat flux, 65.9 W/m^2, and the greatest thermal insulance 0.24 m^2K/W despite having the greatest temperature difference across its first and last layer. Based on the desk study, 5595 Silicone/polyethylene pad supplied by 3M^{TM} was the most promising candidate for experimentation based on its thermal conductivity, electrical insulation and price. Edu Pack modelling showed that filling a polyimide (PI) matrix with thermally conductive fillers like hexagonal boron nitride (h-BN) and alumina (Al_2O_3(85)) enhances the thermal conductivity of the composite. At filler loadings greater than 40%, the thermal conductivity of the filler influences significantly the total thermal conductivity of the composite. Equal filler volume fraction of 50.6% in a h-BN/PI composite offers 34% greater thermal conductivity and 3 folds electrical resistivity than the its Al_2O_3(85)/PI counterpart. The h-BN composite exhibited better performance than Al_2O_3(85) composite.

Sammendrag

En innovativ metode for å forbedre effektiviteten til fotovoltaiske (PV) solceller ved økt omgivelsestemperatur er å benytte et fotovoltaisk/termisk (PV/T) system. Systemet tilbyr en kjølemekanisme for PV-modulen ved å utnytte overflødig varme for rom- eller vannoppvarming. Dette arbeidet forsøkte å foreslå et termisk grensesnittmateriale (TIM), som gir maksimal varmeoverføring fra PV-modulen til varmematten. To scenarioer for en sandwichstruktur til et PV/T-system er undersøkt i denne rapporten, hvor varmematten var en aluminiumsplate. Scenario A siktet på å sette inn et TIM mellom en glass/glass PV-modul og aluminiumsplaten. Scenario B forsøkte å erstatte det bakre glasset til PV-modulen med en TIM. Arbeidet ble utført i to deler. Under den første delen ble eksperimentering utført ved hjelp av SINTEFs spesialbygde varmestrømningsapparat for begge scenarier. For den andre delen ble det gjennomført en studie om scenario B for tilgjengelig TIM på markedet; videre ble enkel Edu Pack modellering på kompositter gjort for å finne et godt valg for TIM.

Feil bruk av varmestrømningsapparatet innebar at størst varmeoverføring mellom PV-modulen og aluminiumsplaten ikke kunne bestemmes. Imidlertid viste apparatets innebygde monitorer at kobberteip som TIM for scenario A ga den største varmestrømmen, 96.9 W/m², og den laveste termiske isolasjonen, 0.14 m²K/W, gjennom sin sandwichstruktur. PVC-matte som TIM for scenario B hadde laveste varmestrømmen, 65.9 W/m², og den største termiske isolasjonen 0,24 m²K/W til tross for at den har den største temperaturendringer over sitt første og siste lag. Basert på studien var 5595 silisium/polyetylenmate levert av 3M^{TM} den mest lovende kandidaten til eksperimentering basert på termisk ledningsevne, elektrisk isolasjon og pris. Edu Pack-modellering viste at fylling av en polyimidmatrise (PI) med termisk ledende fyllstoffer som heksagonal bornitrid (h-BN) og alumina (Al_2O_3(85)) forbedrer termisk ledningsevne for kompositten. Ved fyllfraksjoner større enn 40% påvirker fyllstoffets varmeledningsevner den samlede termiske ledningsevne for kompositten betraktelig. Tilsvarende volumfraksjon ved 50.6% i en h-BN/PI-kompositt gir 34% høyere termisk ledningsevne og 3 ganger lavere elektrisk resistivitet enn dens Al_2O_3(85)/PI motpart. h-BN-kompositten viste bedre ytelse enn Al_2O_3(85) kompositten, og bør utforskes i fremtiden for å vurdere om h-BN-kompositten vil gi størst termisk ledning fra PV-modulen til varmematten.

Abbreviations

AMS - Advanced metering system

ARC – Antireflection coating

ASTM - American Society for Testing and Materials

BIPV-T - Building integrated photovoltaic thermal

CPU - Central processing unit

csv - Comma Separated Value

DECC - Department of Energy & Climate Change

DEE - Department of Electrical Engineering

DSO - Distribution system operators

Gen-I - First generation

Gen-II - Second generation

Gen-III – Third generation

GHP - Guarded hot plate method

h-BN - Hexagonal boron nitride

IEA - International Energy Agency

N.I.C.E - New Industrial Cell Encapsulation

PSA - Pressure sensitive adhesive

PV - Photovoltaic

PV/T - Photovoltaic/Thermal

SINTEF - Stiftelsen for industriell og teknisk forskning

TIM- Thermal interface material

XRF- X-ray fluorescence

ZEB - Zero energy building

Nomenclature

A	Area [m^2]
h	Convective heat transfer coefficient [W/m^2K]
i_u	Unit vector in x-direction
j_u	Unit vector in y-direction
k	Thermal conductivity [W/mK]
k_f	Thermal conductivity of the filler in a composite [W/mK]
k_i	Thermal conductivity of a layer in a sandwich structure [W/mK]
k_m	Thermal conductivity of the matrix in a composite [W/mK]
k_u	Unit vector in z-direction
L	Lorentz number [2.44×10^{-8} $\Omega W/K^2$]
P	Power [W]
Q	Heat [J]
$\dot{Q}$	Heat flow [J]
$\dot{Q}_i$	Heat flow in stationary situation [J]
$\dot{Q}_{in}$	Heat flow in [J]
$\dot{Q}_{out}$	Heat flow out [J]
q''	Heat flux [W/m^2]
q_x''	Heat flux in x-direction [W/m^2]
q_y''	Heat flux in y-direction [W/m^2]
q_z''	Heat flux in z-direction [W/m^2]
$R_{i,\,cond}$	Conductive thermal resistance [K/W]
R_{val}	Thermal insulance [m^2K/W]
T	Temperature [K]
$\triangle T$	Temperature difference [K]
T_f	Fluid temperature [K]
T_s	Surface temperature [K]
$wt\%$	Weight percent
x	Thickness of a layer [m]
x_i	Thickness of a layer in a sandwich structure [m]
$\triangle x$	Change in distance [m]
∇	Vector differential, nabla
α	Thermal diffusivity [m^2/s]
σ	Electrical conductivity [$\Omega^{-1}m^{-1}$]
σ_s	Stefan Boltzmann's constant [5.67×10^{-8} W/m^2K^4]
$\in$	Emissivity [0-1]

Contents

Preface i

Abstract ii

Sammendrag iii

Abbreviations iv

Nomenclature v

1. Introduction 1

2. Theory 5

2.1 Energy active building 5

2.2 Heat Transfer 9

2.2.1 Radiation 10

2.2.2 Convection 11

2.2.3 Conduction 12

2.2.4 Heat conductors 19

2.2.5 Thermal conductivity measurement 25

2.3 Thermal management 28

2.3.1 Heat pipes 30

2.3.2 Thermal interface materials 32

2.4 Photovoltaic cells 34

2.4.1 Structure and mechanism 36

2.4.2 Performance 38

2.5 Solar thermal collectors ……..… 40

2.5.1 Heat pipe solar collectors ……..… 41

2.6 Photovoltaic/Thermal system ……43

3. Material and Method 45

3.1 Heat flow experiment ……45

3.1.1 Materials ……45

3.1.2 Apparatus and calibration ……..…47

3.1.3 Preparation of samples ……...……48

3.1.4 Experiments ……....50

3.2 Desk study on scenario B ……..……53

3.2.1 Materials in the market ……..…… 53

3.2.2 Simple Edu Pack modelling ……..…… 54

4. Results 55

4.1 Heat flow experiment …… 55

4.1.1 Reference experiment……..……56

4.1.2 Scenario A ……...…58

4.1.3 Scenario B ……..…60

4.1.4 Summary of results from Apparatus' monitors ……..…62

4.2 Desk study on scenario B ……..…… 63

4.2.1 Materials in the market ……...… 63

4.2.2 Simple Edu Pack modelling ……..…… 64

5. Discussion 67

5.1 Heat flow experiment ……67

5.1.1 Errors in the experiment ……70

5.1.2 Improvements in the experiment ……...72

5.2 Desk study on scenario B ……..……73

5.2.1 Materials in the market ……..…… 73

5.2.2 Simple Edu Pack modelling ……..… 74

5.3 Future Work ……..…… 77

6. Conclusion **78**

7. Bibliography **82**

Appendix

1. Introduction

With the increase in global energy demand, it is necessary to utilize the sustainable energy sources. Renewable sources are classified as clean and sustainable sources and they have had a high growth rate of any other fuel recently. Figure 1 shows the growth in energy demand based on the different types of fuels in different regions of the world. It can be seen that gas has had the highest growth rate followed by the renewables and oil. Global energy demand grew by 2.3% in 2018 which was mainly driven by a robust global economy and higher heating and cooling requirements. Renewables, which grew up by 4% in 2018, met 25% of the increase in energy demand. Although, this growth rate is appreciable, it is far from being sufficient to combat global warming and the climate change. For this reason, it is crucial to obtain a maximum output from the natural energy sources and also to make an efficient energy usage [1].

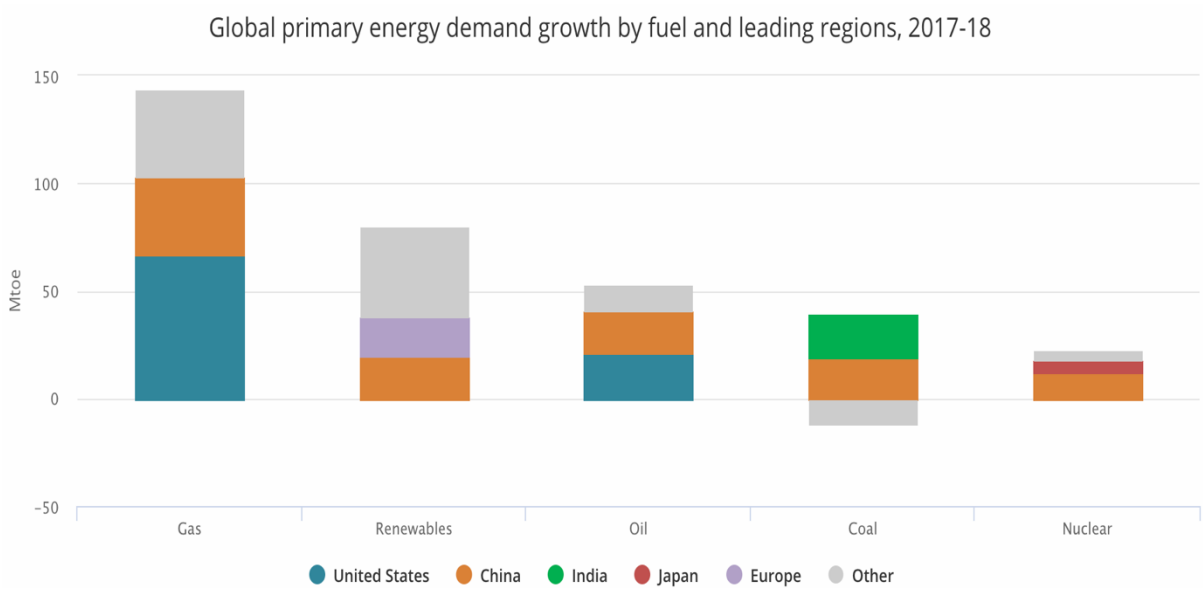

Figure 1: Global primary energy demand growth by fuel from 2017 to 2018. Gas has had the highest demand growth whereas nuclear energy has had the least demand growth. China and Europe are the leading regions of the renewable energy growth [1].

Energy is consumed in many different ways. The energy usage can be classified based on various sectors like residential, commercial, industrial and transportation. For the purpose of this thesis, energy in producing electricity and in heating systems shall be investigated. Solar energy shall be the focal point of this report and the methods for maximal exploitation of energy from the sun shall be explored.

Solar energy is the radiant light and heat from the sun which is harnessed using various technologies. One such technology is the photovoltaic (PV) cell, or solar panels, where energy from the sun is absorbed to generate electricity. Photovoltaics are a renewable energy source and do not produce greenhouse gases; although, the materials used to assemble the photovoltaics are not entirely clean and sustainable in their fabrication. An issue with the PV cell is that it only utilizes a small fraction of the incoming sunlight to produce electricity and most of the energy in the solar cells is converted into thermal energy. This thermal energy can be catastrophic for the PV module as the cell's efficiency decreases drastically with the increase in PV module's temperature. Therefore, there is a need to develop a technology which solves this problem such as a photovoltaic/thermal (PV/T) system [2] [3].

A PV/T system has a sandwich structure where a PV module is connected to a solar collector, i.e. the heat mat. This system not only regulates the cooling mechanism in the PV module, but also acts as a hybrid structure where the thermal energy gained upon heating of the PV cell is used for other beneficial purposes. This report builds up on the previous investigation conducted on the PV/T systems; especially on the experiments conducted by the researchers in Cardiff, UK. The Department of Energy & Climate Change (DECC) project in Cardiff made comparative energy and performance analysis where it concluded that a PV/T system is highly efficient in enhancing electrical output of the PV cell and is also effective in solar/thermal conversion. A full-scale PV/T structure was built and was integrated as a building envelope on a roof top in Cardiff. In this experiment, 15% increase in efficiency in the PV module was recorded after it was provided with the homogeneous cooling. Figure 2, on the following page, is obtained from the research done in Cardiff. It shows the electrical output of a PV system and a PV/T system during the day. The figure indicates how the output energy of a PV module significantly increases when a suitable cooling mechanism is incorporated into the system. Thus, approving that the efficiency of the cooled PV/T system is greater than the uncooled PV system [2].

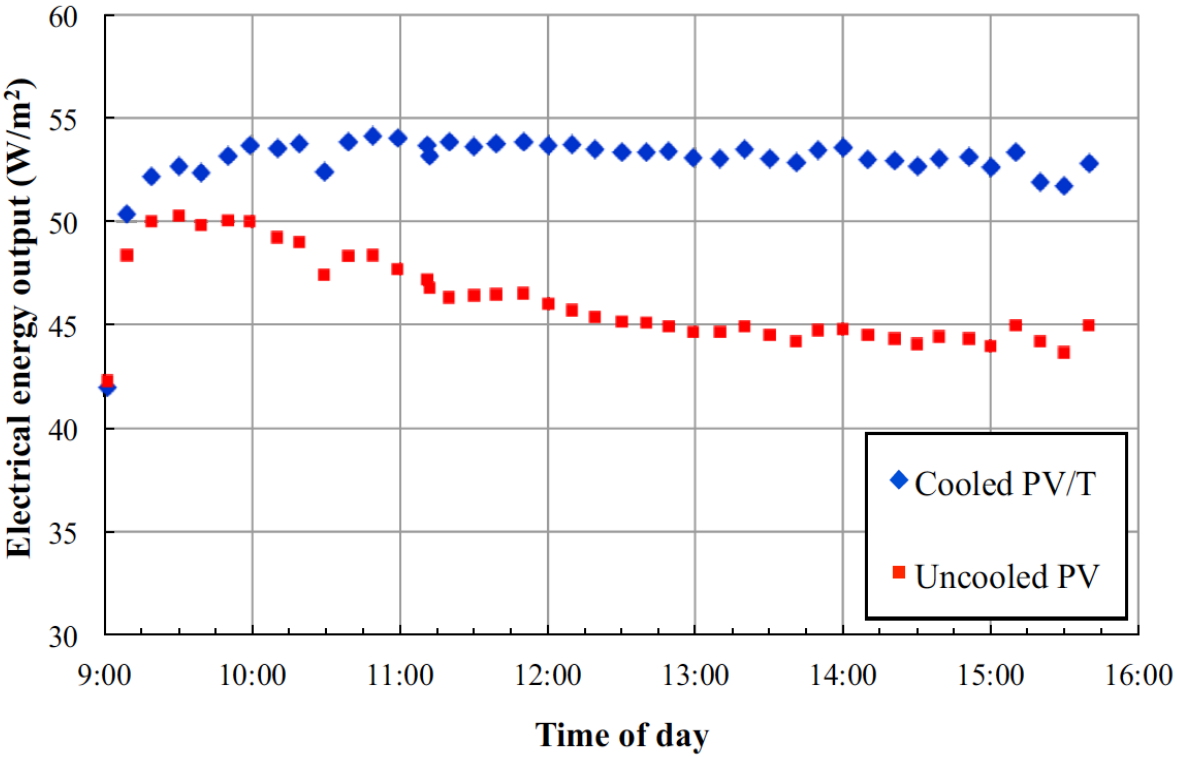

Figure 2: Effect of cooling on the electrical energy output from the PV/T system. An increase in electrical output is obtained when a PV module is provided with a cooling mechanism [2].

The task of this thesis is to conduct a thorough literature and experimental research to find the most suitable interface in a PV/T system. The report aims to answer the following question: What is the best thermal interface material which allows for the maximum heat transfer in a PV/T system? This research is part of the European Project, PVadapt, which aims to transform a traditional building into an energy active building. This shall be achieved by connecting Apollon Solar's PV module with a heat mat. New Industrial Cell Encapsulation (N.I.C.E) is Apollon Solar's module technology which is based on fully automated production of photovoltaics. The technology is based on first generation crystalline silicon solar cells sandwiched in between two glass plates. The heat mat is adhered to the backside of this photovoltaic module which results in a hybrid system, i.e. a PV/T system. Heat mat is made of aluminium with channels for the working fluid, ammonia. Building integrated photovoltaic thermal (BIPV-T) system shall replace traditional elements such as windows, cladding or roofs with a functional component able to generate energy. The main goal of PVadapt project is to provide a cost effective and a sustainable BIPV-T [4].

For the purpose of this report, a most suitable interface for heat transfer from the PV module to the heat mat is determined. For this reason, a thorough literature, experimental and

simulated research based on two scenarios for a PV/T system is conducted. Risk evaluation sheets for the experimental part of this report are presented in appendix attachment 2. At the start of the experimental part of this project, a reference experiment is conducted with no thermal interface in the PV/T system. The results from this experiment are used as literature values and are compared with the results obtained from the different scenarios. The idea behind this thesis is to conduct experiments and simulation which mimic the real-life production line of the PV/T systems. Therefore, the two scenarios which are investigated are both based on a sandwich structure. Only after an in-depth literature research, suitable materials are identified for each scenario and are experimented or simulated. Later, comparisons based on thermal conductivity, electrical insulation and price are drawn from the results. Heat flow chamber is used for the experimentation. Experimental results are treated quantitatively by conducting heat flow calculations.

This thesis is organized as follows: firstly, the theory behind this investigation is reported. Secondly, the experimental phase is reported where all the screening processes for the materials and the eventual experimental setup is documented. Thirdly, comparisons based on the experimental results are drawn. Based on the results from these calculations, a conclusion is drawn for the most suitable interface for heat transfer from the PV module to the heat mat.

2. Theory

2.1 Energy-active building

Buildings have a great impact on the environment and on the energy usage. According to the International Energy Agency (IEA), buildings account for 36% of global energy consumption and about 40% of total direct and indirect CO_2 emissions. This energy usage will only increase as new buildings are being constructed faster compared to the old ones being destroyed. Moreover, it will also increase due to improved access to energy in the developing countries and greater ownership and use of energy-consuming devices. This will continue to be the case until the buildings can be designed in such a way that they are self-sustainable and have zero net energy consumption [5]. Buildings use energy for lighting, cooling/heating of the air, heat water and power other personal (electrical) devices. Even after installing a private system of energy production e.g. a solar cell, there is still a heavy energy load which needs to be resolved. This issue is resolved by using an external power grid but due to the increasing number of buildings, the usage of external power systems is not an effective solution. Consequently, a transition to a smarter power system is required where buildings can play an active role to meet their energy demands [2].

Energy active building is a concept where active elements are integrated in the building material which contribute to an efficient energy usage. These elements produce electricity but mostly focus on controlling the heat flow between the internal and the external environment of the building. According to the IEA, about 40% of energy is used in space heating in the residential and non-residential sectors. Energy requirement for space heating has increased recently as seen from the Figure 3, on the following page. This is because of the increased number of buildings in the last decade and also due to the improved standard of living. Heating is the largest single end-use within buildings. Therefore, adequate methods such as introducing BIPV-T can make buildings more efficient than they are today [5].

Figure 3: Percentage of the final energy used for space heating in the residential and non-residential sector from the year 2000 to 2016 [5].

Buildings are mainly classified into four types: low energy house, passive house, energy-plus house and zero energy house or Zero energy building (ZEB). This classification is based on the different building standards for energy use in buildings. A low energy house uses considerably less energy than ordinary houses. It is an energy efficient house which is designed without any active cooling or traditional heating system. Solar panels are often mounted on such buildings which reduce the house's total energy expenditure. Standards for such buildings differ from country to country but an overall building design is compact and has a well-insulated building envelope [6].

A passive house is a building standard which is energy efficient and ecological at the same time. These buildings require little or no energy for cooling and space heating as they utilize energy already present in the building. This energy can include the heat from electrical appliances like computers, refrigerators etc., as well as the heat emitted by the users of the building. The building utilizes passive measures like extra insulation in walls and windows, dense and compact building body, minimal bridges and a good ventilation system with good heat recovery. Heat recovery means managing the heat that disappears from the building and reusing to heat the clean air that is supplied to the building by means of a ventilation system. Figure 4, on the following page, is a graphic illustration of the energy savings in a passive house compared to the low energy house. Annually, these heating energy savings can rise up to 75% with efficient energy usage [6] [7].

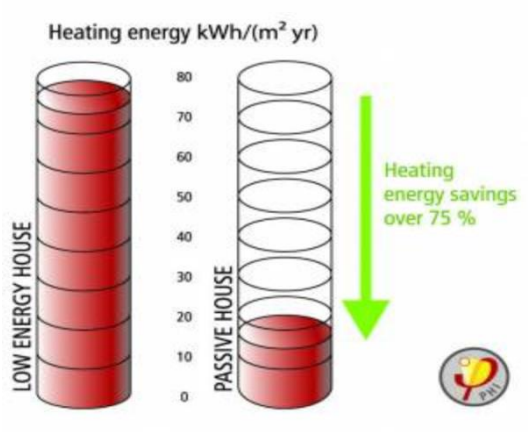

Figure 4: Energy savings obtained from a passive house by utilizing passive energy saving techniques. The comparison is made with a low energy house [7].

Energy-plus house is a building which generates more energy than the energy which was required for the production of the building materials, construction, operation and demolition of the building. Over the course of a year, the energy produced in such buildings is greater than the annual energy import from external sources. This is achieved by utilizing low-energy building techniques, such as: insulation, passive solar building design and careful site selection. These buildings use the most efficient power generators and appliances throughout the house which allow for energy savings. Later, the excess energy produced is either sold or transferred to an external power grid for storage [6] [8].

The fourth type of building is a ZEB. These buildings are also known as zero-carbon buildings and have a zero net energy consumption. This means that on an annual basis, the total amount of energy consumed by the building is completely offset by the renewable energy produced on or around the building. When the conditions are unsuitable for the building to produce its own energy e.g. a rainy day for a building integrated with a solar cell, the building draws energy from an electrical grid to meet its needs. When the conditions improve, the onsite renewable energy systems will cover the building's energy requirement and will transfer the excess energy to the grid. Over the course of a year, the building transfers as much energy as it takes from the external power grid. Thus, maintaining the energy balance, i.e. zero net energy consumption [6] [8].

The European project, PVadapt, is an innovative project which expects to contribute to the implementation of ZEB. The EU's revised building energy directive stipulates that all new buildings should be "almost zero-energy buildings" by the end of 2020. Many innovative

ideas have been investigated for a feasible and a cleaner energy production aiming at zero-carbon emissions. One such idea is combining highly energy efficient buildings, solar panels and solar collectors for electricity and heating requirements. Similar to the investigation conducted in Cardiff by the DECC, an energy-active building envelope material has proved to be an answer to the growing demand of the energy-efficiency. The experiments in Cardiff mounted a PV/T system on a rooftop with a large surface area [2]. However, for high-rise buildings, it is not feasible to install a PV/T system on the rooftop as the rooftop has a relatively smaller surface area for energy production. Therefore, a more innovative building design which transforms traditional building envelopes into active building envelopes is needed. This idea utilizes the building surface in a more ingenious way by making it a primary site for electricity production and thermal management [4].

Traditionally, the exterior of a building simply aims to preserve the inner environment from the outer environment. For example: during winter, the building-exterior aims to keep the cold out and during summer, the building-exterior aims to keep the heat out. Upon the introduction of BIPV-T systems, reduction in the running cost of the building can be expected with a more efficient energy usage. This new building design will control the heat flow between the internal and the external environment in a flexible way. Figure 5 shows the BIPV-T module which comprises of a thermal component (PV system and a heat mat) joined to the structural component of the building. These components are produced separately and later joined together. The combination of the PV system and the heat mat provides with the building block while the structural component is made up of a steel frame attached to the building block. The figure also describes the key features of the PV module, the heat mat and the structural component [2] [9]

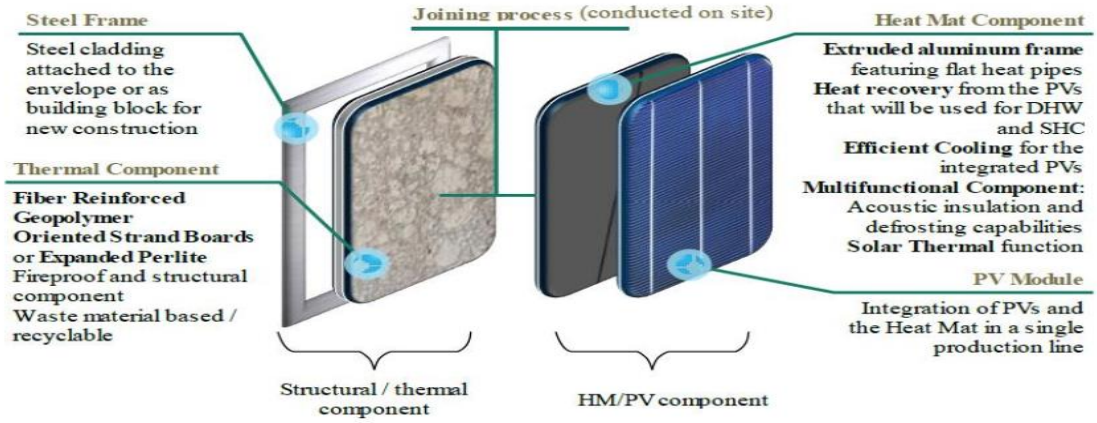

Figure 5: Building block comprising of a PV/T system joined to the structural component for an active building envelope. These two components are produced separately and later assembled together [9].

2.2 Heat transfer

Heat is a form of energy exchange due to temperature difference. The direction of a heat flow is always from high to low temperature. For systems, heat is defined as positive if it is transmitted to the system from the environment. The SI unit of heat is joule [J]. A conventional symbol, Q, is used to represent the amount of heat transferred in thermodynamic processes. Heat is a process variable, i.e. a variable whose value is measured as current value at a particular part of a process. Heat flux or thermal flux is defined as amount of heat transferred per unit area per unit time. The SI units of heat flux are watts per square meter [W/m^2]. Heat flux is a vector quantity; it has both magnitude and a direction. A conventional symbol, *q"*, is used to represent heat flux in thermodynamic calculations [10].

Heat transfer is a phenomenon in thermal engineering that concerns with the generation, usage, conversion and exchange of heat. Heat is also referred to as thermal energy and heat transfer is a stream of thermal energy that arises from temperature differences. Thermal energy represents the cumulative effect of microscopic activity in a material and is related to temperature. These microscopic activities include the vibration and movement of atoms or molecules in a body. Heat flows from hot bodies to colder bodies, i.e. from area of high temperature to an area of low temperature. This heat flow is based on three mechanisms: radiation, convection and conduction which are discussed in the following chapters [10]. Figure 6 is a graphic illustration of these mechanisms.

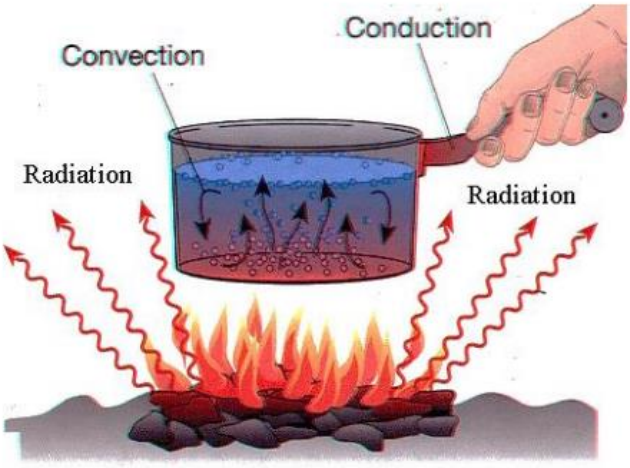

Figure 6: The three mechanisms of heat transfer. Radiation is the heat coming directly from the fire; convection is the heat transfer inside the pan; conduction of heat is the heat spread through the pan's handle [11].

2.2.1 Radiation

Thermal radiation occurs through a vacuum or any transparent medium. This type of heat flow does not rely on any contact between the heat source and the heated object. It is the result of random movements of particles in matter. As electrons and protons are charged particles, their movement results in emission of electromagnetic radiations in the form of infrared radiations. Heat waves radiate out from hot objects and travel at the speed of light in vacuum. An example to this is the radiation from the sun which travels through vacuum i.e. space. This heat energy can either be absorbed or reflected depending on the receptor. Solar radiation is key in harnessing the heat energy from the sun. These radiations are directed onto PV absorbers using various reflectors in order to harness maximum energy from the sun. This method is used to generate electricity in a solar cell [16]. Heat flux, q'' [W/m^2], through radiation can be expressed with the help of Stefan Boltzmann's law given in Equation 1

$$q'' = \epsilon \sigma T_s^4 \tag{1}$$

Where ϵ is the emissivity of the object which varies between 0 and 1; σ is Stefan Boltzmann's constant [σ = 5.67 x 10^{-8} W/m^{2}K^4]; T_S is the surface temperature [K]. All objects emit electromagnetic radiations at non-zero temperature. The intensity of such radiations depends on the surface of the body and also on body's temperature. The emission of these radiations occurs at all temperatures, with the rate of emission increasing with the increase in temperature. Radiative heat transfer is proportional to the temperature to the fourth power. This signifies that thermal transfer through radiation becomes more important at higher temperature. There aren't large temperature variations in the real-life scenario for the usage of a PV/T system; temperature variations of ± 50 K are considered nominal variations. Therefore, heat transfer through thermal radiation in the experimental samples is considered to be negligible [11].

2.2.2 Convection

Convection occurs due to the movement of fluids. It occurs when a liquid or a gas carries heat along its flow of matter in the fluid. For example, when air is heated, the air particles gain energy. Thus, these particles move faster and further apart. They carry heat energy with them, and as hot air is less dense than cold air, the hotter air with highly energized particles rises above the cooler air. The cooler air moves in below to replace the hotter air that has risen. Later, when this cooler air heats up, it replaces the air above it, forming a continuous and a circular flow. This circular flow is called convectional current and the fundamental idea behind this is the difference in the fluid's density. In convective heat transfer, heat energy is transferred by the circulation of air. An example to this is the boiling of water in a pan. The water bubbles that arise at the top of the pan constitute of hotter fluid which replaces the colder fluid. The convectional current inside the pan transfers heat energy in water inside the pan [11]. Heat flux through convection can be expressed by Equation 2, Newton's heat law

$$q'' = hA(T_f - T) \tag{2}$$

Where h is the heat transfer coefficient [W/m^{2}K]; A is area of the object [m^2]; T_f and T are temperature [K] of the fluid and the temperature of the object respectively. The PV/T system which is experimented in this report is stacked up vertically (sandwich structure) with little or no fluid trapped between the different layers. Therefore, heat transfer through convection in the sandwich is considered to be negligible [11].

2.2.3 Conduction

Heat conduction is the transfer of heat in solids because of direct contact of the material with the heat source. This is the result of the direct exchange of kinetic energy of particles on a microscopic level. All matter is composed of particles called atoms. These particles are always in motion; vibrating back and forth or colliding into each other. Figure 7 shows the arrangement of atoms in the different states of matter.

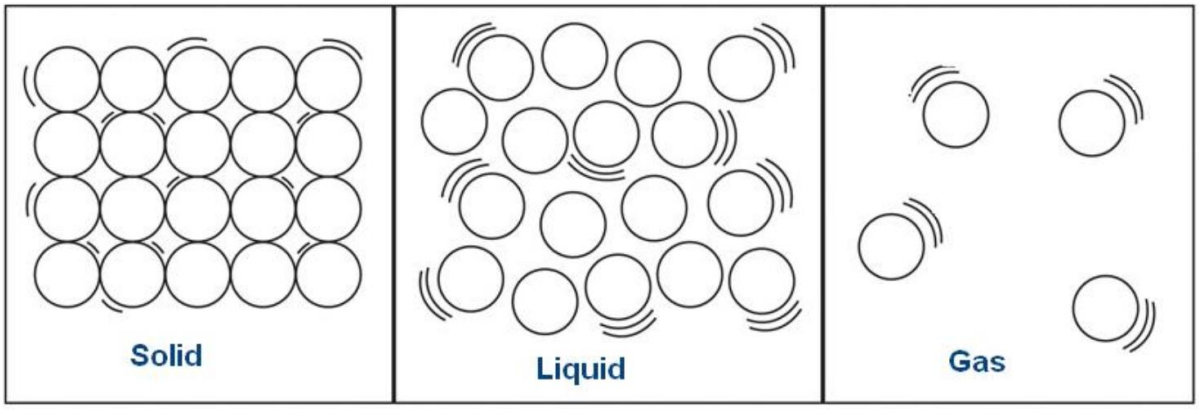

Figure 7: Arrangement of atoms in the three different states of matter. Solids have tightly packed arrangement so they can only vibrate; liquid particles lie at a distance and so can vibrate and roam freely; gaseous particles are free flowing particles as they are furthest away [10].

The motion of these particles gives rise to thermal energy. This is the underlying principle of heat transfer through conduction. As atoms are tightly packed in a solid, conduction occurs either due to the collision of particles, vibration of these particles or because of the presence of free electrons. At higher temperature, the particles have greater energy. Some of this energy is transmitted to particles at lower temperature due to vibration or collision of atoms. A hotter atom has greater velocity and energy than the colder atom. At the time of collision between a hotter particle and a colder particle, the hotter atom gives some of its energy to the colder atom. The colder and the slower atom now gains more thermal energy and collides with other molecules in the colder area of the material. The bumping of these particles into each other allows for the transfer of kinetic energy from a hot area to the colder area. This process continues until thermal equilibrium is reached where the temperature is uniform across the material. As particles are closer together in solids, heat conduction is better in solids than in liquids and gases [10].

Presence of free electrons in solids, especially metals and semi-conductors, is another means of heat conduction. Greater the concentration of these free electrons, greater the conduction.

As metals have more free electrons than the semi-conductors, they are better conductors of heat. Metals have metallic bonds within them which allows them to have free-moving electrons around their nuclei. These electrons form an electron cloud around the nucleus of the conductive metallic solid which conducts most of the heat flux. Generally, metals which are good heat conductors are also good electrical conductors. According to Wiedemann–Franz law, the thermal conductivity, k, and the electrical conductivity, σ, of a metal are proportional to the temperature [3]. This can be expressed using Equation 3

$$LT = \frac{k}{\sigma} \tag{3}$$

Where L, known as the Lorentz number [$\Omega W/K^2$] is the proportionality constant; T is temperature [K]; k is the thermal conductivity [W/mK] of the material i.e. material's ability to conduct heat; σ is the electrical conductivity [$\Omega^{-1}m^{-1}$] of the material i.e. material's ability to conduct electric current. The theoretical value for L, when based on conduction of heat through free electrons, is 2.44 x 10^{-8} $\Omega W/K^2$ [3]. Figure 8 affirms the Wiedemann–Franz law where metals and alloys lie at the bottom of bubble chart. Electrical resistivity is plotted against thermal conductivity for different material groups. Technical ceramics are a unique material group which defies the Wiedemann–Franz law. They are discussed later in the report.

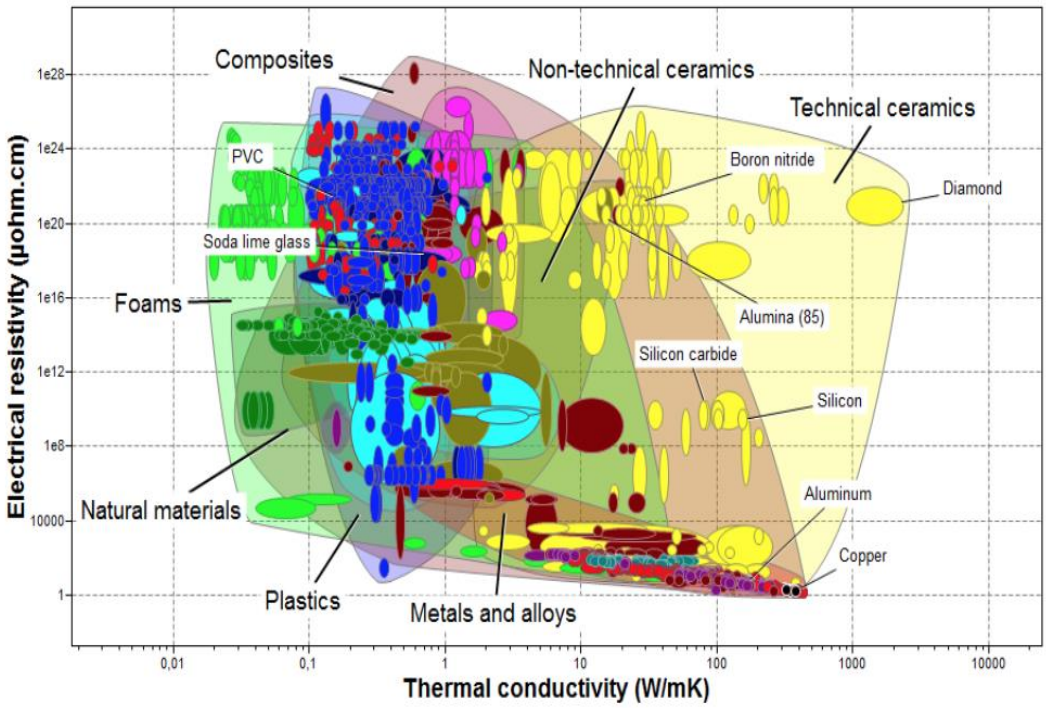

Figure 8: Electrical resistivity and thermal conductivity of different materials. Different material groups are shaded in different colours in the bubble char [12].

Heat conductivity in non-metals is mainly due to lattice vibrations as there are little or no free-moving electrons. Vibration of particles is essentially the process of absorption of heat. These vibrations propagate in the form of waves within a material which is described in terms of the phonons. Phonon is a unit of vibrational energy that arises from the oscillation of atoms. Solid crystals are made up of 3-dimensional array of atoms which are bounded in repeating units. These atoms behave like springs and upon the increase in their thermal energy, the lattice vibrates generating mechanical waves that carry heat across the material. As atoms vibrate, the more energetic particles transfer energy to the less energetic neighbouring atoms until thermal equilibrium is achieved in the material. Figure 9 shows how the lattice position of atoms is displaced because of vibrations. This displacement results in the conduction of heat [3].

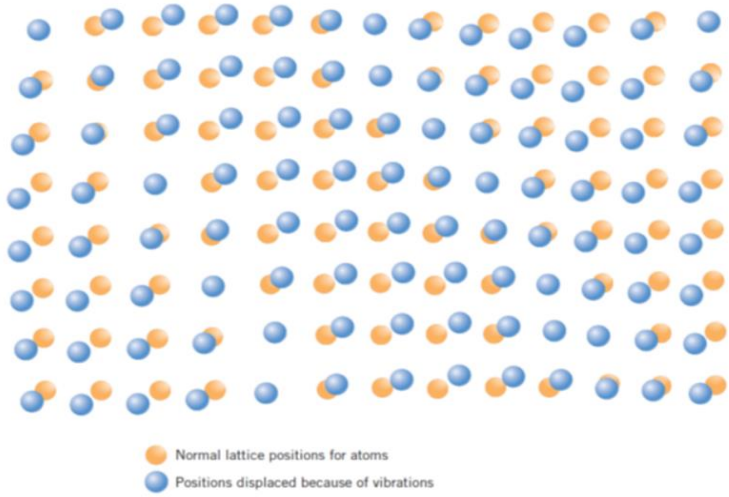

Figure 9: Displacement of lattice position of atoms because of vibrations in the material. Orange circles represent the original lattice positions with no vibrations whereas the blue circles represent the new lattice positions after vibration is experienced in the material [3].

The total thermal conductivity is the sum of the conductivity contributions from the free electrons and the vibration of particles [3]. Temperature difference, ΔT, is the driving force for conduction in a material. Mathematically, heat flow through conduction in a material can be described using Fourier's law. The law states that the heat flux resulting from thermal conduction is proportional to the magnitude of the temperature gradient and opposite to it in sign. This can be expressed using Equation 4

$$q'' = -k \frac{\Delta T}{\Delta x} \tag{4}$$

In this equation, q'' is the heat flux [W/m^2]; k is a material and temperature dependent property called thermal conductivity [W/mK] of the material; ΔT is the temperature difference [K];

$\triangle x$ is the distance [m]. The term $\frac{\triangle T}{\triangle x}$ is referred as the temperature gradient and is generally written as $\frac{dT}{dx}$. Some assumptions of the Fourier equation include:

- No internal heat generation in the material.
- Steady state heat conduction.
- Thermal conductivity, k, is constant in all directions as the material is considered to be isotropic and homogeneous [11].

If A is the cross-section area [m^2] of the heat transferring surface, heat flow, $\dot{Q}$ [J], in terms of Fourier's law can be described using Equation 5

$$\dot{Q} = q'' A \frac{\triangle T}{\triangle x} = -k A \frac{dT}{dx} \tag{5}$$

For 1-dimensional heat flow, temperature varies linearly between two points in a material. Figure 10 describes this situation.

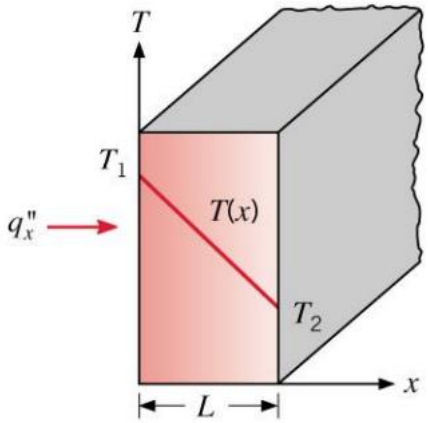

Figure 10: 1-dimensional heat flow in a material with a rectangular cross-section, A [m^2]. Figure shows the heat flux, q_x'' [W/m^2] in the material; T_1 and T_2 are two different points on the surface of the material. L represents the distance, $\triangle x$ [m] of the heat flow [11].

It is important to realise that if $T_2 = T_1$, $q'' = 0$. The negative sign in Equation 5 suggests that the temperature gradient has an opposite direction to the heat flow. For a stationary problem, heat flux is constant. This means that the thermal conductivity and the temperature gradient will also be constant [11]. In general, temperature may vary in all spatial directions i.e. x, y

and z directions. Therefore, heat flux through a material is calculated based on all the directions. Partial derivatives are used to express this in Equation 6

$$q_x" = -k\frac{\partial T}{\partial x}\ ,\quad q_y" = -k\frac{\partial T}{\partial y},\quad q_z" = -k\frac{\partial T}{\partial z} \tag{6}$$

In Equation 6, partial derivative is used as the temperature, T [K], differs in every direction i.e. T (x, y, z). The total heat flux, thus, points out in a certain direction and can be expressed as a vector as follows:

$$q" = q_x"i_u + q_y"j_u + q_z"k_u \tag{7}$$

In Equation 7, i_u, j_u and k_u are unit vectors in x, y and z direction respectively. Using nabla, ∇, as vector differential operator, Equation 8 can be written as

$$q" = -k\nabla T \tag{8}$$

Equation 8 is the general expression of heat flux. It highlights that the heat flux in conduction is proportional to the gradient of the temperature. It is important to emphasize that in real life situation, the materials are mostly anisotropic in nature. This is especially true on surfaces, grain boundaries and in splices/joints. However, for the sake of simplicity in the experimentation part of this report, the materials are considered to be isotropic in nature. Thus, the thermal conductivity of a material is considered to be constant [16]. Moreover, only the conductive heat flow in various sandwich structures is investigated in this report. A sandwich structure can be thought of as a wall with different layers; each layer with the same area, A [m^2] but different thickness, x [m], and thermal conductivity, k [W/mK]. In such scenarios, heat flow, $\dot{Q}$ [J], from the entire structure is the area of interest. This is based on the $\dot{Q}_{in}$ [J] and $\dot{Q}_{out}$ [J] from the structure when the wall thicknesses and temperatures are known. Figure 11 illustrates the heat flow, $\dot{Q}$ [J], in a wall with different layers [11].

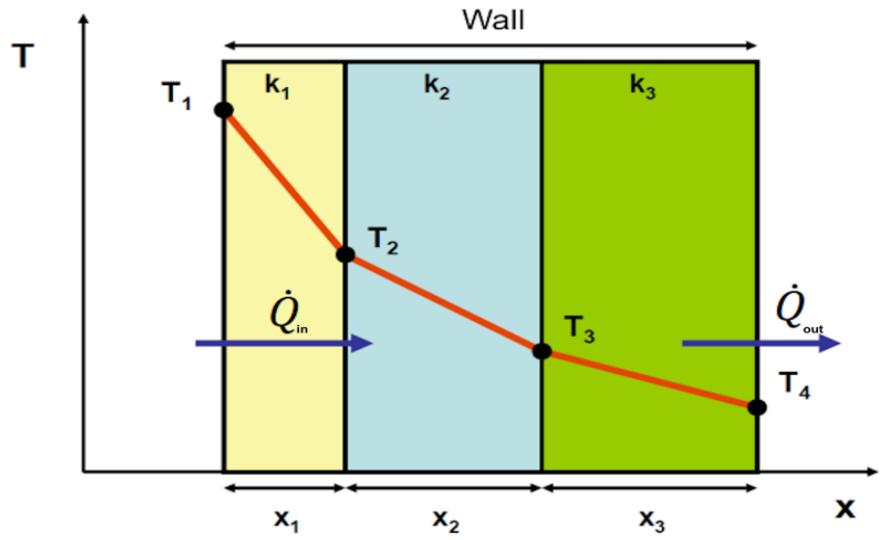

Figure 11: Heat flow [J], $\dot{Q}_{in}$ and $\dot{Q}_{out}$, in a wall with different layers. Each layer is represented with a different colour, and has a different thickness, x [m]*, and value for thermal conductivity, k* [W/mK]*. The wall is sketched on 2-axis; temperature (T) and distance (x). Temperature readings are made on the surfaces of each layer.*

The total heat flow in such structures is calculated by calculating heat flow in each layer separately [11]. This is done using Equation 5. For a stationary heat flow situation in a sandwich structure, $\dot{Q}_{in} = \dot{Q}_{out} = \dot{Q}_i$. Simplifying heat flow equations based on each layer for the sandwich structure results in Equation 9

$$\triangle T = \frac{\dot{Q}_i}{A} \Sigma \frac{x_i}{k_i} \tag{9}$$

In Equation 9, $\triangle T$ is the temperature difference [K] between the first layer and the last layer i.e. $\triangle T = T_1 - T_4$ on Figure 11. A is the area [m^2]; $\dot{Q}_i$ is the stationary heat flow [J]; x_i is the thickness of a layer [m], k_i is the thermal conductivity of a layer [W/mK].

Using the conductive thermal resistance, $R_{i,cond}$ [K/W], simplifies the aforementioned equation [11]. Conductive thermal resistance is expressed as

$$R_{i\,cond} = \frac{x_i}{Ak_i} \tag{10}$$

Where x_i is the thickness of a layer [m]; A is the area [m^2] and k_i is the thermal conductivity of a layer [W/mK] in a sandwich structure. Therefore, $\dot{Q}$ [J] for the sandwich structure can now be expressed as Equation 11

$$\dot{Q} = \frac{\triangle T}{\Sigma R_{i,cond}} \tag{11}$$

Where $\dot{Q}$ is the heat flow [J]; $\triangle T$ is the temperature difference [K] between the first layer and the last layer in a sandwich structure and $\Sigma R_{i,cond}$ [K/W] is the sum of all thermal resistances. Equation 11 is analogous to the Ohm's law for electrical circuits where $\dot{Q}$ [J] resembles the electric current; $\triangle T$ [K] resembles the voltage and $\Sigma R_{i,cond}$ [K/W] resembles the electrical resistance [14]. The sandwich structure with different layers is equivalent to an electric circuit with different resistors connected in series. Furthermore, thermal noises and contact resistance due to the surface irregularities in the sandwich structure also contribute to the conductive thermal resistance [11]. Thermal noises are a result of random thermal motion of electrons in a conductor and arise from temperature differences. It results in a disturbance in an electrical signal. Higher temperature and increased layers in a sandwich structure causes greater thermal noises [13]. Various techniques can be used to minimize this thermal resistance which are discussed later in the report [11]. Another important thermal property, especially in the construction industry, is the thermal insulance of a material. It is referred as R-value and is a measure of a two-dimensional layer's resistance to the conductive heat flow. It can be expressed using Equation 12

$$R_{val} = \frac{\triangle T}{\dot{Q}_i} \tag{12}$$

Where $\triangle T$ is the temperature difference [K] and $\dot{Q}_i$ is the heat flux [J] across a material at stationary conditions. Higher R-value indicates greater thermal resistance; therefore, poor conducting but better insulating properties of the material. In this study, only 1-dimenstional heat flow in the vertical direction, q_z", is examined. Moreover, heat transfer through convection and radiation are considered to be negligible as an ideal sandwich structure for the PV/T is documented. Consequently, convective thermal resistance- where the trapped fluid (air) acts as an extra layer in the sandwich structure- is also considered to be negligible. In practice, all resistances i.e. conductive thermal resistance, contact resistance and convective thermal resistance affect the heat flow in a sandwich structure.

2.2.4 Heat conductors

A good heat conductor is the one with the greatest thermal conductivity, *k*. In order to use Fourier's law, it is important to know the thermal conductivity of the material. Usually, material properties like thermal conductivity, density, electrical resistivity, tensile strength etc. are provided by the material-supplier. Based on the technical data sheet, one concludes if the desired material is a good heat conductor or not. Thermal conductivity values depend on the material; metals and technical ceramics have high conductivity whereas polymers typically have low conductivity. Figure 12 confirms this relationship. On the chart in Figure 12, it can be seen that on average, metals (shown in red) and technical ceramics (shown in yellow) have the highest thermal conductivity of any material group. Metal's conductivity varies between 2-600 W/mK. This is because in addition to the vibration of atoms in a metal, availability of free electrons allows for a greater amount of kinetic energy to be carried out in the lattice. Technical ceramics are also known as advanced ceramics and often have manipulated microstructures to obtain enhanced performances. However, diamond is a naturally occurring technical ceramic which has the highest thermal conductivity, 1440 W/mK, of any known material. Non-technical ceramics like clay and concrete generally have low thermal conductivities. Polymers and natural materials have the lowest thermal conductivity and are often termed as good heat insulators [3] [12].

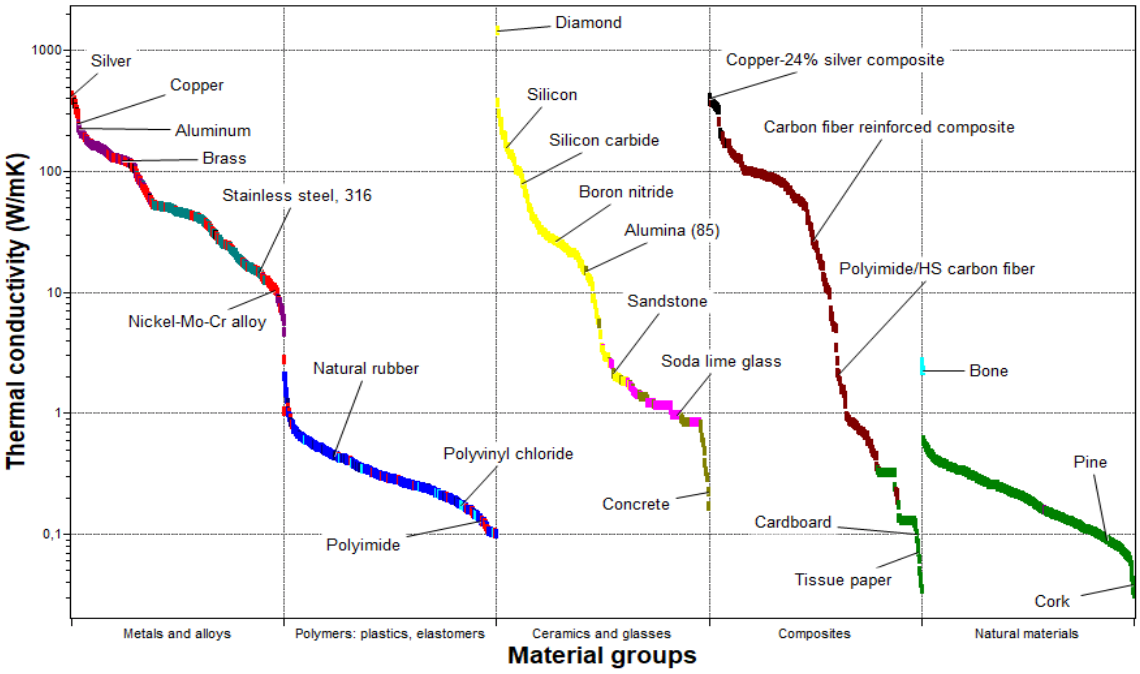

Figure 12: Chart of thermal conductivity of different materials. These materials are classified into groups. Different material groups are represented with different colours [12]

Moreover, since conduction is dependent on the vibration or collision of the microscopic particles, it is typically higher for high density materials than low density materials. Table 1 shows thermal conductivity of some materials labelled in Figure 12. Diamond and copper have the highest thermal conductivity of the materials mentioned in the table. At great temperature variations, it has been experimentally observed that the thermal conductivity of a material is dependent on the temperature. As there is a little temperature variation in the experimental part of this report, the thermal conductivity's dependence on temperature is considered to be negligible in the experimental part of this report [3].

Table 1: Thermal conductivity of some materials labelled in Figure 12 [12].

Material	**Thermal conductivity [W/mK]**
Alumina (85)	15.0
Aluminium	225.0
Boron nitride	26.8
Copper	275.0
Diamond	1440.0
Polyimide	0.13
Polyvinyl chloride	0.2
Silicon	160.0
Silicon carbide	80.0
Soda lime glass	1.0

Impurities in metals decrease the metal's thermal conductivity. Alloying agents are considered as metal impurities; therefore, metal alloys have lower conductivity than pure metals. This is observed in Figure 13 where increase in impurities in the aluminum metal decreases the overall thermal conductivity of the alloy. The graph is obtained after different metals were mixed in different content, weight percent (wt%), with aluminum. The "impurity" metals include copper, iron, magnesium, manganese and silicon. Alloys are a combination of different metallic elements and are manufactured to obtain desired properties like increase in shear strength, fracture toughness etc. As compared to pure metals, alloys have atoms of varied sizes which vibrate at different rates. Different types of atoms in the metal alloy have different values of thermal conductivities. Thus, the heat flow changes from atom to atom causing the change in pattern for thermal conductivity. This change in the

pattern of thermal conductivity acts as a resisting force in alloys which results in lower thermal conductivity in them as compared to pure metals [3] [15].

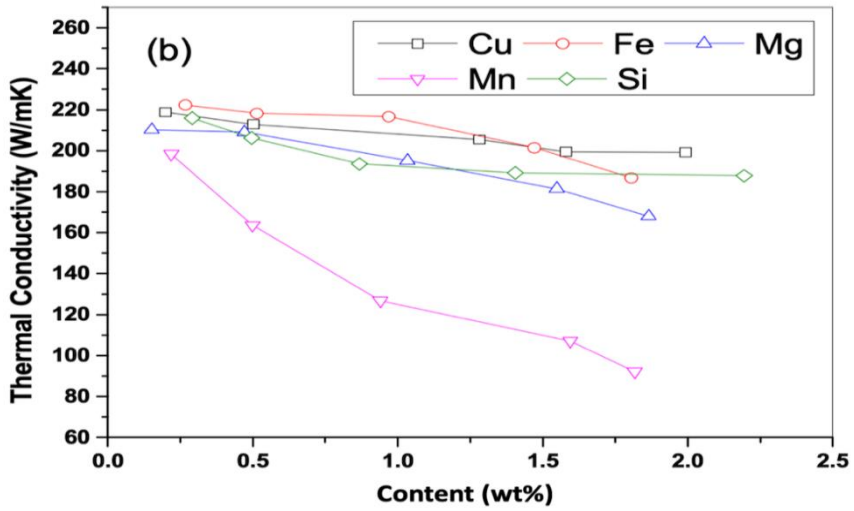

Figure 13: Decrease in thermal conductivity of an aluminium alloy with an increased in alloying content (wt%). Different alloying metals include: copper (Cu), iron (Fe), magnesium (Mg), manganese (Mn) and silicon (Si). They are represented with a different coloured line on the graph. Aluminium mixed with manganese results in the lowest thermal conductivity [15].

Polymers are thermal/electrical insulators made up of long repeating chain of molecules. Just like ceramics, they do not have free-moving electrons in their atoms. Thus, only the vibration of atoms contributes to the thermal conductivity in polymers. Polymers are light weight, flexible and are easy to process. Plastics are the most common type of polymers. Increase in crystallinity increases the thermal conductivity of polymers. Crystallinity in polymers refers to the partial alignment of their molecular chains. These chains form ordered regions called lamellae which are dispersed within the amorphous region of the material. Crystallinity in polymers ranges from 0-95% but mostly varies between 10-80%. Crystallized polymers are often referred as semi-crystalline polymers and their thermal conductivity depends on the degree of crystallinity and the orientation of the molecular chains. Density of crystalline polymers is greater than amorphous polymers as the molecular chains are closely packed in the crystalline structure. Moreover, thermal conductivity can also improve if fillers are introduced in polymers [16]. Fillers are used to improve the properties of various materials. For polymers, metal or carbon fillers are mostly used to enhance its thermal conductivity. These fillers have varied forms; precise geometry like short fibres or irregular masses. Depending on the size, geometry, quantity and the dispersion technique of the fillers, enhanced properties in polymers can be obtained. Typically, pure polymers have thermal conductivity value of 0.3-0.6 W/mK [3] [12].

Traditional ceramics are inorganic, thermal/electrical insulators with no free-moving electrons. The thermal conductivity in such ceramics is solely based on the vibration of atoms. Vibration of atoms has a lower contribution to the overall thermal conductivity of the material compared to the contribution from the free-moving electrons. Thus, traditional ceramics have lower thermal conductivity than metals. However, technical ceramics like diamond and silicon have unique properties with high thermal conductivity. This can be seen in Figure 12 where diamond, labelled in yellow, lies at the top of the graph. This is due to the strong covalent bonds in diamond's microstructure. Similar to polymers, crystalline ceramics have a more orderly microstructure than the amorphous ceramics. This allows them to have a distinct microscopic pattern which is uniform in the material. This results in greater thermal conductivity in crystalline ceramics than amorphous ceramics. Amorphous ceramics like glass, shown in pink in Figure 12, have a disordered microstructure which limits the propagation of phonons in thermal conductivity. Moreover, pores and surface irregularities also decrease the thermal conductivity of ceramics [3].

Composites are multiphase materials which are made by combining two or more materials. The final material exhibits new properties which are not present in any individual component. A key difference between composites from mixtures and solid-solutions is that the individual components of the composite remain separate and distinct within the finished product. Most composites are made up of two materials; a matrix and the reinforcement (fillers). Composite materials tend to be anisotropic in nature. Hence, the composite interface, the alignment of the matrix and the filler with respect to each other, is important to obtain effective properties. The shape of the filler is determined by the aspect ratio, which is defined as the ratio between the length and the diameter of the filler. Mainly, there are two types of fillers: fibre fillers and particulate fillers. The overall performance of the composite depends on the individual properties of the fillers and the matrix. Some composites perform better when the filler is in form of fibres whereas others perform better when the filler is a particulate. However, aligned and continuous fillers in the matrix exhibit better properties than discontinuous fillers. This is in accordance with the Hasselman-Johnson model proposed in 1980s [17]. The model states that the thermal conductivity in composites depends on the type of matrix, the type and the geometry of the filler. The model also highlights the importance of the nonzero interfacial thermal resistance which is achieved by a continuous matrix phase with adequate amount and geometry of the fillers. Usually, three types of matrices are used in composites i.e. polymer-matrix, metal-matrix and ceramic-matrix [18]. Metals and polymer matrices are commonly

used when some ductility is desirable; whereas, ceramic-matrix composite is used to increase the mechanical strength of the final material. However, one issue with ceramic matrices is that upon incorrect filler/matrix interface, a brittle composite is obtained [19]. Magnesium and titanium matrices are the most common metal matrices while polyimide, polypropylene and nylon are the most common polymer matrices. Typically, silicon carbide is used with continuous fibre fillers as a ceramic matrix. However, metal-matrix composites offer the greatest thermal and electrical conduction e.g. copper24%-silver composite highlighted in black in Figure 12. This is because both metals in this composite are excellent thermal/electrical conductors. Additionally, as silver is more ductile than copper, it is used as the matrix material. Experiments have shown that 24wt% of copper fillers with silver provides thermal conductivity value between 400-410 W/mK, the maximum thermal conductivity of any known composite. Generally, the thermal conductivity of composites varies from as low as 0.02 W/mK to 410 W/mK [3] [12].

Polymer based composites are used in the electronic industry for heat dissipation. Technical ceramics like boron nitride (BN) and alumina (Al_2O_3(85)) are often the filler choice because of their superior thermal conductivity and electrical insulation as seen from Figure 8. Such composites have feasible processability and good breakdown strength. They also provide strong interface interaction and allow desirable dispersion. However, high concentration of these fillers results in the loss of polymeric material which increases the thermal conductivity but massively reducing the electrical resistance in the composite. It also makes the composite denser and stiffer in some cases. This also affects the composite's mechanical properties by making it brittle [3] [20]. Thermal conductivity in composites can be expressed through the geometric mean model, Equation 13

$$k = k_m^{(1-Q)} k_f^{Q} \tag{13}$$

Where k, k_m and k_f are the thermal conductivities [W/mK] of the composites, the polymer matrix and the filler, respectively. According to this equation, the thermal conductivity of the filler has a greater impact on the thermal conductivity of the composite [21].

The most stable form of boron nitride ceramic is the hexagonal boron nitride (h-BN). It is a synthetic material with a two-dimensional planar, layered structure. It has a similar crystal structure as graphite and has a soft texture. It is often referred as "white graphite" but unlike

graphite, this ceramic offers electrical insulation. h-BN has a thermal conductivity value of 26.8 W/mK [12]. When the h-BN filler is oriented parallel to the heat transfer in a polymer matrix, maximum thermal conductivity and electrical insulation is obtained. This is due to the anisotropic nature of h-BN [22].

Alumina (Al_2O_3(85)) has a trigonal crystalline structure with octahedral coordination geometry between its atoms. This ceramic has a thermal conductivity value of 15 W/mK and has 85 wt% aluminium oxide in it [12]. Al_2O_3(85) in a polymer matrix offers a dense composite with good thermal properties. Thermal conductivity depends on the purity of alumina, size and the type of filler. Spherical alumina in a polyimide matrix offers greater thermal conductivity than short fibre alumina [12]. Increased volume fraction alumina enhances the thermal conductivity of the composite. Alumina has low reflectivity and is abrasive in nature. Thus, it requires various processing techniques before it can be used as fibres in a polymer matrix [3].

2.2.5 Thermal conductivity measurement

Thermal conductivity of a material can be measured using two methods: non-stationary and stationary method. The choice of the method depends on the type of material, its thermal properties and the medium temperature. Temperature plays a pivotal role in both of these techniques. Hence, temperature measurement is central in the thermal conductivity measurements [11].

Non-stationary methods, also known as transient methods, for thermal conductivity are based on the variation in material's temperature with time. The sample to be tested is placed next to the energy source (heat source) and the samples response is noted. This method is based on the time-dependent heat equation

$$\alpha \frac{\partial}{\partial x}\left(\frac{\partial T}{\partial x}\right) = \frac{\partial T}{\partial t} \tag{14}$$

Where α is the thermal diffusivity [m^2/s] of the sample material, $\left(\frac{\partial T}{\partial x}\right)$ is the change in temperature [K] with respect to distance [m] and $\frac{\partial T}{\partial t}$ is the change in temperature with respect to time [s]. This is a complex technique of measuring thermal conductivity which utilizes differential equations. However, it can be used for large temperature intervals of -100°C - 3000°C with an accuracy of 3-5% [11].

Stationary methods are thermal conductivity measurement techniques are based on two assumptions: the temperature gradient does not change with time and that the insulating material is in thermal equilibrium with its surroundings. This means a constant heat flux from the heat source is observed. The operating principle behind this method relies on sending a known $\dot{Q}$ [J] through a material with a known thickness [m], area [m^2] and later the temperature difference [K] is measured across the material. Thereafter, using the Fourier law, Equation 5, the thermal conductivity of the material can be calculated as follows

$$k = \dot{Q}\frac{x}{A\triangle T} \tag{5}$$

The exact configuration for the experimental setup for the stationary method depends on the type of sample. Guarded hot plate method (GHP) is the most common stationary method for

measuring thermal conductivity. A simplified apparatus setup involves a central heating plate sandwiched in between two sample plates. Cold plates are connected on either ends of the sample plates. The sides of the apparatus are well insulated to avoid heat losses to the environment. Heat flows from the heating plate to the sample and eventually to the cold plates. Temperature is recorded when steady state heating conditions are achieved using thermocouples at four different points: at top and bottom of the heating plate, and at the sample plate/cold plate interfaces, labelled in the sketch of GHP method, Figure 14. Once the entire system has reached thermal equilibrium, temperature increase of the cold plates is used to calculate the thermal conductivity of the sample. Often the temperature increase is smaller than the accuracy of the temperature measurement. In such cases, the sample is often made as long as possible so that the temperature difference becomes as large as possible. Thus, resulting in a more accurate thermal conductivity measurement. Two sample plates are typically chosen to control the heat flow as the heat flows symmetrically from the heating plate. This technique can be used for temperature interval of -160°C - 250°C with an accuracy of 2%. American Society for Testing and Materials (ASTM) has developed three methods: C177, C1043 and C1044 for GHP thermal conductivity measurements. The standard used to measure the thermal conductivity depends on the apparatus setup [11] [23].

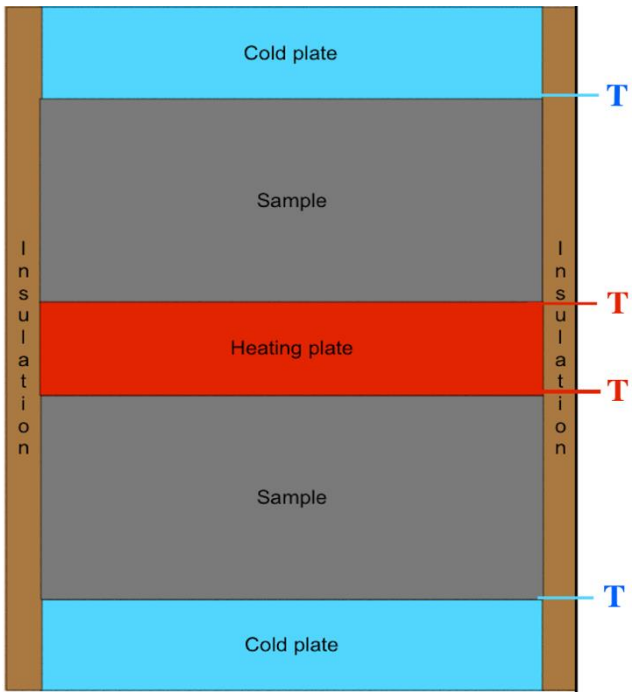

Figure 14: A simplified sketch of the guarded plate method used to determine thermal conductivity of a sample. The hot plate and the sample plates are well insulated from the sides so that heat losses are minimal [11].

Stiftelsen for industriell og teknisk forskning (SINTEF) has a custom-built chamber for heat flow measurements. It is based on plate-apparatus and is a stationary method of measuring different thermal properties. These properties include thermal conductivity, heat flow, thermal resistance etc. which are recorded at constant temperature difference over the specimen. Figure 15 shows a sketch of this apparatus set according to the standard ISO 8301 [24].

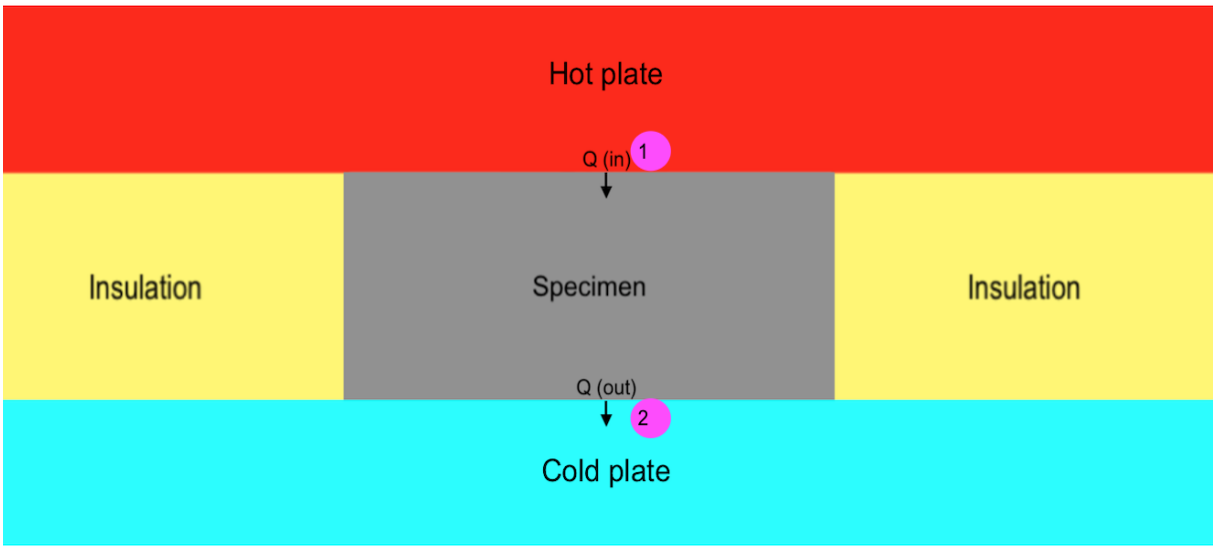

Figure 15: Sketch of SINTEF's heat flow chamber. The hot plate and the cold plate can be seen in red and blue; insulating material, represented in yellow, is put on the sides of the specimen to avoid heat losses.

The apparatus has a hot plate on top, a cold plate on the bottom, and the specimen is sandwiched in between them. The sides of the specimen are well insulated using mineral wool. The temperature of the hot and the cold plate is controlled using a circulating liquid, water/glycol, which circulates through insulated channels inside both plates. Difference in temperature in the hot plate and the cold plate results in one-dimensional, uniform heat flow in vertical direction. Dimensions of the hot plate and the cold plate are 600 mm x 600 mm whereas the heat flow measuring-area for the integrated heat flow meters is 300 mm x 300 mm. Heat flow meters incorporating 625 Type-T (Copper-Constantan) thermocouples are integrated inside the hot plate and the cold plate of the apparatus to measure the temperatures and the heat flows. They are measured at points 1 and 2, labelled in Figure 15. Moreover, the thermal insulance through the specimen is also recorded by these thermocouples. Thermocouples are connected to a data logger which in turn is connected to a computer which shows real-time variations in thermal properties of the specimen. If a sandwich specimen is being experimented, additional thermocouples are often used to measure temperature in different layers of the specimen. They are either grooved into the layer or taped on the surface of the layer and are extended from the specimen using thermocouple extensions. The outlet to these thermocouple-wires is often under the soft insulation material [24].

2.3 Thermal management

All electronic devices generate heat during their operation and thus require thermal management. The amount of heat generated depends on the input energy and on the ambient conditions of the system. The continued miniaturization of electronics has resulted in a dramatic increase in the amount of heat generated per unit volume. The increased rates of heat generation results in increased operating temperatures for electronic systems, thus, jeopardizing their performance and safety. Researches show that a temperature increase of as little as 10 K can shorten the lifetime of various electrical appliances by more than 50% [25]. Figure 16 shows the reasons of failures in electronics during operation. It can be seen that unsuitable temperature has the greatest impact on the degradation of the electrical appliances. This degradation is temporary when based on the temperature fluctuations, but constantly high temperatures can lead to a permanent failure [25].

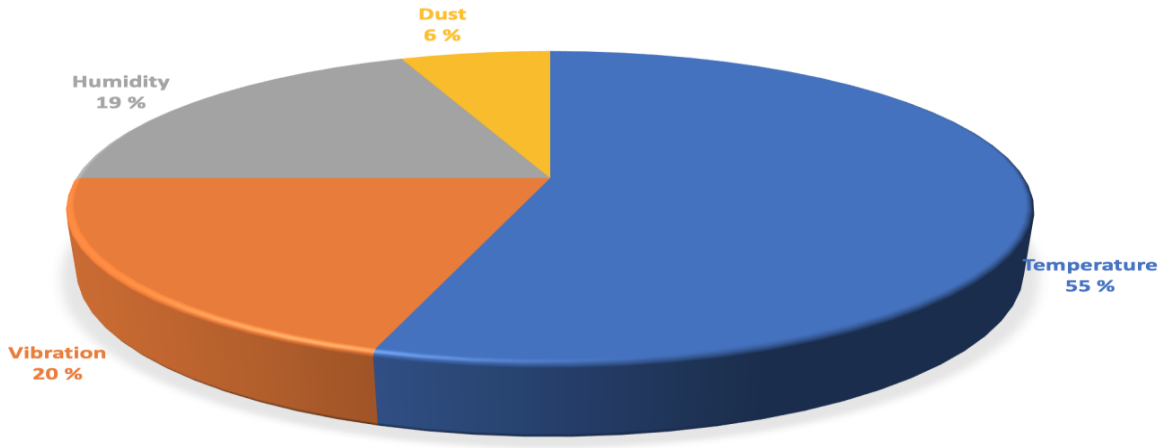

Figure 16: Main reasons for the failures in electronic components. It can be seen that temperature has the greatest impact while dust has the least impact [25].

In thermal management, temperature is the most important variable for the system. Thermal management includes various concepts like heating and cooling, heat removal, cycling and temperature homogenization in a system. The primary use of these concepts is to enhance the heat transfer and active cooling in an electrical system. In general, thermal management is categorized into two techniques: active cooling and passive cooling. Active cooling allows higher cooling capacity where the system can be cooled below the ambient temperature. This technique relies on external devices to enhance the heat transfer e.g. forced air through a fan or a blower. In contrast, passive cooling technique is not assisted by any mechanical equipment. The technique involves the use of heat spreaders like heat pipes, thermal interface

materials etc. An advantage in passive cooling technique is that it is more economical and energy efficient than active cooling techniques [25].

Various investigations have been conducted on thermal management and the effect of temperature on the PV performance. One such task was conducted by the Department of Electrical Engineering (DEE), Islamic Azad University, Iran. This investigation was based on Gen-1 crystalline PV module and its results are shown graphically in Figure 17 [26].

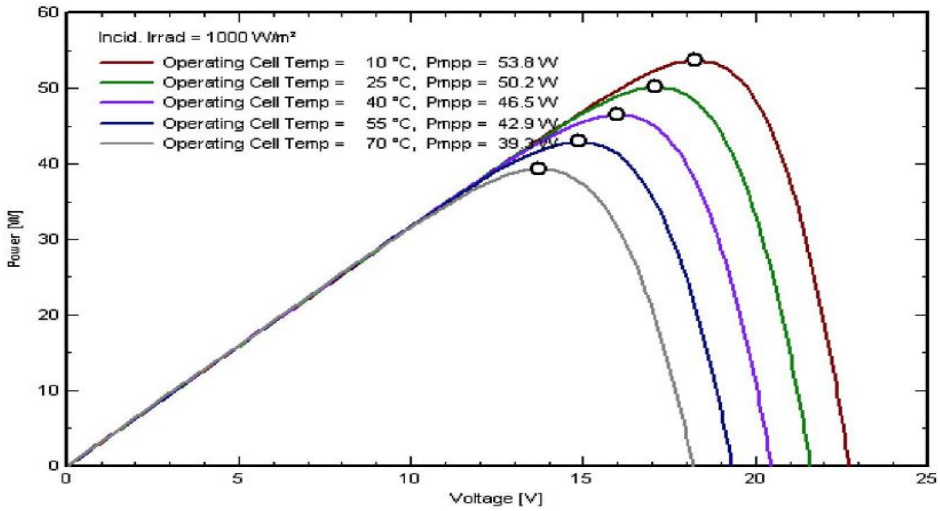

Figure 17: Power-Voltage characteristics of a PV module at different operating temperatures. The different operating temperatures are shown in different coloured curves [26].

From the graph, it can be seen that the performance of solar cells varies under temperature changes. These recordings were made at constant solar radiation of 1000 W/m^2. Figure 17 highlights the strong dependence of voltage on the temperature and an increased temperature decreases the voltage. The figure indicates the decrease in output electrical power as the temperature of the PV module increases. This highlights the significance of thermal management which is the ability to control the temperature of an electronic system to avoid its premature degradation. Many innovative technologies are used to avoid such degradation and are described later in the report. These technologies are based on thermodynamics and may include all possible processes like conduction, convection, condensation, radiation etc. Based on the system, the temperature is either increased/decreased or distributed accordingly to achieve better efficiency. This optimized thermal management not only protects the equipment and improves its performance but also saves costs in repair and maintenance [2] [26]. This report focuses on passive cooling techniques, especially on the TIMs for the PV/T system.

2.3.1 Heat pipes

A heat pipe is a passive two-way heat transfer device that uses evaporation and condensation of a coolant to transfer large quantities of heat. The coolant is often referred to as a two-phase "working fluid". Typically, a heat pipe is an evacuated, sealed vessel with a cylindrical cross-section. The working fluid flows inside the cylindrical hollow tube which is made up of a thermoconductive metal such as aluminium or copper. When the heat pipe is heated on the evaporator interface, the working fluid vaporizes. This results in a pressure difference which is the driving force for the vapour to move through the adiabatic section to the condenser interface. Here, the working fluid condenses back into liquid and releases the latent heat. The condensed liquid saturates and is pumped back into the evaporation section because of the creation of the capillary pressure. This loop continues as long as the heat is applied on the evaporator section. Figure 18 shows a sketch of a heat pipe with wick structure. Although, the sketch is rectangular, it is usually cylindrical in shape because it is often more practical; offering greater strength and other advantages in thermomechanical terms. Heat pipes have a wick structure which utilize the axial grooves on the inner wall of the heat pipe vessel to transfer heat. [27] This structure uses the capillary action- the ability of a fluid to flow in narrow spaces without any assistance like gravity- to move the working fluid from the condensed section back to the evaporated section. Capillary effect is efficient when the heat pipe has a very small diameter. The surface tension and the adhesive forces between the liquid and the container lift the flowing liquid and is even able to work against the gravity. Copper and aluminium are mostly used as the vessel materials; methanol, ammonia or water are widely used as the working fluid. The choice of working fluid depends on the operating temperature. Methanol is used if the operating temperature is below the freezing point of water and ammonia is used for electronics cooling in space [25] [27].

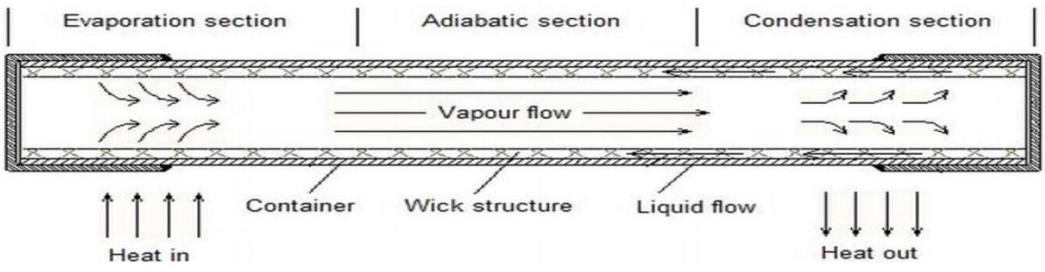

Figure 18: Rectangular heat pipe with three sections: evaporation, adiabatic and condensation. The sealed envelope has a wick structure with the working fluid inside. Vapor flows through the center while liquid flows along the wick to the evaporator side using the capillary action [27].

The advantages of using heat pipes is that they are highly efficient in the thermal conductivity over long distances. It is a passive heat dissipation technique and so does not require any input energy to operate other than heat. Moreover, they have a long life-time because of the protective coatings on the envelope and also because there is no liquid-loss due to the evacuated vessel. Typical applications include the solar/thermal systems, computer systems, heat exchangers etc. [27].

2.3.2 Thermal interface materials

A TIM is any material that is used between two components to improve the thermal transfer. It is inserted in between the heat producing and heat dissipating device to enhance the thermal conductivity in z-direction; thermal conductivity in x and y directions is unaffected. The most important function of a TIM is to replace air or vacuum with a more effective heat conducting material and to provide an adequate path for cooling of the electric component. They are widely used in commercial applications like CPU, graphics processing units (GPU), telecommunication etc. There are several types of TIMs as they depend on the application and the desired characteristics [28]

Thermal grease is a substance, in the form of a liquid or a paste, mostly used in electronics to transfer heat from the heat producing source to the heat sink. Typically, they have a polymer-based material formulated with silicone or hydrocarbon oils. They provide with a thin bond line which addresses the surface irregularities; thus, providing a better contact between the heat source and the heat dissipater. Typically, the grease has no mechanical strength and may require external fixation mechanism. As the grease does not cure, it is applied where the material can be contained or in thin application where the viscosity of the grease does not damage the system. There are various other kinds of thermal grease such as ceramic based and metal based. Metal based grease is the most efficient type of grease as it has metal particles in it which increase the thermal conductivity of the grease [28] [29].

Similar to the thermal grease, thermal glues are applied in many electronics to improve the thermal conductivity. An additional quality of the glue is that it provides mechanical strength to the bond after curing. Usually, thermal glues include metal oxide particles e.g. aluminium oxide (Al_2O_3) and boron nitride (BN), in a polymer matrix, usually silicone based. This provides thermal stability to the glue and offers enhanced heat dissipation. Typically, the thermal conductivity of such glues is in the same range as thermal grease i.e. from 0.7 – 1.5 W/mK. Figure 19 shows two imperfect surfaces in contact. They can be thought of as the heat source and the heat sink. Figure 20 shows how the surface irregularities between the two surfaces is cured by thermal greases and thermal glues. The gaps in the adjoining components are filled with a thin bond line which improves the thermal conductivity and better heat dissipation from the electrical device is obtained [29].

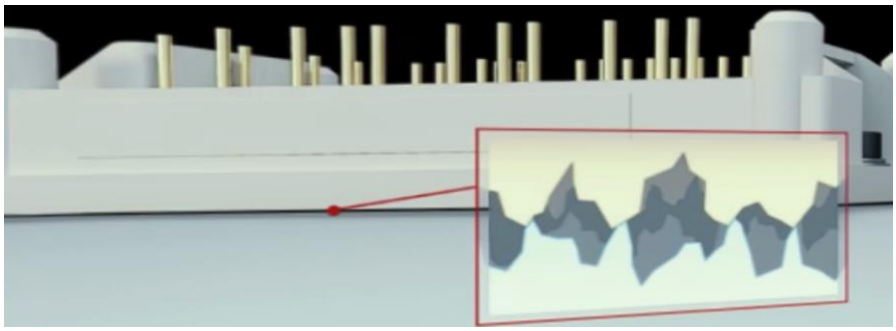

Figure 19: The module and the heat sink in contact with gaps in between them. The grey and black spots in the red window highlight these gaps [29].

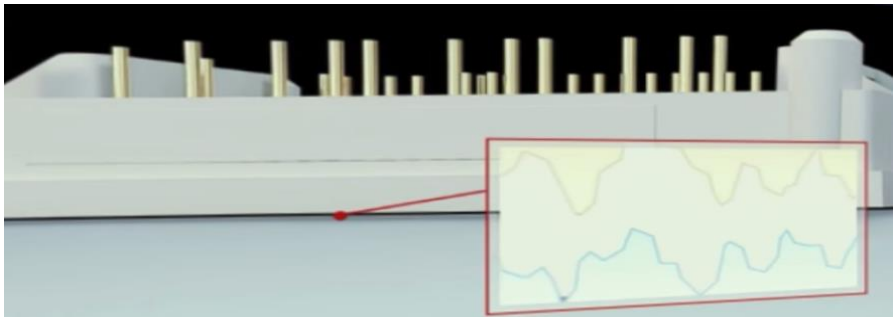

Figure 20: Gap between the module and the heat sink is filled by the grease/glue. The grease/glue is the off-white layer between the blue and yellow layers [29].

Unlike the aforementioned TIMs, thermal pad is a solid-state pad which is often soft and flexible. The most common type of thermal pad is made up of silicone and is either rectangular or square shaped. They have a typical thickness of 2 mm and include fillers like BN and a woven fiberglass to provide better conductivity and handling. The main advantage of these pads is that they are easy to apply and remove, especially when they are to be inserted in a sandwich structure. These pads are elastomeric in nature and have a high dielectric strength which provides long term electrical insulation between the heat source and heat dissipater. Thermal conductivity of these pads typically ranges from 1.0 – 3.0 W/mK [30].

Thermal tapes are easy to apply and are used to attach the electrical device to the heat dissipater. They adhere to the surface and require no curing time. These tapes are acrylic or silicone-based pressure sensitive adhesive (PSA) loaded with thermally conductive fillers. Adhering properties of these tapes is the primary reason of their usage while the thermal conductivity for heat dissipation is a secondary consideration. They readily conform to the complex module geometries and are also able to fill in the surface-gaps ranging from 0.1 mm to 0.6 mm [28] [30].

2.4 Photovoltaic cells

A PV cell is a technology which harnesses energy from the sun to produce electricity. At atomic level, it utilizes the phenomenon known as photovoltaic effect to absorb photons of light and release electrons. The usage of semiconductors allows the capturing of these photons which results in producing electric current. A PV system comprises of many solar cells which are grouped together and are either mounted on rooftops, wall mounted or ground-mounted. After its installation, it offers advantages like no greenhouse gas emissions and no other form of pollution as compared to electricity produced by fossils. There are three classes of PV cells, namely: first generation PV cells, second generation PV cells and third generation PV cells. All of these systems utilize different optical phenomenon including transmission and absorption of light by the solar cell, producing clean energy. Their efficiency and cost [US $] per square meter [$m^2$] increase in the order of their name (numbering) as shown in Figure 21. From the figure, the third generation PV cells seem the most promising class. However, as it is a relatively new technology, there is still a long way to go to exploit the maximum output from them [31] [32].

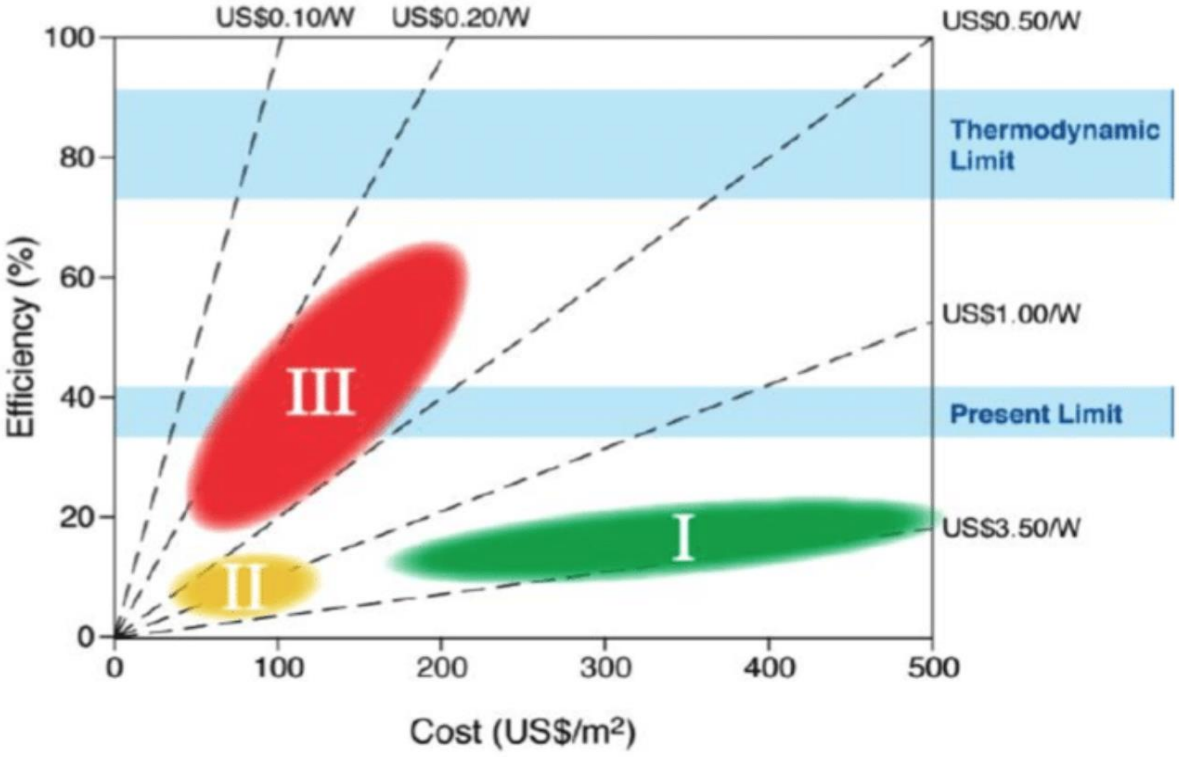

Figure 21: Efficiency and electricity production cost per m^2 of the different classes of PV cells. It can be seen that the third generation PV cells are more efficient than first- and second-generation PV cells. Moreover, the electricity production cost per m^2 is also lower for the third generation PV cells than the others. The figure also shows the present limit of efficiency i.e. 40% and the thermodynamic limit of efficiency of the PV cells. [32].

First generation solar cells (Gen-I) are mostly used in the solar panels. They account for about 80% worldwide sales of solar panels and are a prime candidate for PV cells for residential purposes. This is because of their long life-time and relatively straightforward manufacturing as compared to the other classes of PV cells. Gen-I PV cells are based on crystalline silicon which are cut into wafers. A silicon wafer has varied dimensions but with a typical thickness of 100-500 μm. The efficiency of the PV cells is influenced by the output voltage, module temperature and the solar light intensity. Theoretical efficiency limit of such cells is 30%; the PV cell efficiency ranges from 6-15%. Figure 22 shows a conventional Gen-I PV cell [31] [32].

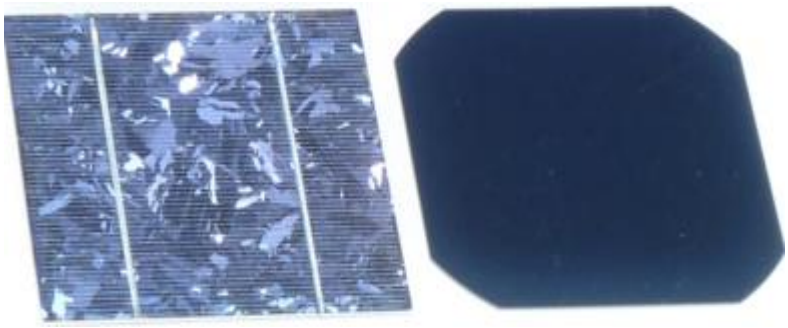

Figure 22: Gen-I crystalline silicon PV solar cell. It has a wafer structure and a thickness of 200 μm [33].

Second generation cells (Gen-II) are based on thin-film cells which also incorporate other semi-conductors. They require less material (silicon) and so are cheaper in their fabrication. They offer an advantage over the Gen-I cells as Gen-II cells are flexible because of the glass or plastic substrates used in their fabrication. They are mostly based on amorphous silicon, cadmium telluride (CdTe) and copper indium gallium selenide (CIGS). A disadvantage of Gen-II cells is that they offer shorter lifetime than Gen-I cells and their efficiency reduces drastically over time. Efficiency of amorphous silicon cells varies between 10-14% whereas efficiency of CdTe in laboratory is tested to be around 20% [31] [32].

Third generation cells (Gen-III) are an innovative technology which is still under development. They are based on various materials including organic solar cells, perovskite solar cells, tandem cells and dye sensitized solar cells. These cells can be thought of as a combination of Gen-I and Gen-II solar cells, a hybrid version which promises to offer greater efficiency and lifetime. They have various configurations and are expected to exploit greater energy from the sun. Currently, most of the research on Gen-III cells is still in its testing phase and they are not commercially available [31] [32].

2.4.1 Structure and mechanism

A PV cell comprises of layers of different materials contributing to the generation of electricity. A PV cell power generation employs many solar cells connected to each other in a solar module. This module is arranged in an array; mounted onto a building which is facing direct sunlight resulting in the production of electricity. Single modules are designed to generate electricity of distinct voltage, usually 12 volts. The resulting current depends on the intensity of sunlight, the area of the module and module temperature. Figure 23 shows a typical solar panel. PV modules can either be connected in series or parallel electrical arrangements. Increased number of cells in series produces a greater voltage while an increased number of cells in parallel produces a greater current [31] [34].

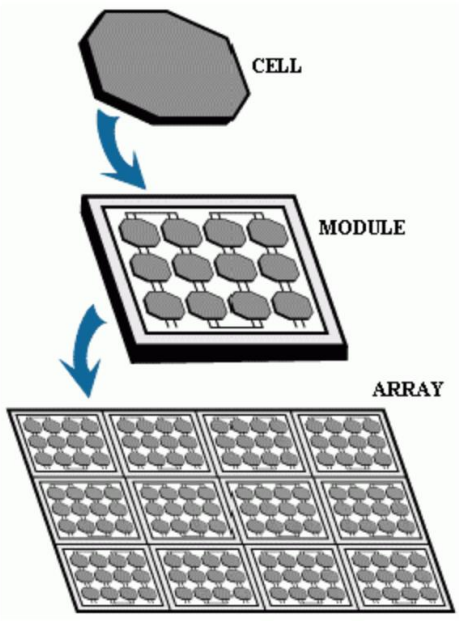

Figure 23: A typical solar panel. Multiple modules are aligned together to form an array which is called a solar panel. These panels produce direct current upon solar insolation [34].

Most of today's PV cells are based on a single junction, p-n interface. This p-n interface is part of the semi-conductor layer in the PV cell which has two distinct layers:
p-type and n-type. This semi-conductor is responsible for the absorption of light and in the generation of electricity, a mechanism known as PV effect. Figure 24, on the following page, shows the mechanism of electricity generation in the solar panel. When sunlight strikes the p-n junction, energy is absorbed by the electrons. Electrons move to a higher energy state and move towards the positive side (p-side) of the semiconductor. Consequently, the holes move towards the negative side (n-side) of the semiconductor. The combination of electrons and the

holes because of the diffusion through the p-n junction results in an electrical voltage. If an external electrical contact on the end of the p-type semi-conductor is made positive and the contact on the end of the n-type semiconductor is made negative, an electrical current is obtained through the external circuit i.e. from n-to-p semi-conductor [33]. A critical factor in the absorption of light by the electrons is the wavelength of the photons of light. Photons are bundles of electromagnetic radiation with varying wavelengths. As atoms have distinct energy levels, only the photons with energy equal to or greater than the bandgap-energy of the semiconductor are absorbed by the electrons in the semiconductor. These photons are solely responsible for the excitation of the electrons to the conduction band and electrons' eventual mobility to the p-side semi-conductor as depicted by the arrows in the figure X [31] [33].

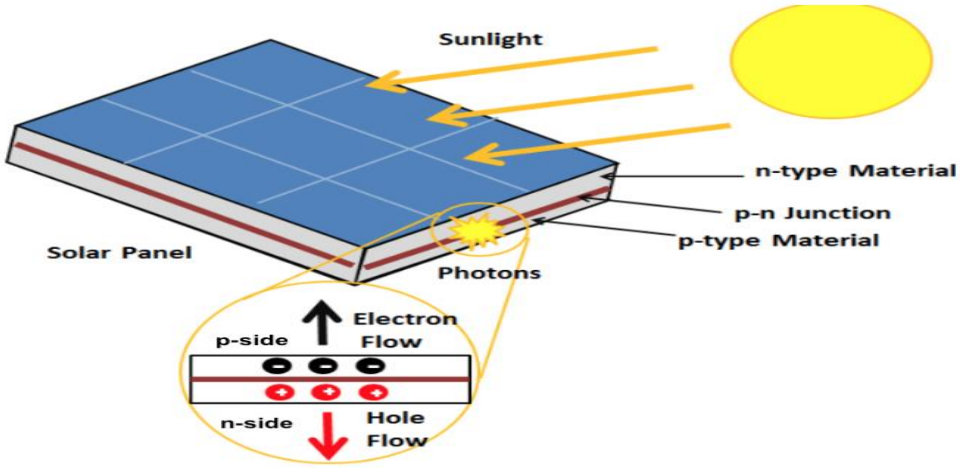

Figure 24: Electricity generation from the solar panel. The p-type and n-type semiconductors are critical in utilizing the PV effect, creating the electron/hole pair. It is important that the solar panel is facing the sun for maximum performance [33].

Figure 25 shows the structure of the PV cell used in the production line of the PV/T systems. This PV cell has no encapsulation and has a double edged sealing from the sides, shown in grey and black. It is a glass/glass module based on Gen-I crystalline silicon cells connected in series. Unlike conventional Gen-I cells, this module offers advantages like no lamination, no soldering. It uses a neutral gas, N_2, than an encapsulant which saves the material cost as the incident ultraviolet light is not cut-off, avoiding the yellowing of the cell [35].

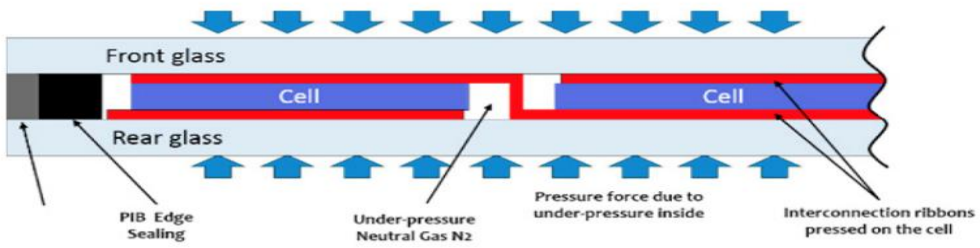

Figure 25: PV module used in the production line of PV/T system. The module is tightly sealed from the sides for better performance [35].

2.4.2 Performance

¼ of solar energy to Earth cannot be converted into electrical energy in a PV cell. This is due to the photons of light having lower energy than the bandgap energy of the semi-conductor. When these photons are unable to excite the electrons in the semiconductor to the conduction band, they are absorbed as thermal energy. This energy is catastrophic for the PV cell as the increase in system's temperature drastically reduces the performance. Moreover, the peculiar properties of semi-conductors used in PV cells is another reason for their limited performance. Increase in temperature reduces the bandgap inside the semi-conductor. Lower energy is therefore needed to surpass the bandgap energy. This leads to a greater number of electrons in the conduction band which produce greater current. As the temperature of the PV cell increases, the output current increases exponentially while the voltage output reduces linearly. This is due to a phenomenon known as recombination where electron/hole pairs generated after the absorption of photons fall back to their ground state. Recombination happens when a semi-conductor is not in thermal equilibrium because of increased illumination or the injection of current in it. The falling back of these electron/hole pairs releases phonons, unit of vibrational energy. The release of phonons is an energy loss in the form of heat which decreases the performance of the PV cell [31].

Figure 17 shows the temperature dependence of the output voltage from the PV cell. Another important result drawn during the investigation by DEE, Iran, was the variation in efficiency with temperature at 1000 W/m^2. Efficiency in a PV system is defined as the percentage of power from sunlight converted to electrical power by the solar cell. The results from the DEE research in Iran on PV efficiency are shown graphically in Figure 26.

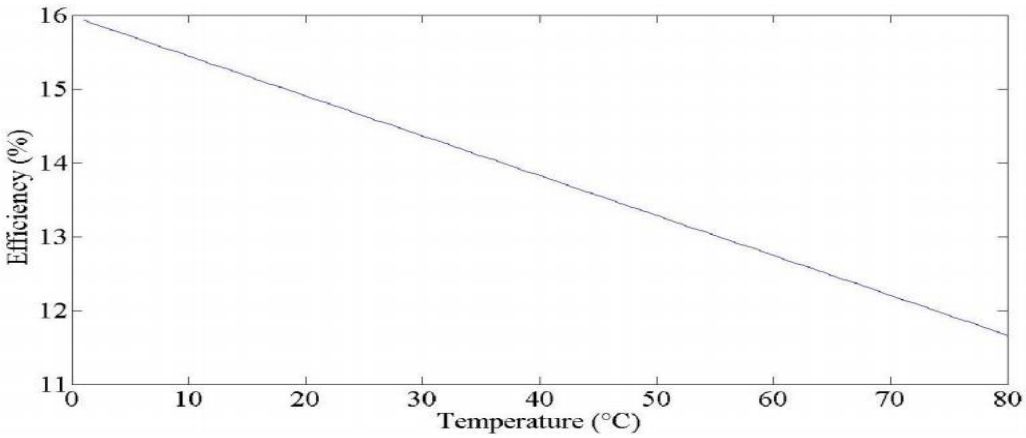

Figure 26: Variation in efficiency of the PV module with ambient temperature. A linear relationship can be observed [26].

The research by Department of Electrical Engineering (DEE), Iran, signified an important issue with the PV cells. The research by Department of Energy & Climate Change (DECC), UK, proposed a solution to this issue which consisted of a cooling mechanism incorporated with the PV cells. The research by DECC reported a hybrid system which involves the use of a heat mat which acts as a coolant and an efficiency enhancer [2] [26]. This report is based on the investigation of Gen-I PV cells in a PV/T system and it further the aforementioned researches. It attempts to conclude by providing the best possible interface between the PV cell and the heat mat in a PV/T system.

2.5 Solar thermal collectors

A solar collector is a device that collects and utilizes solar radiation to heat a circulating medium. They are often referred as solar thermal collectors and they collect solar radiation for space heating or water heating. Water is the most common circulating medium and adding anti-freeze like glycol help in the colder weather conditions. These devices are usually mounted on rooftops and are facing the sun to exploit maximum solar energy [36]. They provide endless amounts of energy which is free of charge with no CO_2 emissions during operation. There are two types of solar collectors, concentrating and non-concentrating solar collectors. A concentrating solar collector has a very large surface area for the solar radiation interceptor. The greater sunlight interceptor reflects the sunlight to the smaller absorber. An example to this is the parabolic dish reflector, shown in Figure 27 (a) [37]. In a non-concentrating solar collector, the collector area is the same as absorber area; relatively smaller than the concentrating collectors. The entire solar collector absorbs the sunlight and actively participates in the usage of solar insolation. Typically, they are shaped like a box containing a transparent cover with the enclosure insulated to minimize heat losses to the environment. Usually, a metal absorber plate is used with water/anti-freeze as the circulating fluid in the tubes which lie underneath the absorber. When the water heats up upon solar insolation, it circulates around the piping system as long as the sunlight is strong enough to increase the water's temperature. This heated water can either be directly used or stored in a hot water tank for later usage. The advantages with such solar collectors are that they have low initial and maintenance costs and are best suited for low-temperature systems [37] [38]. Figure 27 (b) shows a non-concentrating solar collector.

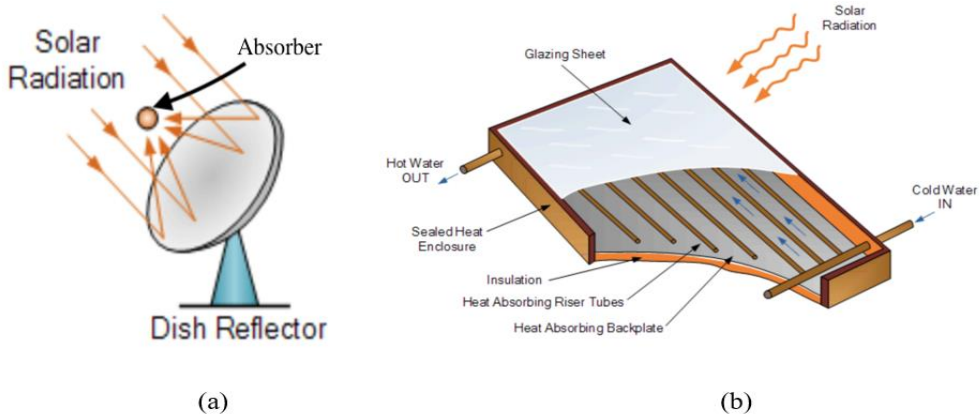

Figure 27: Two types of solar collectors. (a) Concentrating solar dish is formed into a paraboloid which collects and concentrates the solar energy onto the absorber [37]. *(b) Non-concentrating solar collector. The covering layer, the absorber plate and insulation are the key components of such solar collectors* [39].

2.5.1 Heat pipe solar collectors [2]

Heat pipe solar collectors used in the PV/T production line are based on non-concentrating solar collectors. They are rectangular in shape containing a dark cover with an absorber plate and fluid circulation passageways underneath. In addition to harnessing solar energy, this solar collector is capable to act as a building envelope material. Its mechanism involves: using the heat pipe technology, using phase change materials, a hydraulic based cooling system referred to as water cooling and ammonia as the circulating fluid. Phase change materials are important when adhering this technology onto the PV module for greater efficiency. These materials stabilize the PV cell temperature and demonstrate a total of 6% increase in PV's efficiency, as reported by DECC, Cardiff. However, only after incorporating the flat heat pipe technology with integrated cooling channels can the waste heat from the PV system be utilized by this heat pipe solar collector. This type of solar collector is referred to as the PV/T heat mat. Apart from its primary goal of providing energy for space/water heating, it converts the building envelope from a passive to an active component for energy generation.

The heat mat used in the production line of PV/T systems has been validated by Flint engineering and can be thought of as a non-concentrating solar collector. It is made of aluminium with ammonia as the working fluid in the integrated heat pipe channels. These channels are based on heat pipe technology and incorporate flat head heat pipes with rectangular cross-section. However, they do not utilize the wick structure for thermal dissipation. Instead of axial grooves, they utilize internal finning and the heat pipe technology for an effective thermal dissipation from the PV system. Subsequently, this becomes the cooling mechanism for the PV module which provides a greater utilization of solar energy in the PV/T system. Figure 28 shows a snapshot of heat mat used by DECC, Cardiff during their investigation.

Figure 28: Heat mat experimented as a building integrated material during DECC's investigation in Cardiff [2].

Figure 29 illustrates the principle behind this design. Heat absorbed by the heat mat can either be used in heat pumps for space heating or can be directly used/stored for water heating.

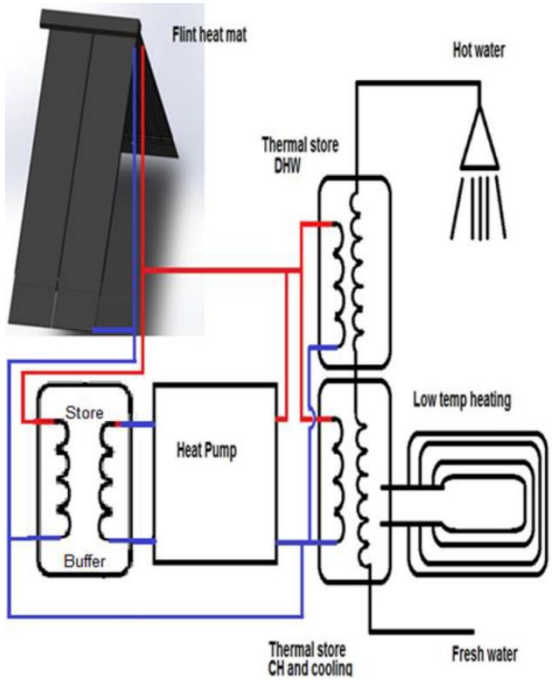

Figure 29: Sketch of the mechanism of Flint heat mat used in the production line of PV/T systems. Heat absorbed by the heat mat can either be stored or directly used for space/water heating [4].

2.6 Photovoltaic/Thermal system

A PV/T system has a sandwich structure where a PV module is adhered to a solar collector, i.e. a heat mat. As this building integrated system has not been commercialized yet, different module designs and scenarios are being investigated by the researchers. This report aims at finding the best thermal interface material (TIM) which allows for the maximum heat transfer within a PV/T system. It takes inspiration from the successful research conducted by the DECC, Cardiff, and investigates the joining mechanism in the hybrid system [4].

In this report, two scenarios for a PV/T system are investigated; shown in Figure 30. The idea behind this thesis is to conduct experiments which mimic the real-life production line of the PV/T systems. Figure 30 (a) shows scenario A which aims at investigating the best way to connect/bond the glass/glass PV module with the heat mat. Figure 30 (b) shows scenario B which aims at investigating the best TIM upon the removal of the rear glass from the PV module. In addition to the experiments, a desk study is conducted on scenario B.

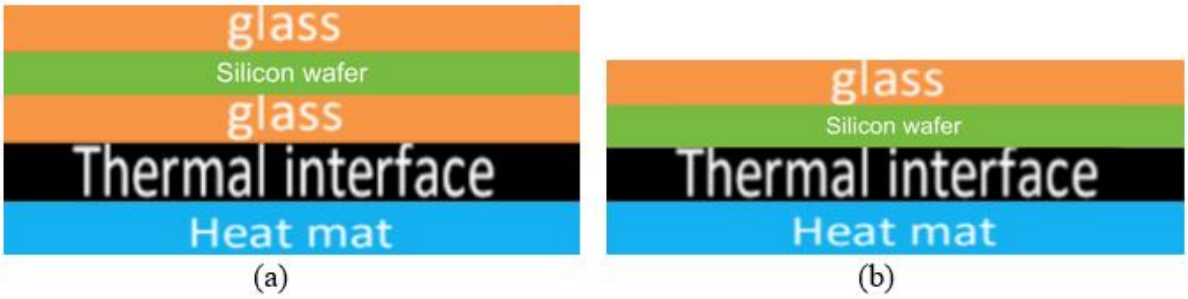

Figure 30: PV/T systems investigated in this report. (a) Scenario A where glass/glass PV module is attached onto the heat mat with a suitable TIM and (b) Scenario B where rear glass of the PV module is replaced by TIM and adhered to the heat mat.

TIM for scenario A must have a thermal conductivity greater than the thermal conductivity of the rear glass. Electrical conductivity is not important in this scenario as it is expected that the PV module will utilize maximum electrical energy; the rear glass is expected to provide good electrical insulation.

TIM for scenario B must be an electrical insulator for direct application. Electrical insulation is important to avoid the premature degradation of the system. This is due to the absence of the rear glass which provided such insulation in scenario A. Table 2, on the following page, presents the objectives and requirements in these scenarios for the production line. As the

PVadapt, BIPV-T project is still in its initial stages, there are not many definitive parameters and constraints regarding the scenarios.

Table 2: Requirements in TIM for the two PV/T scenarios.

Requirement	**Scenario A**	**Scenario B**
Thermal conductivity	>1W/mK*	Maximum
Electrical insulation	Not important	Maximum*
Mechanical properties	Can be elastomeric	Glass-like*
Thickness	≤ 3 mm	≤ 3 mm
Flammability	No*	No*
CO_2 footprint	Minimum	Minimum
Price	Economical	Economical

*Critical requirements for the scenario.

3. Material and Method

3.1 Heat flow experiment

3.1.1 Materials

The PV/T system for heat flow experimentation had a sandwich structure. It was based on soda-lime glass plates, Gen-I crystalline silicon wafer and an extruded aluminium plate. The TIM used for scenario A was a copper tape whereas a polyvinyl chloride (PVC) pad was used as TIM for scenario B. Table 3 shows different properties of the materials used for experimentation.

Table 3: Properties of the materials used for heat flow experiments [12]

Material	**Thermal conductivity [W/mK]**	**Thickness [mm]**	**Area [m^2]**	**Dimension [10^{-3} m]**
Soda-lime glass	1	3	0.045	180 x 250 x 3
Silicon wafer	160	3	0.023	150 x 150 x 3
Aluminium plate	225	10	0.045	180 x 250 x 10
Copper tape	275	0.01	0.045	180 x 250 x 0.02
PVC pad	0.2	1	0.045	180 x 250 x 1

Pilkington Optifloat™ glass plates were obtained from Riis Glass og metall AS, Trondheim. Silicon wafer and the aluminium plate were supplied by the PVadapt project-group. The silicon wafer was doped with boron of unknown concentration. The aluminium plate simulated the heat mat and had 15 hollow grooves in it. In an actual heat mat, these grooves are channels for the working fluid. Figure 31, on the following page, shows the aluminium plate which was stacked at the bottom of the PV module for experimentation. Copper tape was manufactured by Stokvis Tapes and was obtained from Clas Ohlson, Trondheim. MultiSafe PVC pad was obtained from Oldroyd AS, Kragerø. Moreover, Murplate 32 mineral wool was used for insulation. It is manufactured by Glava AS and was obtained from SINTEF, Trondheim. 3 Type-T thermocouples, supplied by SINTEF, Trondheim, were

connected to a DT80 data logger and a computer. Online dEX software was used for temperature measurements inside the sandwich structure.

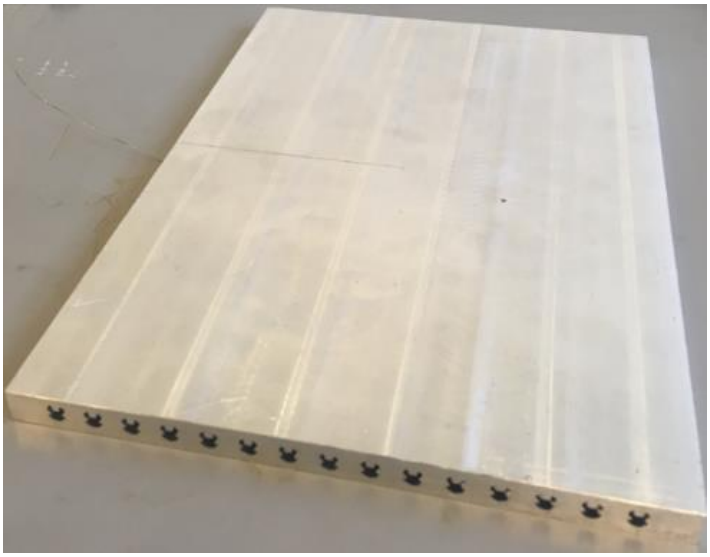

Figure 31: Aluminium plate used for experimentation. 15 hollow grooves can be seen which incorporate working fluid in the PV/T production line.

3.1.2 Apparatus and calibration

Figure 32 shows a snapshot of the experimental setup. SINTEF's custom built heat flow apparatus was used for these experiments which measured a unidirectional heat flow at stationary conditions. Dimensions of the hot plate and the cold plate are 600 mm x 600 mm whereas the heat flow measuring-area for the integrated heat flow meters is 300 mm x 300 mm. All experiments were set up according to Figure 32, with the only change in the specimen type and the duration of the experiment.

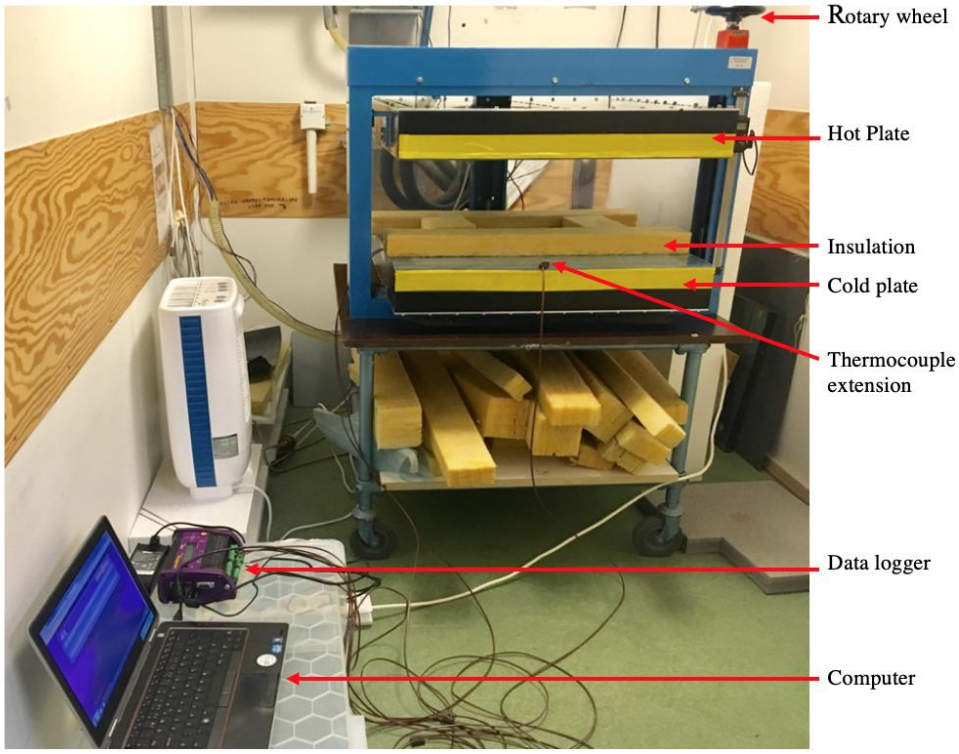

Figure 32: Both scenarios and the reference experiment were set up as shown in the figure. For insulation, the specimen was bordered with mineral wool inside the chamber. The rotary wheel used to bring down the hot plate can be seen in black, on top of the chamber.

External thermocouples were used to record temperature of the different layers in the sandwich specimen. They were calibrated before their usage. Two calibrations were done: in 500g crushed ice at 0℃ and in a kettle of boiling water at 100℃. The data logger was connected to the thermocouples and the computer running dEX application. Thermocouples were extended using extension cables to a length of 3 meters to record temperature. Due to its soft texture, thermocouples were placed underneath the mineral wool and extended outwards using extension cables. The temperature of the hot plate was set at 16℃ whereas the temperature of the cold plate was set at 4℃. This difference in temperature led to a heat flow, $\dot{Q}$ [J], from the top plate to the bottom plate, going through the sandwich specimen. Room temperature was held constant at 10℃.

3.1.3 Preparation of samples

Materials mentioned in Table 3 were cleaned using rectified spirit before experimentation. A clean cloth was soaked in the spirit and gently rubbed over the glass surfaces, aluminium plate, silicon wafer and the PVC pad until it appeared clean. In order to obtain accurate temperature values, the thermocouples were grooved in the centre of the glass plates and the aluminium plate. Glass plates had a groove depth of 0.2 mm and they were made manually using a cutter. Aluminium plate had groove depth of 0.5 mm and it was made using a milling machine. After the grooves were made, a rapid glue was used to glue the thermocouple probes in the centre of the different surfaces.

Copper tape was chosen as TIM for scenario A. This tape had a 99.4 wt% copper content, attachment 3 in appendix. X-ray fluorescence (XRF) scan using SPECTRO xSORT handheld XRF scanner was done to determine the copper content in the tape. The back side of the rear glass was taped; first horizontally and later vertically, filling up the entire glass surface, 180 mm x 250 mm. Additional care was taken while applying this tape to avoid trapping any air between the tape and the glass surface. This was done by pressing the tape smoothly over the glass plate. The glass was coated twice, thus, resulting in 0.02 mm of total thickness of the TIM. Figure 33 shows the finished version of the rear glass after being taped.

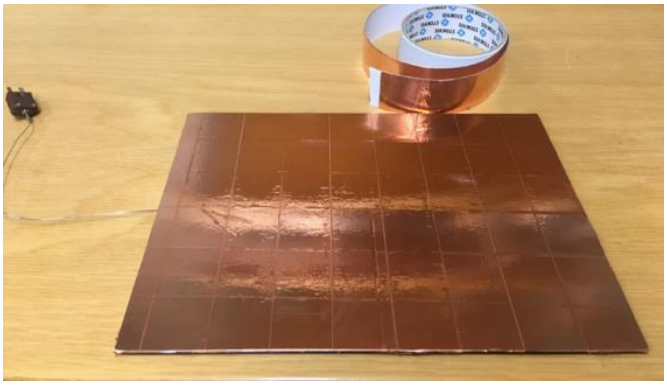

Figure 33: Rear glass which was taped using the copper tape. The thermocouple which was grooved inside the rear glass can also be seen in the figure.

A thin polymer interface, PVC pad, was chosen as TIM for scenario B. Plastic identification flow chart, attachment 4 in appendix, was used to test the material. No special preparation was required for this TIM. Figure 34 shows the pad used in this experiment.

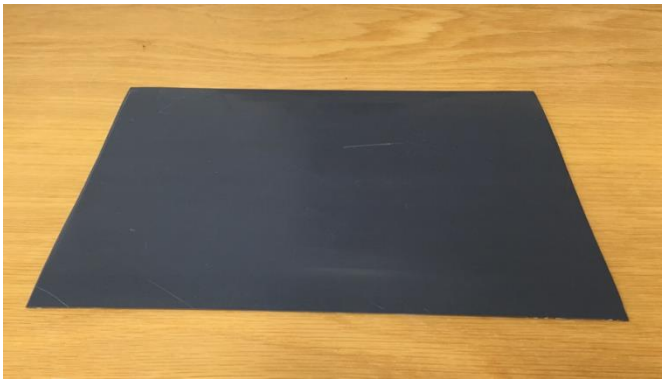

Figure 34: PVC pad used for scenario B. This pad replaced the rear glass of the PV module and was directly inserted for experimentation.

3.1.4 Experiments

Reference experiment

A reference experiment was conducted without a thermal interface between the PV module and the aluminium plate. This experiment was conducted to obtain literature values for heat flow. The equipment was stacked up vertically in the following order, top to bottom: front glass, silicon wafer, rear glass and aluminium plate. Figure 35 shows a sketch of the sandwich structure placed inside SINTEF's heat flow apparatus. Temperature and heat flow values at points 1 and 5 were recorded by chamber's in-built monitors. Temperature at points 2, 3 and 4 were recorded by external thermocouples grooved into the different layers. Thermocouples were connected at the bottom of the front glass, the second on top of the rear glass and the third on top of the aluminium plate, shown in curved red lines.

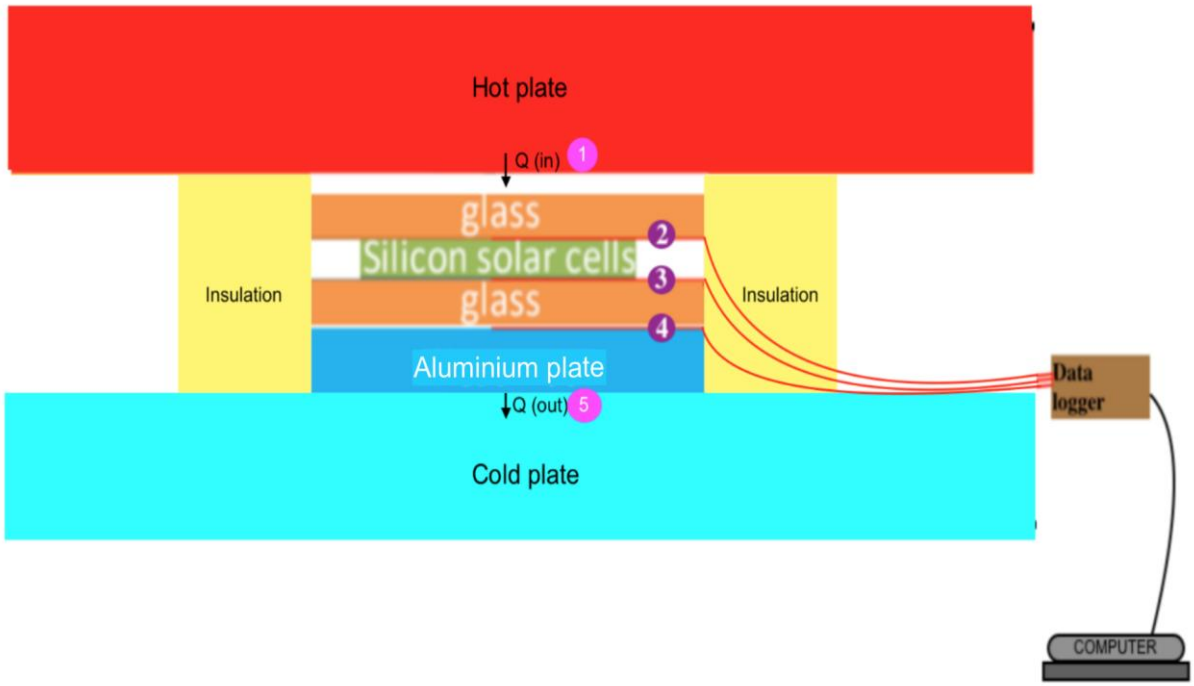

Figure 35: Sketch of the PV/T system for the reference experiment. Three type-T thermocouples, shown in red lines, recorded temperature of different layers. The sketch is not drawn to scale.

The distance between the hot plate and the front glass was 3 mm. This was done to avoid excessive pressure on the glass. Moreover, mineral wool did not fully enclose the chamber's measuring area. The data logger was connected to the thermocouples and a computer. The dEX software was launched on the computer and temperature was recorded every 5 seconds for 2 hours.

Scenario A

Figure 36 shows the entire specimen for scenario A. Backside of the rear glass was taped using the copper tape. Similar to the reference experiment, three thermocouples were used.

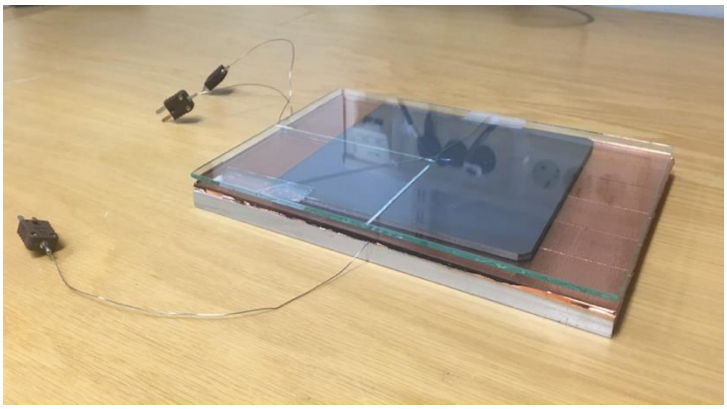

Figure 36: The specimen setup of scenario A. Front glass, silicon wafer, rear glass coated at the back-side with copper tape, the aluminium plate and the three thermocouples can be seen in the figure.

Figure 37 shows the configuration of the specimen for scenario A inside the apparatus. The distance between the hot plate and front glass was 3 mm. Using the data logger and the dEX software, temperature was recorded every 5 seconds for 15 hours. This was done to observe any change in temperature readings with a longer experimental time. Temperature and heat flow values at points 1 and 5 were recorded by chamber's in-built monitors. Temperature at points 2, 3 and 4 were recorded by external thermocouples, shown in curved red lines.

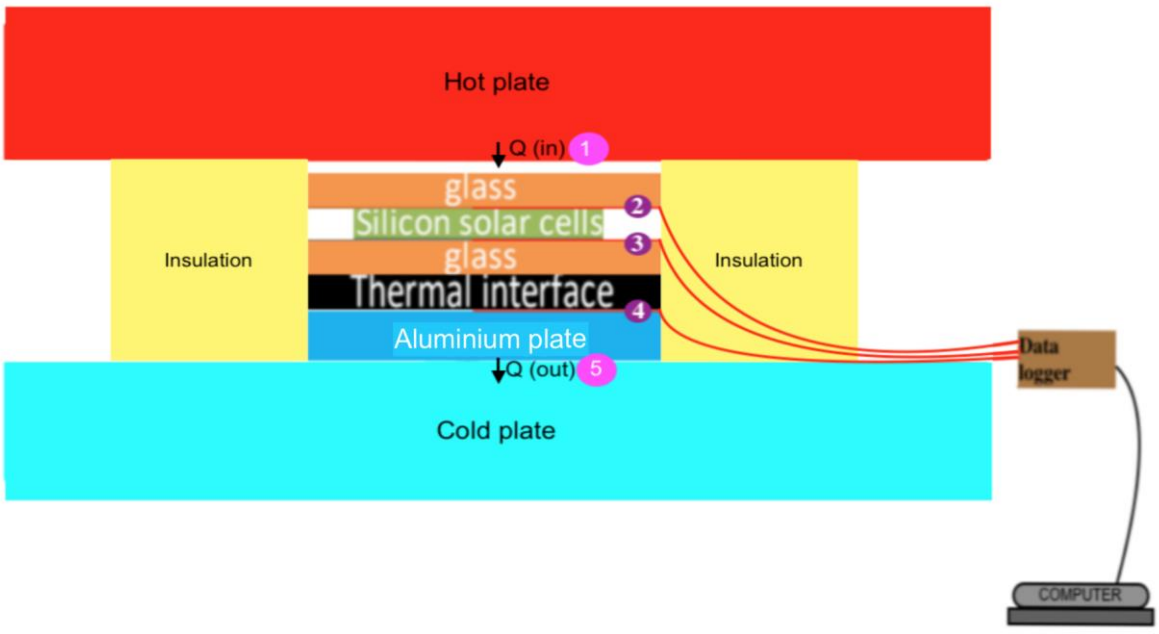

Figure 37: Sketch of the specimen for scenario A placed inside the heat flow apparatus. Three thermocouples were used to record the temperatures. The thermal interface was attached to the back side of the rear glass. The sketch is not drawn to scale.

Scenario B

Figure 38 shows the specimen for this experiment. As the rear glass was removed from this specimen, only two thermocouples were used to record the temperatures with respect to time. One thermocouple was attached on the back side of the front glass and the second thermocouple was attached on the top of the aluminium plate, underneath the PVC pad.

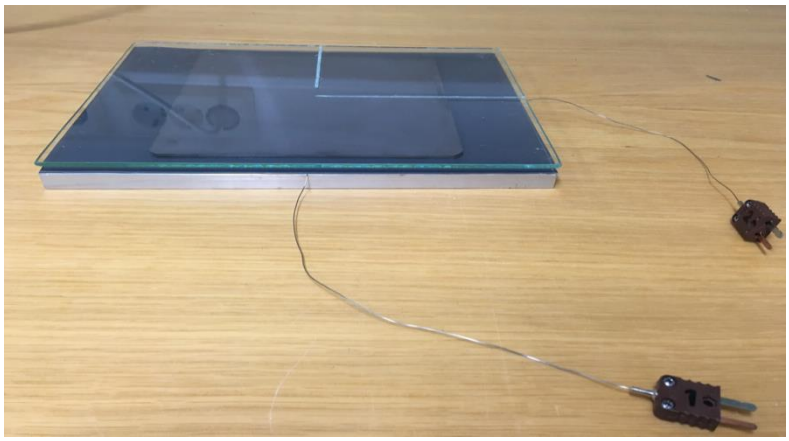

Figure 38: Specimen setup for scenario B. The PVC pad can be seen through the transparent glass layer. Two thermocouples can also be seen in the figure.

Figure 39 shows a sketch of this scenario inside the heat flow chamber. The distance between the hot plate and front glass was 3 mm. Temperature and heat flow values at points 1 and 4 were recorded by chamber's in-built monitors. Temperature at points 2 and 3 were recorded by external thermocouples. Temperature was recorded every 5 seconds for 2 hours.

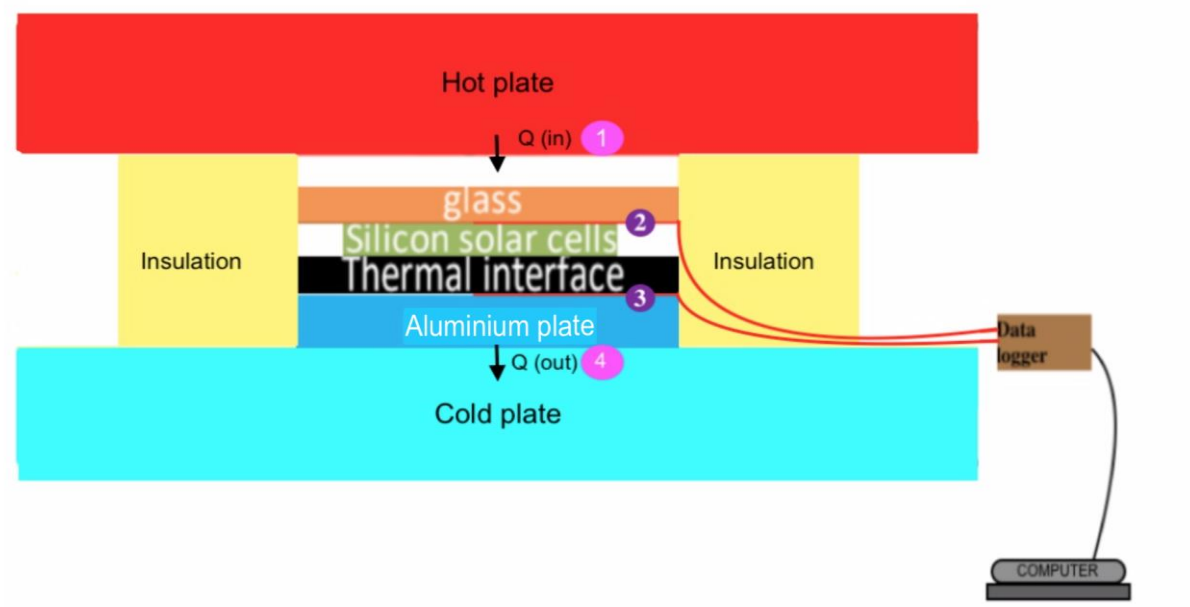

Figure 39: Sketch of the specimen for scenario B placed inside the heat flow apparatus. Two thermocouples were used to record the temperature which are shown in curved red lines. The PVC thermal interface was placed between the silicon wafer and the aluminium plate. The sketch is not drawn to scale.

3.2 Desk study on Scenario B

3.2.1 Materials in the market

Material exploration was conducted on scenario B for experimentation. Elastomeric thermal pads, composite materials, were chosen as TIM for this desk study. This short research was done in two steps: firstly an online research on TIMs available in the market and secondly, using Edu Pack. As PVadapt is still in infancy, there are not many concrete parameters or constraints for the scenario. Thus, the criteria for the online research was simple and straightforward. It was based on the thermal pads which offered maximum thermal conductivity and maximum electrical insulation. This criteria is slightly different than the one presented in Table 2. The difference in mechanical properties arises because these pads are considered for experimentation where elastomeric nature of the pad is not an issue. Moreover, only the materials supplied by the renowned companies which offered material data sheet and safety data sheets were investigated. Individual suppliers were rejected based on the uncertainty in their product. Table 4 summarizes the objectives of this material exploration.

Table 4: Objectives behind the investigation on thermal pads available in the market.

Parameter	**Objective**
Thermal conductivity	Maximum
Electrical Insulation	Maximum
Mechanical	Can be elastomeric
Price	Cheapest
Supplier's reliability	Maximum

3.2.2 Simple Edu Pack modelling

The second material investigation on composites was done in Edu Pack, Level 3 version 18, 1, 1, 0. To obtain an elastomeric pad, polymer matrix was chosen because they are light weight and flexible. Filler choice was based on superior thermal conductivity and electrical insulation. Hexagonal boron nitride (h-BN) and alumina (Al_2O_3(85)) were chosen; firstly; because they are increasingly being used in the electronic industry for heat dissipation and secondly, because they exhibit desirable qualities as shown in Figure 8 [12] [20]. From Figure 8, diamond seems the best filler choice but due to it being an expensive material, it was rejected. The notion for this material exploration was to obtain material-results that are as realistic as possible with an idea of using them in the production line of the PV/T systems.

Short fibres of h-BN and Al_2O_3(85) were used as the filler materials in an unfilled polyimide (PI) matrix. The "Synthesizer" tool in Eco Design (Level 3) was used to simulate these two composites. 9 different values were simulated between 0 - 100% filler volume fraction. Fibre aspect ratio was held constant at 30 for both reinforcements. This simplistic composite modelling in Edu Pack is based on the general rule of mixtures where a weighted mean is used to predict properties of a composite at 25℃. The composite is made of continuous and unidirectional fibres. The model assumes properties for the composite when the filler is in parallel orientation. The composite is assumed to have a good fibre-matrix interfacial bonding and the orientation and distribution of the reinforcement is considered perfect. Price of the constituent materials without being processed are accounted when estimating the price of the finished composite [40].

4. Results

4.1 Heat flow experiment

Data was plotted on graphs as Temperature [℃] vs. Elapsed time [minutes]. Different temperature readings are distinguished on the basis of the thermocouples and are represented using different colours in the following figures; dark blue for the aluminium plate thermocouple, orange for the rear glass thermocouple and grey for the front glass thermocouple.

It took 40-60 minutes before the temperature reading became "stable". Stable readings are defined as temperature fluctuations between a mean temperature value. Mean temperature value is used to calculate heat flux between different layers. Therefore, new graphs were plotted which were moved 60 minutes to the right of the initial plots. Moreover, for the scenario where copper tape is used as TIM, longer experimental time did not affect the temperature measurements. Temperature fluctuated about the same mean temperature, accurate to $\pm$ 0.1 ℃, in the second hour as it did in any other hour. This is shown in Table 5 where average temperature for all thermocouples in scenario A was taken at three different time intervals. Moreover, as silicon wafer had the smallest surface area of all the sandwich layers in the specimen, it was used in heat flux calculations.

Table 5: Mean temperature of different thermocouples at different intervals for scenario A. Longer experimental time gives the same mean temperature values as the second hour of the experiment with an accuracy of $\pm$ 0.1 ℃.

Time interval [minutes]	**Front glass Mean Temperature [℃]**	**Rear glass Mean Temperature [℃]**	**Aluminium plate Mean Temperature [℃]**
60 - 120	9.6	9.2	7.6
480 - 540	9.6	9.3	7.7
840 - 900	9.6	9.2	7.6

4.1.1 Reference Experiment

This experiment lasted 2 hours. Figure 40 shows the raw experimental results. Figure 41 shows the mean temperature values for the different thermocouples in the second hour of the experiment, i.e. after stable readings were obtained.

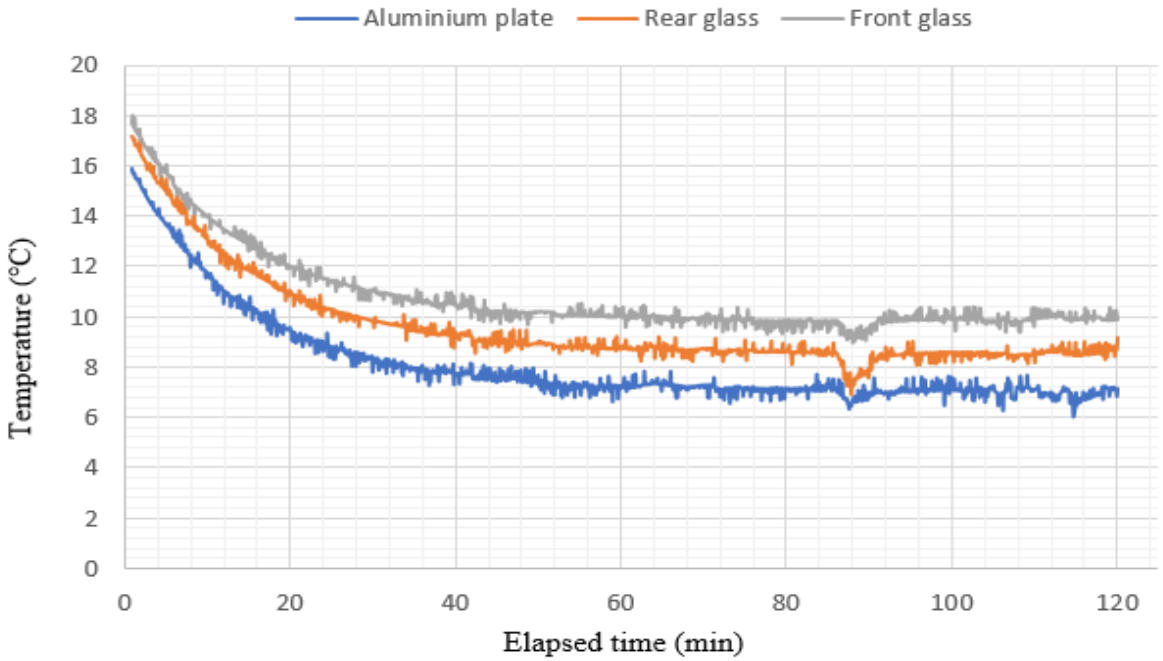

Figure 40: Plot of raw experimental data of the reference experiment. Temperature readings of the different thermocouples are represented with different colours.

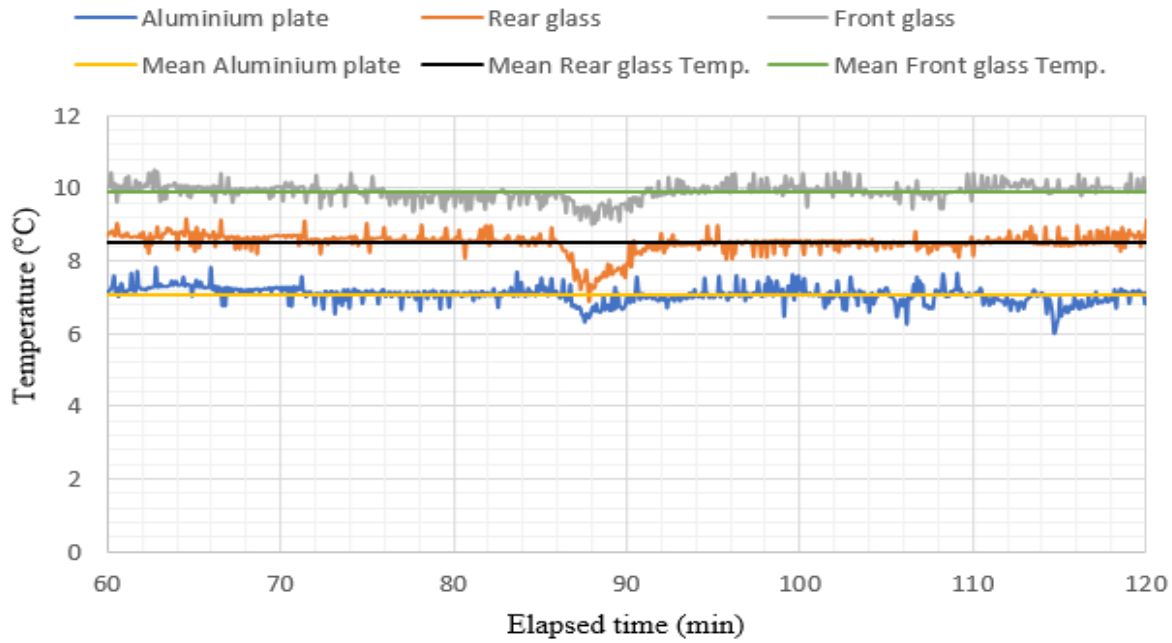

Figure 41: Mean temperature readings of the different thermocouples. Horizontal lines are drawn for each thermocouple, about which, the temperature of the thermocouple fluctuated. Yellow line is sketched for the aluminium plate, black line and green line for the rear glass and front glass temperatures, respectively.

Heat flow apparatus' monitors gave temperature and heat flow values at point 1 and point 5, attachment 5 in appendix. Table 6 shows temperature values obtained from the apparatus' monitors and the mean temperature values obtained from the thermocouples.

Table 6: Temperature values obtained from the apparatus' monitors and the mean temperature of different thermocouples.

Point	**Description**	**Temperature [℃]**
1	Hot plate	15.7
2	Front glass	9.9
3	Rear glass	8.5
4	Aluminium plate	7.1
5	Cold plate	3.6

Using Equation 5, area and the thermal conductivity values presented in Table 3, and temperature values presented in Table 6, heat flux through different points in the reference experiment was calculated. This is presented in Table 7.

Table 7: Heat flux through different points in the reference experiment. Heat flux at points 1 and 5 was calculated by apparatus' monitors.

Point(s)	**Description**	**Heat flux [W/m^2]**
1	Hot plate	90.3
1-2	Between hot plate and front glass	44.5
2-3	Between front glass and rear glass	1717.3
3-4	Between rear glass and aluminium plate	10.7
5	Cold plate	90.2

Thermal energy dissipated from the PV module to the aluminium plate in the reference experiment is 10.7 W/m^2. Table 8 shows the temperature difference between the hot/cold plates, mean heat flux and R-value obtained from apparatus' monitors.

Table 8: Values obtained from the heat flow apparatus for reference experiment.

△ *T* hot plate and cold plate [℃]	**Mean heat flux [W/m^2]**	**R-value [m^{2}K/W]**
12.1	90.3	0.15

4.1.2 Scenario A

This experiment lasted 15 hours. Figure 42 shows the raw experimental results. Figure 43 shows the mean temperature values for the different thermocouples in the second hour of the experiment, i.e. after stable readings were obtained.

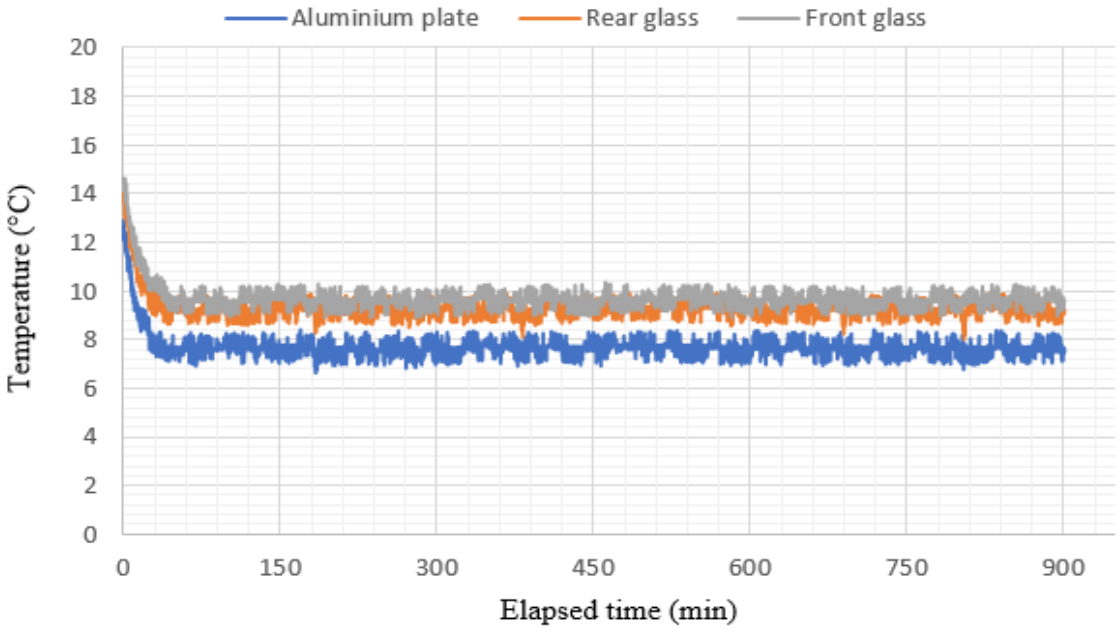

Figure 42: Plot of raw experimental data of scenario A. Temperature readings of the different thermocouples are represented with different colours.

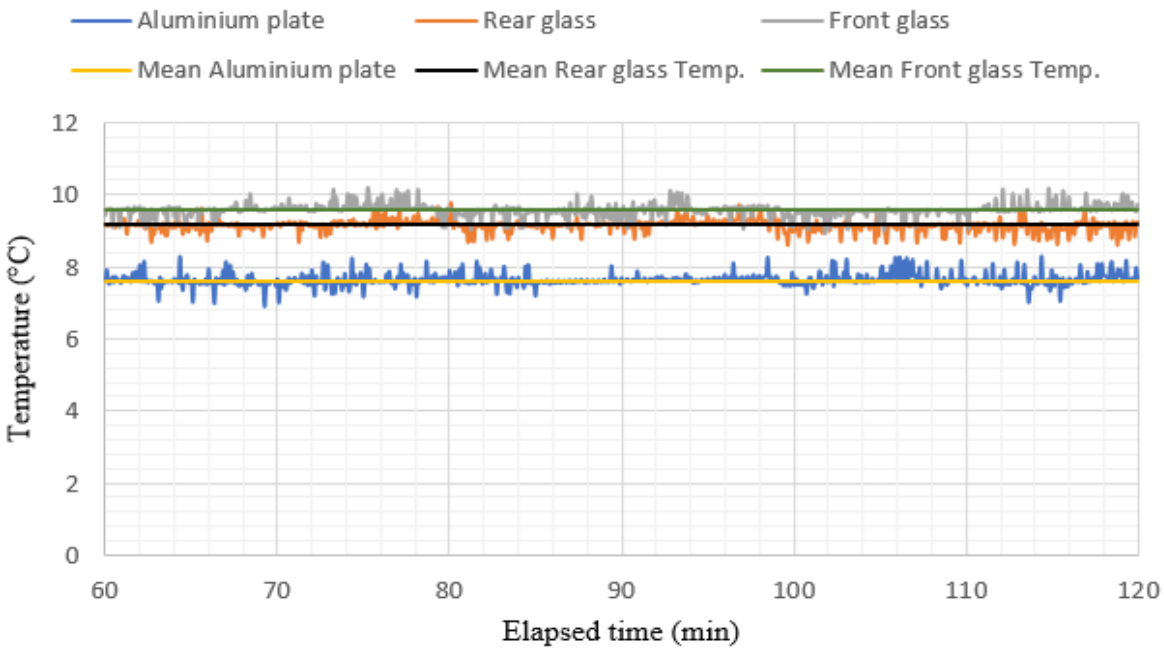

Figure 43: Mean temperature readings of the different thermocouples. Horizontal lines are drawn for each thermocouple, about which, the temperature of the thermocouple fluctuated. Yellow line is sketched for the aluminium plate, black line and green line for the rear glass and front glass temperatures, respectively.

Heat flow apparatus' monitors gave temperature and heat flow values at point 1 and point 5, attachment 5 in appendix. Table 9 shows temperature values obtained from the apparatus' monitors and the mean temperature values obtained from the thermocouples.

Table 9: Temperature values obtained from the apparatus' monitors and the mean temperature of different thermocouples in scenario A.

Point	**Description**	**Temperature [℃]**
1	Hot plate	15.5
2	Front glass	9.6
3	Rear glass	9.2
4	Aluminium plate	7.6
5	Cold plate	4.0

Using Equation 5, area and the thermal conductivity values presented in Table 3, and temperature values presented in Table 9, heat flux through different points in the experiment for scenario A was calculated. Heat flux between points 3-4 was calculated using Equations 10 and 11. This is presented in Table 10.

Table 10: Heat flux through different points in the experiment for scenario B. Heat flux at points 1 and 5 was calculated by apparatus' monitors.

Point(s)	**Description**	**Heat flux [W/m^2]**
1	Hot plate	97.0
1-2	Between hot plate and front glass	45.2
2-3	Between front glass and rear glass	490.7
3-4	Between rear glass and aluminium plate	12.3
5	Cold plate	96.7

Thermal energy dissipated from the PV module to the aluminium plate in scenario A is 12.3 W/m^2. Table 11 shows the temperature difference between the hot/cold plates, mean heat flux and R-value obtained from apparatus' monitors.

Table 11: Values obtained from the heat flow apparatus for experiment on scenario A.

$\triangle T$ hot plate and cold plate [℃]	**Mean heat flux [W/m^2]**	**R-value [m^{2}K/W]**
11.5	96.9	0.14

4.1.3 Scenario B

This experiment lasted 2 hours. Figure 44 shows the raw experimental results. Figure 45 shows the mean temperature values for the different thermocouples in the second hour of the experiment, i.e. after stable readings were obtained.

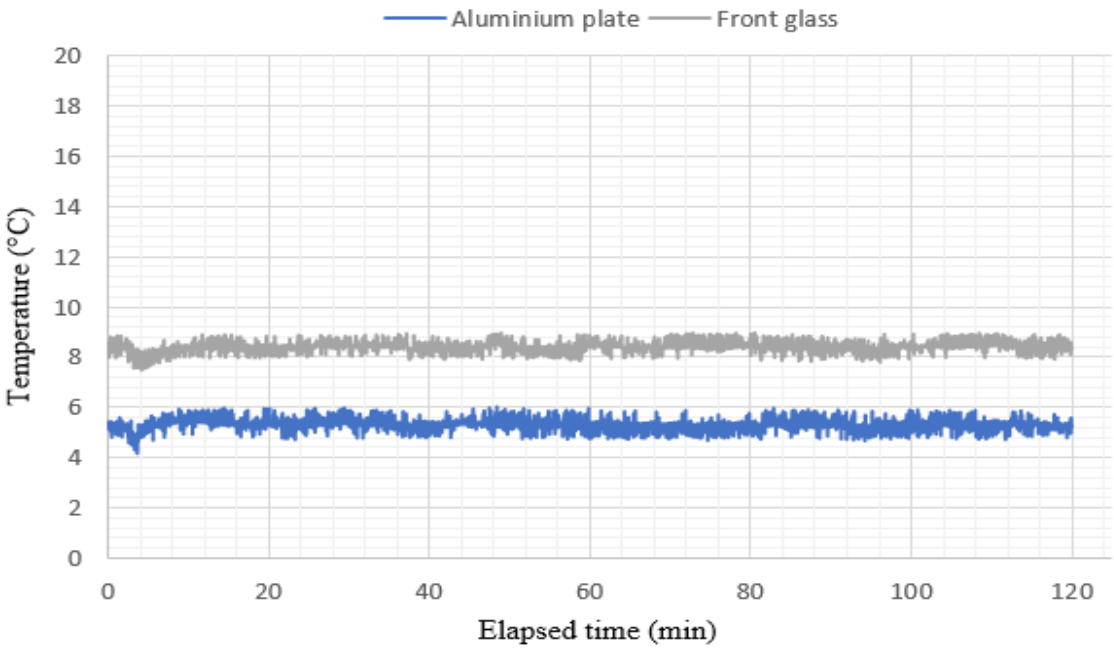

Figure 44: Plot of raw experimental data of scenario B. Temperature readings of the different thermocouples are represented with different colours.

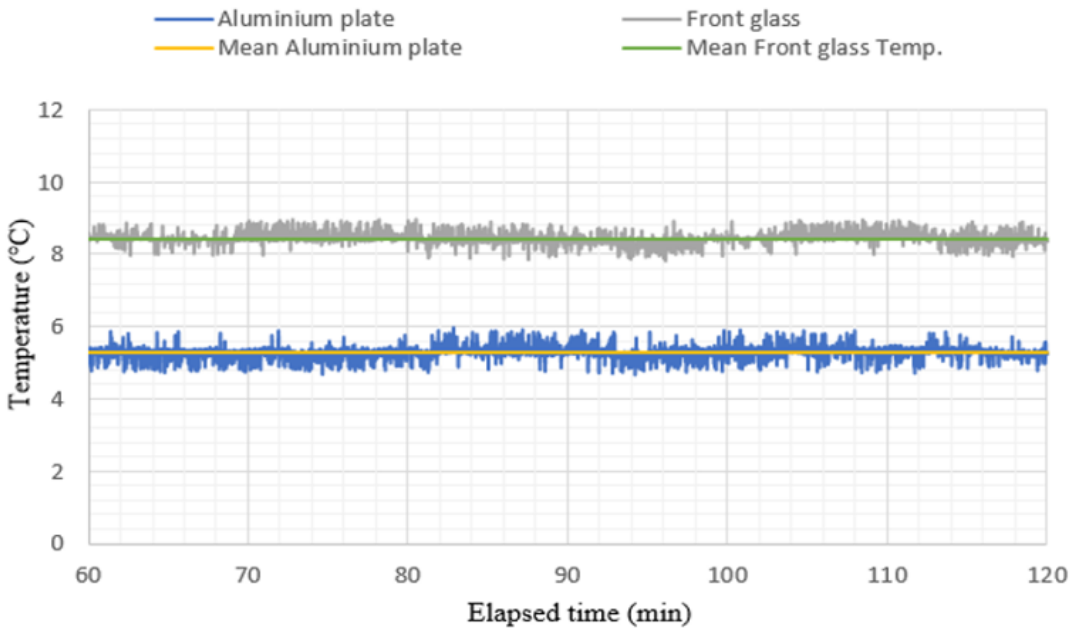

Figure 45: Mean temperature readings of the different thermocouples. Horizontal lines are drawn for each thermocouple, about which, the temperature of the thermocouple fluctuated. Yellow line is sketched for the aluminium plate temperature and green line for the front glass temperature.

Heat flow apparatus' monitors gave temperature and heat flow values at point 1 and point 4, attachment 5 in appendix. Table 12 shows temperature values obtained from the apparatus' monitors and the mean temperature values obtained from the thermocouples.

Table 12: Temperature values obtained from the apparatus' monitors and the mean temperature of different thermocouples in scenario B.

Point	**Description**	**Temperature [℃]**
1	Hot plate	17.8
2	Front glass	8.4
3	Aluminium plate	5.3
4	Cold plate	2.4

Using Equation 5, area and the thermal conductivity values presented in Table3, and temperature values presented in Table 12, heat flux through different points in the experiment for scenario B was calculated. Heat flux between points 2-4 was calculated using Equations 10 and 11. This is presented in Table 13.

Table 13: Heat flux through different points in the experiment for scenario B. Heat flux at points 1 and 5 was calculated by apparatus' monitors.

Point(s)	**Description**	**Heat flux [W/m^2]**
1	Hot plate	65.8
1-2	Between hot plate and front glass	72.1
2-3	Between front glass and aluminium plate	14.1
4	Cold plate	65.9

Thermal energy dissipated from the PV module to the aluminum plate in scenario A is 14.1 W/m^2. Table 14 shows the temperature difference between the hot/cold plates, mean heat flux and R-value obtained from apparatus' monitors.

Table 14: Values obtained from the heat flow apparatus for experiment on scenario A.

$\triangle T$ hot plate and cold plate [℃]	**Mean heat flux [W/m^2]**	**R-value [m^{2}K/W]**
15.4	65.9	0.24

4.1.4 Summary of results from Apparatus' monitors

Table 15 shows the temperature difference between the hot/cold plates, mean heat flux and R-value obtained from apparatus' monitors for all experiments

Table 15: Values obtained from the heat flow apparatus for all experiments.

Experiment	△ *T* between hot/cold plates [°C]	Mean heat flux [W/m²]	R-value [m²K/W]
Reference	12.1	90.3	0.15
Scenario A	11.5	96.9	0.14
Scenario B	15.4	65.9	0.24

Figure 46 is a graphic illustration in the form of a bar chart on the values from Table 15.

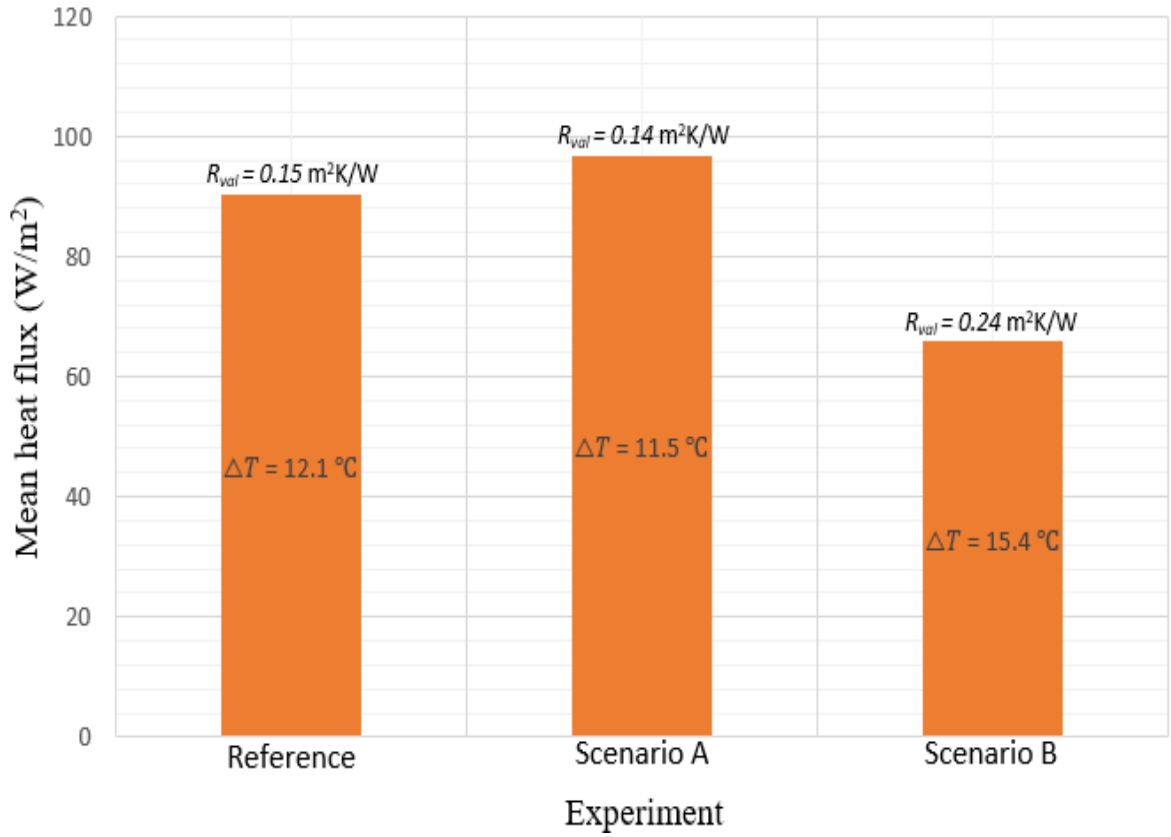

Figure 46: Summary of the results obtained from the heat flow apparatus. These results are classified based on individual experiments. The chart shows the heat flux, thermal insulance and △T hot/cold plates for different experiments.

4.2 Desk study on Scenario B

4.2.1 Materials in the market

After a comprehensive research on the internet and after contacting several renowned companies, a list of thermal pads was made. This list is presented in Table 16 showing key attributes of the pads. The table also shows the price per kilogram for the pads in Norwegian kroner.

Table 16: Thermal pads available in the market. All these pads are patented and are available for commercial usage.

Product Name	**Filler/Matrix**	**Thermal Conductivity [W/mK]**	**Electrical Resistance [10^{13} Ω m]**	**Price [NOK/kg]**
3M 5595	Silicone/polyethylene	1.6	500	1142
3M 5578H	Firm arcylic/Soft arcylic	3.5	0.0017	781
Sil-Pad A1500	Silicone/Fibreglass	2.0	0.01	3900
Sil-Pad 400	Silicone rubber/Fibreglass	0.9	0.01	1460
HF300P	Hi-Flow/Polyimide	1.6	0.1	1510
SSP-1850C	Silicone/Polyester	1.5	2800	-

Filler volume fraction for these pads was not provided in the data sheet. Test methods for thermal conductivity and electrical resistance for these pads are as follows:

Thermal conductivity- ASTM D5470

Electrical resistance- ASTM D257

Appendix attachment 6 gives more details on these products.

4.2.2 Simple Edu Pack modelling

Hexagonal boron nitride (h-BN) fillers in a polyimide (PI) matrix offer a greater thermal conductivity than the Al_2O_3(85) fillers in the polyimide matrix at 25℃. At a low filler volume fraction, thermal conductivity of both composites is similar. The thermal conductivity of the composite increases with an increased filler volume fraction; greater increase for h-BN composite than the Al_2O_3 composite. Figure 47 shows the results on thermal conductivity obtained from the simple modelling in Edu Pack. It also shows thermal conductivity results for 0% filler volume fraction i.e. pure PI matrix, and 100% filler volume fraction i.e. pure fillers.

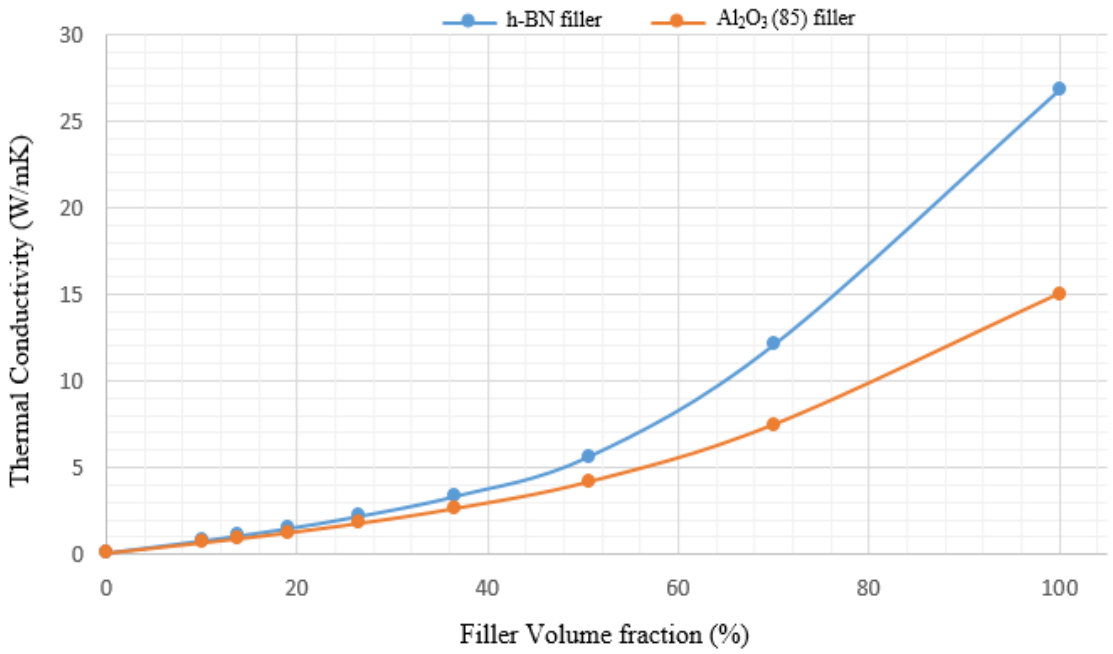

Figure 47: Increase in thermal conductivity of the composites with an increase in filler volume fraction. h-BN thermal pads exhibit a greater increase in thermal conductivity than the Al_2O_3(85) thermal pads.

h-BN thermal pads offer greater electrical insulation than the Al_2O_3(85) pads at 25℃. The electrical resistance decreases for both pads with an increase in filler volume fraction. This decrease in resistance is similar in both composites. Figure 48 shows the results obtained on electrical resistance from the simple modelling in Edu Pack for 0%-100% filler volume fraction.

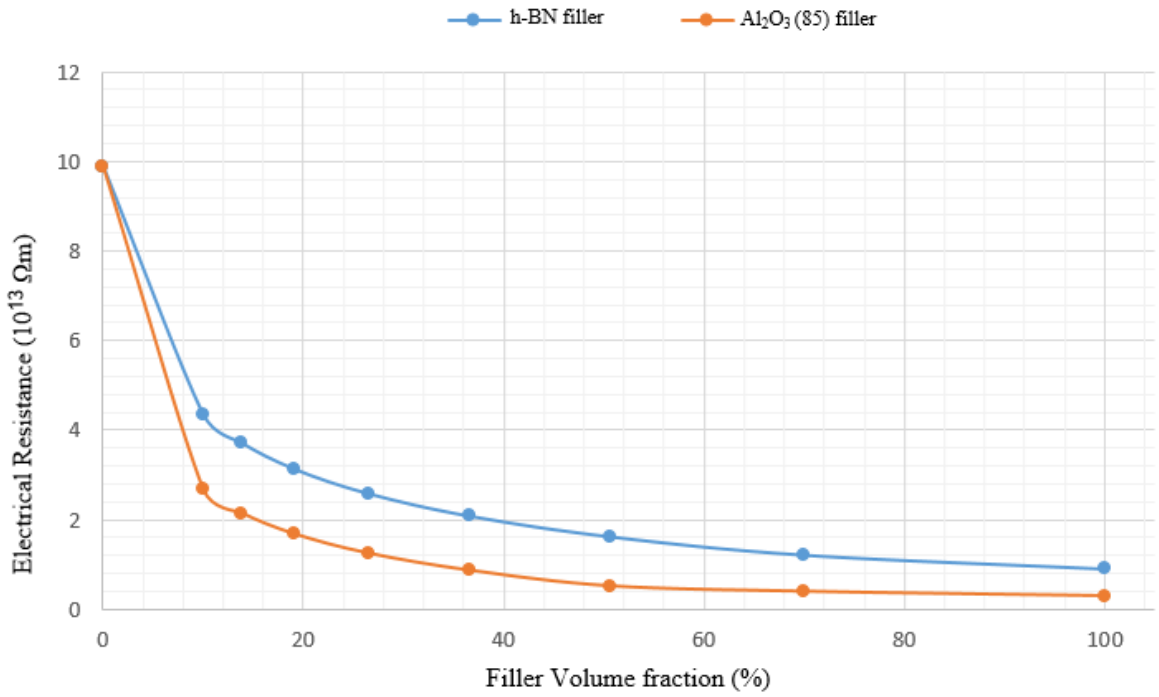

Figure 48: Decrease in electrical resistance with an increase in filler volume fraction. Al_2O_3(85) thermal pads exhibit a greater decrease than the h-BN pads.

h-BN and Al_2O_3(85) fillers in a PI matrix have distinct properties depending on the filler volume fraction. These properties are presented in Table 17 and Table 18. Table 19 shows density and price of individual fillers and the matrix.

Table 17: Properties of h-BN thermal pad with varied filler volume fraction. These values were obtained after simulation in Edu Pack [12].

h-BN Filler volume fraction [%]	**Thermal conductivity [W/mK]**	**Electrical resistance [10^{13} Ω m]**	**Density [10^3 kg/m^3]**	**Price [NOK/kg]**
0	0.13	9.9	1.38	482
10	0.8	4.35	1.47	461
13.8	1.09	3.72	1.5	453
19.1	1.52	3.13	1.55	443
26.5	2.22	2.58	1.61	430
36.6	3.38	2.08	1.71	414
50.6	5.66	1.62	1.82	394
70	12.1	1.21	1.99	370
100	26.8	0.99	2.25	340

Table 18: Properties of Al_2O_3 thermal pad with varied filler volume fraction. These values were obtained after simulation in Edu Pack [12].

Al_2O_3(85) Filler volume fraction [%]	**Thermal conductivity [W/mK]**	**Electrical resistance [10^{13} Ω m]**	**Density [10^3 kg/m^3]**	**Price [NOK/kg]**
0	0.13	9.9	1.38	482
10	0.69	2.67	1.59	379
13.8	0.92	2.15	1.67	347
19.1	1.27	1.68	1.79	307
26.5	1.81	1.25	1.94	259
36.6	2.67	0.87	2.16	205
50.6	4.2	0.52	2.45	146
70	7.48	0.04	2.87	84
100	15.0	0.03	3.5	16.2

Table 19: Price per kilogram of individual materials which were used to make the composites [12].

Material	**Density [10^3 kg/m^3]**	**Price [NOK/kg]**
Hexagonal boron nitride (h-BN)	2.25	340
Alumina (Al_2O_3(85))	3.5	16.2
Polyimide (PI)	1.38	482

5. Discussion

5.1 Heat flow experiment

Calculated heat flux, $\dot{Q}$ [J], results from the heat flow experiments do not agree with the stationary heat flow principle. This can be seen from the heat flux values shown in tables 7, 10 and 13 in results. For a stationary heat flow situation in a sandwich structure, $\dot{Q}_{in} = \dot{Q}_{out}$. Therefore, heat flux must be constant through the different layers of the sandwich-specimen. As the calculated values of heat flux within the different layers of the specimen did not match the $\dot{Q}_{in}$ and $\dot{Q}_{out}$ obtained from the apparatus' monitors, they were discarded and not interpreted as successful results. Thus, it is impossible to answer the topic question regarding the best thermal interface material which allows for the maximum heat transfer in a PV/T system.

However, the heat flux values recorded by the apparatus' monitors were approximately constant for each experiment. These values are interpreted as $\dot{Q}_{in}$ from top of the specimen and $\dot{Q}_{out}$ from the bottom of the specimen, and are accurate to ± 0.1 W/m^2 for the reference experiment and scenario B. For scenario A, this value is accurate to ± 0.3 W/m^2. These values, along with other important measurements from the heat flow apparatus are shown in Table 15. It can be seen from the table that heat flux and thermal insulance results obtained from the reference experiment lie in between the results of scenario A and scenario B. This indicates that the thermal properties recorded by the apparatus are fairly reliable, appendix attachment 5. These results are used to make a comparison between the two scenarios, scenario A and scenario B.

As observed from this Table 15, maximum heat flux was obtained from the experiment on scenario A, i.e. 96.9 W/m^2. Moreover, copper tape as TIM for scenario A also contributed to the least thermal insulance from the sandwich specimen, i.e. 0.14 m^{2}K/W. This could be because this TIM had the smallest thickness of all TIMs used for experimentation but is mainly due to copper being a metal. As a metal, it conducts heat due to the vibrations of atoms and the availability of free electrons. Copper tape comprised of 99.4 wt% copper and 0.6wt% of various alloying metals, appendix attachment 3. The low alloying content and the similar atomic size of the alloying elements to copper, like iron and zinc, meant that the tape

was able to retain its copper-like properties i.e. good thermal conduction. High copper content enhanced the thermal flux from the specimen. Greater thermal conductivity of copper meant lower thermal resistance which resulted in lower R-value. Therefore, the experimental results from this experiment conform to the theory.

TIM for scenario A, copper tape, had a thickness of 0.02 mm. This thickness resulted in a decrease in thermal insulance by 0.1 m^2K/W, when compared to the reference experiment, Table 15. Therefore, it can be deduced that a greater thickness of the copper tape could have provided a greater insulation. Subsequently, a greater thermal flux than 96.9 W/m^2 could also have been obtained from the specimen. This makes copper tape a good choice as TIM for scenario A. However, copper would have been a poor choice of TIM for scenario B where electrical insulation is desired. Copper is a metal and according to the Wiedemann–Franz law, Equation 3, electrical conductivity and thermal conductivity are proportional to the temperature of a metal. Higher thermal conductivity would also have resulted in higher electrical conductivity (low electrical resistance), as seen from Figure 8. Hence, this would have adversely affected the PV/T system in scenario B and would have led to its ultimate degradation.

The lowest heat flux and consequently the greatest thermal insulance was obtained from scenario B. PVC pad was chosen as TIM which resulted in mean heat flux of 65.9 W/m^2 and a total thermal insulance of 0.24 m^2K/W. Despite having the greatest $\triangle T$ between hot/cold plates of the heat flow apparatus, it resulted in the lowest heat flux. This defies the Fourier's law, Equation 5, which states that the thermal conduction is proportional to the magnitude of the temperature gradient; thus, increased temperature difference should result in a greater heat flux. However, PVC pad's superior insulating properties compensated for this. Thus, a conclusion that can be drawn from this experiment is that thermal conductivity of a material is, in fact, the most dominant force in calculating heat fluxes at lower temperature variations. PVC is a polymer and the polymer material group, along with the natural materials, have the lowest thermal conductivity. This is also evident from Figure 12 and the low thermal conductivity value of PVC seen in Table 1. These materials only conduct heat based on the vibration of their atoms and are mostly amorphous in nature. Therefore, PVC is mainly used as an insulating material in building, electronic and other sectors.

Some improvements for this scenario may include using a more crystallized PVC pad. The degree of crystallinity of the PVC pad used for experimentation was unknown; but, according to the theory, increase in crystallinity would have improved the thermal transfer. This is due to increased aligned molecular chains in the material's microstructure.

5.1.1 Errors in the experiment

It is evident from the experimental results that there were errors in the experimental setup. Initially, temperature inside the heat flow apparatus could not be kept constant due to the limited time for experimentation. The circulating liquid inside the hot plate and the cold plate of the chamber had to be adjusted after the completion of each experiment. Due to scarce time, these adjustments were not made. Thus, different temperature values for the upper plate and the lower plates were obtained during different experiments. These are documented in appendix attachment 5. Therefore, during heat flux calculations, a slightly different $\triangle T$ was obtained for each experiment, shown in Table 15. This resulted in varied heat fluxes through the specimen which are not consistent with the principle of stationary heat flow. Therefore, these results were discarded and only the results from the heat flow apparatus are analysed.

However, varying $\triangle T$ was not the only error in the experiment. The incorrect usage of the heat flow apparatus and the inconsistency in the experimental specimen were the major flaws. The heat flow measuring area inside the heat flow apparatus was not fully covered by the specimen. The total heat flow measuring area was 300 mm x 300 mm whereas the specimen was 180 mm x 250 mm. The remaining measuring area was not fully enclosed by the mineral wool either. This allowed the heat to flow directly from the hot plate to the cold plate with air as the only medium. Moreover, as 3 mm gap was left between the hot plate and the front glass during experimentation, it is possible that convective thermal resistance influenced the results. Earlier, convective resistance was considered negligible in this unidirectional, stationary heat flow investigation. The poor contact between the hot plate and the front glass and due to the heat flow measuring area not being fully covered by the specimen/insulation allowed for the convective resistance which affected the results.

Moreover, silicon sample area was smaller than the corresponding layers in the sandwich structure. Although, it was accounted for during the heat flux calculations; yet, incorrect results were obtained. In a sandwich structure, area of layers must be constant. The gap left by the silicon wafer allowed for the lateral heat to pass through air, another source of convective thermal resistance. Silicon wafer was also doped with boron of unknown concentration. Literature value of thermal conductivity of pure silicon was used during heat flux calculations. This also resulted in an incorrect heat flux through the specimen as alloyed

materials have different properties than the pure materials. Also, the usage of glue to fasten the thermocouples onto the different layers in the experimental specimen could have affected the heat transport. The quantity of the glue used and its thermal properties were unknown and were not accounted during calculations. Thus, incorrect heat flux values were obtained.

Another reason for error in the obtained results could be the imperfect contact between the surfaces in the specimen. These surfaces were only cleaned using rectified spirit and no special surface treatment was done before their usage. It is likely that due to surface irregularities, there were gaps in the adjoining components which increased the thermal resistance; thus, affecting the results.

5.1.2 Improvements in the experiment

It can be expected that an improvement in the experimental setup can give better results. These improvements include keeping a constant temperature difference over the specimen for all experiments. This could be achieved by monitoring the temperature of the hot plate and the cold plate of the apparatus regularly and adjusting the circulating fluid accordingly. Also, by incorporating the entire heat flow measuring area for thermal calculations inside the heat flow apparatus. This includes using a bigger experimental specimen, i.e. 300 mm x 300 mm, which covers the entire apparatus' measuring area; also, use more insulating material to fill up the voids. Moreover, there must be a direct contact between the specimen and the hot/cold plates of the chamber to avoid convective resistances. For this, no gaps should be left between the specimen and the apparatus' plates. These are, in fact, the standard operating principles of SINTEF's heat flow chamber as shown in Figure 15. Furthermore, the sandwich specimen should have equal surface area for all layers. For this, bigger silicon wafer of dimension 180 mm x 250 mm x 3 mm should be used. This would avoid air being trapped inside the sandwich structure and would give improved results.

In addition, the usage of thermocouples over-complicated the experiment. Instead, TIMs could have been experimented individually inside the heat flow apparatus and their thermal conductivity and insulance values recorded using the apparatus' monitors. This would save the equipment costs in buying thermocouples and utilizing the data logger and the computer. This would also have reduced the thermal noises obtained from the stacked sandwich specimen. The fluctuations in temperature from the temperature vs. time graphs of all experiments, especially the reference experiment, shows the thermal noises obtained because of many layers (resistors) in the sandwich specimen.

In order to reduce the surface irregularities, surface treatment prior to the experimentation could be done. This may include surface polishing or grinding of the glass, silicon and the aluminium plate. Moreover, using TIMs like glues/adhesives can also solve the microscopic surface defects. Such materials fill surface gaps by providing thin bond line after curing. This would have reduced thermal contact resistance between surfaces and would have improved the experimental results.

5.2 Desk study on scenario B

5.2.1 Materials in the market

Table 16 shows a list of patented thermal pads available in the market. From the table, 3M 5578H acrylic interface pad has the highest thermal conductivity value of 3.5 W/mK and is also the cheapest thermal pad 781 NOK/kg. This pad will offer the greatest thermal dissipation between the PV system and the thermal collector when used in a PV/T system. However, it offers the least electrical resistance, 0.0017 x 10^{13} Ω m (1.7 x 10^{10} Ω m), of all TIMs presented in Table 16. Thus, this pad is not the best choice as TIM for scenario B. This is due to electrical insulation being the main requirement upon the removal of the rear glass of the PV module. In order to limit the risks of premature degradation of the PV/T system, a TIM with higher electrical insulation would be a better choice. In contrast, SSP-1850C (silicone/polyester) pad offers relatively good thermal conductivity 1.5 W/mK and the greatest electrical resistance 2800 x 10^{13} Ω m. However, as data regarding its price was not available, it is difficult to conclude if this pad is worth buying and experimenting.

Therefore, it seems that a compromise, either regarding the price or thermal conductivity, would have to be made to obtain a good TIM from the market. From Table 16, 3M 5595, Silicone/polyethylene pad appears to be a good choice. It consists of a thermally stable silicone elastomer which is soft and offers good tack. This interface pad with polyethylene naphthalate film has good processability, offers good thermal conductivity and good dielectric strength. It is provided by 3M™, a multinational corporation which aims at providing innovative solutions for thermal dissipation. This 3M™ pad offers good thermal conductivity, 1.6 W/mK; second best electrical insulation from Table 16, i.e. 500 x 10^{13} Ω m and is relatively economical 1142 NOK/kg. This makes it the most promising candidate in the market. As it is an elastomeric pad, its tacky nature will make it perform well under clamping pressure which suits the PV/T experimentation as it has a sandwich structure.

5.2.2 Simple Edu Pack modelling

Figure 47 shows that an increase in filler volume fraction increases the thermal conductivity of both composites. Thermal conductivity of both composites is low at low filler content. This is the result of the poorly-conductive PI matrix which heavily surrounds the filler particles. As the fillers have a lower volume, they are unable to maintain a good contact in the composite's microstructure to conduct heat. Thus, greater thermal resistance is obtained. When the filler content increases beyond 40%, a rapid increase in thermal conductivity is seen. This is due to particles forming a network in the composites microstructure where they are able to conduct heat in a more continuous and a compact manner. This is also due to the loss of the PI matrix material which results in a decrease in contact heat resistance.

Moreover, it can be seen from Figure 47 that h-BN composite offered greater thermal conductivity than Al_2O_3(85) composite at high filler loading. Based on an arbitrary filler volume fraction of 50.6%, h-BN composite offers 34% greater thermal conductivity than Al_2O_3(85) composite. At 70% filler content, thermal conductivity of the h-BN composite is 12.10 W/mK, whereas, it is 7.48 W/mK for the Al_2O_3(85) composite. Greater thermal conductivity of the TIM would lead to a greater heat dissipation from the PV module to the heat mat in a PV/T system. Thus, h-BN filler is more suitable as a filler than Al_2O_3(85) in a PI matrix. At 100% filler volume fraction, thermal conductivity of the individual fillers accounts for the thermal conductivity of the composite. In fact, at 100% filler loading, the PI matrix disappears and the only material left in the composite is the filler material. Therefore, it can be said that the thermal conductivity of the filler has a great influence on the thermal conductivity of the composite at high filler loading. It can also be deduced from Figure 47 that the higher the thermal conductivity of the filler, the swifter increase in the thermal conductivity of the composite with increasing filler concentration. This conforms to the geometric mean model, Equation 13. The model suggests that the thermal conductivity of the filler has a greater influence on the thermal conductivity of the composite than the thermal conductivity of the composite's matrix. The h-BN filler has a greater thermal conductivity than the Al_2O_3(85) filler; hence, the more rapid rise in h-BN composite's thermal conductivity upon increasing filler volume fraction.

Figure 48 shows that an increase in filler volume fraction decreases the electrical resistance of both composites. At low filler loading, the PI matrix has the greatest influence on the composite's properties. As PI is a superior electrical insulator, greatest insulation in the composite is obtained with the highest PI content. Stronger PI interface interaction at low filler volume results in a high electrical resistance. However, as the filler volume increases, conductive masses of filler particles form inside the composite. Although, h-BN and Al_2O_3(85) fillers are good electrical insulators, they are relatively conductive compared to the PI matrix. Increase in filler volume fraction results in the loss of matrix-material and a gradual decrease in the electrical resistance because of weaker filler/matrix interface. From Figure 48, h-BN composite exhibits a lower decrease in electrical resistance than the Al_2O_3(85) composite. Based on an arbitrary filler volume fraction of 50.6%, h-BN composite offers 3 folds electrical resistance when compared with Al_2O_3(85) composite. This is primarily because the h-BN filler has superior electrical insulation than the Al_2O_3(85) filler.

Table 17 and Table 18 show different properties of the h-BN and Al_2O_3(85) composites. 0% and 100% filler volume content means pure matrix and pure filler in the composite, respectively. These tables show that an increase in filler volume fraction increases the density of the composite while becoming more economical. This is because with an increase in filler volume fraction, the composite involves increased filler material with the loss of the matrix material. Individually, h-BN and Al_2O_3(85) fillers are denser but cheaper than PI as seen from Table 19. Thus, increasing filler volume fraction in the PI matrix makes a denser but a cheaper composite in regards to the material cost.

Furthermore, the tables show that Al_2O_3(85) composites are cheaper but denser than the h-BN composites. For filler volume fraction of 50.6%, Al_2O_3(85) composites are half the price of h-BN composites but they are 34% denser than the h-BN composites, too. Taking these properties into consideration, h-BN composites are a better choice. This is due to h-BN filler being a technical ceramic in a crystalline form with a higher thermal conductivity and electrical resistance than Al_2O_3(85). h-BN has a layered structure and is anisotropic in nature. Thus, the parallel filler alignment in the PI matrix during modelling exhibited best possible properties for the h-BN filler. Although, it is double the price of the Al_2O_3(85) composite for 50.6% filler volume fraction, the superior electrical insulation is more important during the operation of scenario B, as a PV/T system. This insulation would avoid the degradation and the maintenance costs of the PV module without the rear glass. Better material choices during

the fabrication of systems are always preferred over the maintenance and repair which could be more costly and even impossible in some situations.

Moreover, as spherical Al_2O_3(85) fillers perform better than the short fibre fillers, Al_2O_3(85) fibre fillers in a PI matrix exhibited lower thermal conductivity and electrical insulation. This is in accordance with Hasselman-Johnson model which suggests that different fillers perform differently according to their filler orientation and individual properties. Had spherical Al_2O_3(85) fillers been used in a PI matrix, the resulting properties would have been better than the ones obtained from short fibre Al_2O_3(85) fillers. Furthermore, a highly pure alumina filler with greater Al_2O_3 content than 85% might have resulted in a noteworthy improvement in the composite's properties.

5.3 Future work

Future work should primarily focus on improving the experimental setup and obtaining rational results based on stationary heat flow principles. Only after achieving that, the research should be continued. To further this research, effect of TIM's electrical conductivity in scenario A could be investigated. Then a conclusion could be made whether metals are a good choice of TIM for this type of PV/T system. Thermal pads available in the market should be examined. Their filler volume fraction should be investigated after contacting the suppliers. Considering their high price, further research should focus on whether they are worth their qualities. Moreover, h-BN composites could be experimented to determine how they influence the thermal transfer and electrical insulation of the system in scenario B. If h-BN fillers show promising results, the next step should be a detailed study on the best volume fraction of fillers in the matrix. As seen from Figure 48, the increased filler content reduces the electrical insulation and it may also affect the mechanical properties of the composite. With the loss of the matrix material, the composite becomes brittle and its processability and handling becomes difficult. The short simulation in Edu Pack allowed 0% - 100% filler volume fraction to be simulated. In reality, there is a theoretical limit to the filler volume fraction. This limit allows for the best possible results to be obtained from the composite without losing its strength and other important properties. In addition, investigation and experimentation on thermal glues/adhesives might also give some interesting results. If the experimental equipment permits, other types of TIMs should also be investigated.

Research on the CO_2 footprint and life-cycle assessment should be the ultimate investigation. The primary goal for European project, PVadapt is to offer sustainable and clean energy BIPV-T systems with reduced running costs. For this reason, a thorough investigation on the environmental impacts during the different stages of the system's life should be done. Individual materials including TIMs in the PV/T system should be assessed in detail from start to their end. This may include every step of material's life until it is disposed. Such processes include analysing the material's CO_2 footprint from raw material extraction through its fabrication, distribution, use, repair and ultimate disposal or recycling.

6. Conclusion

It can be concluded that thorough knowledge of the experimental equipment is vital in obtaining rational results. SINTEF's heat flow apparatus measures heat flux [J] at stationary conditions. This means that $\dot{Q}_{in} = \dot{Q}_{out}$ must be approximately equal through the sandwich specimen; thus, additional thermocouples to determine heat flux through each sandwich-layer is unnecessary. When investigating a sandwich specimen, it is vital that all layers have the same surface area and are void of any surface irregularities to avoid thermal resistance. Moreover, it is easier to investigate TIMs for a PV/T system individually in the apparatus than in a sandwich structure. Also, the entire apparatus' measuring area must be utilized when conducting heat flow experiments. Further work should focus on improving the experimental setup in order to obtain adequate experimental results. Only after accomplishing that, the best thermal interface between the PV module and the heat mat for a PV/T system can be determined.

Based on in-built apparatus' monitors, copper tape as TIM provides the greatest heat flux 96.9 W/m^2 and the lowest R-value 0.14 m^2K/W. This is mainly due to copper being a metal and having superior heat transferring ability. PVC pad offers the lowest heat flux through its sandwich structure. Consequently, it offers the greatest insulation of all experimental specimens according to its R-value 0.24 m^2K/W. This is a good indication to why PVC is mainly used as an insulating material in building, electronic and other sectors. Additionally, composite materials are a better choice as TIM for scenario B than metals, even though copper tape exhibited the greatest heat flux during experimentation. Composites are able to provide unique properties like thermal conductivity and electrical insulation which is necessary for TIM in this type of PV/T system.

5595 Silicone/polyethylene pad supplied by 3M^{TM} is the most promising candidate for experimentation based on its thermal conductivity, electrical insulation and price. However, all thermal pads available in the market should be examined further. Using technical ceramics like h-BN and Al_2O_3(85) in a PI matrix offers enhanced thermal conductivity and good electrical insulation. Thermal conductivity of the filler has a major impact on the thermal conductivity of the composite at high filler loading (greater than 40% volume fraction). Thus, the simple Edu Pack modelling conforms to the geometric mean model. Furthermore, increase

in filler loading decreases the electrical resistivity of the composite due to the loss of matrix material. Equal filler volume fractions of 50.6% offers 34% greater thermal conductivity in h-BN/PI composite compared to the Al_2O_3(85)/PI composite. The same volume fraction offers 3 folds electrical resistance in h-BN/PI composite compared to the Al_2O_3(85)/PI composite. h-BN composite exhibited superior qualities than the Al_2O_3(85) composite; thus, should be investigated further for experimentation.

7. Bibliography

[1] International Energy Agency (IEA). Global Energy & CO_2 Status Report (Internet). Paris: IEA; 10th January 2019 [Updated 10th January 2019; retrieval date 28th January 2019]. Available from: https://webstore.iea.org/global-energy-co2-status-report-2018

[2] Jouhara H, Milko J, Danielewicz J, Sayegh M.A, Szulgowska-Zgrzywa M, Ramos J.B and Lester S.P. The performance of a novel flat heat pipe based thermal and PV/T (photovoltaic and thermal systems) solar collector that can be used as an energy-active building envelope material. Energy. 2016;108(1):148-154.

[3] Callister W, Rethwisch D. Materials Science and Engineering. 9th Edition. Asia: John Wiley and Sons Pte Ltd; 2011.

[4] PVadapt. PROJECT, Vision and objectives (Internet). EU: PVadapt; 19th December 2018 [Updated 19th December 2018; retrieval date 6th February 2019]. Available from: http://www.pvadapt.com/vision-and-objectives/

[5] International Energy Agency. Energy Efficiency, Buildings: The global exchange for energy efficiency policies, data and analysis (Internet). Paris: IEA; 10th January 2019 [Updated 10th January 2019; retrieval date 2nd February 2019]. Available from: https://www.iea.org/topics/energyefficiency/buildings/

[6] BNP Paribas. What types of Energy-efficient buildings are there? (Internet). Paris: BNP Paribas; 14th March 2016 [Updated 14th March 2016; retrieval date 15th February 2019]. Available from: https://companies.bnpparibasfortis.be/en/article?n=what-types-of-energy-efficient-buildings-are-there-

[7] Passipedia. What is a Passive House? (Internet). Darmstadt: Passipedia; 21st February 2019 [Updated 21st February 2019; retrieval date 15th March 2019]. Available from: https://passipedia.org/basics/what_is_a_passive_house

[8] Davor H. Low energy, passive and zero-energy houses (Internet). UK: Our Energy; 11th October 2015 [Updated 11th October 2015; retrieval date 15th March 2019]. Available from: https://www.our-energy.com/low_energy_passive_and_zero_energy_houses.html

[9] alchemia-nova. European Projects, PVadapt (Internet). Vienna: PVadapt; 10th October 2018 [Updated 10th October 2018; retrieval date 15th March 2019]. Available from: https://www.alchemia-nova.net/projects/pvadapt/

[10] Atkins P, Paula J. Physical Chemistry- Thermodynamics, Structure, and Change. 10th Edition. Oxford: Oxford University Press; 2014.

[11] Geankoplis C. Transport Processes and Separation Process Principles. 4th Edition. Essex: Pearson Education Ltd; 2014.

[12] CES Edu Pack 2018 version: 18.1.1 Copyright Granta Design Limited, Built 18, 1, 1, 0 Level 3 Eco Design.

[13] Electronics notes. RF Thermal Noise: Johnson-Nyquist Noise (Internet). London: Electronics Notes; 1st June 2016 [Updated 1st June 2018; retrieval date 5th May 2019]. Available from: https://www.electronics-notes.com/articles/basic_concepts/electronic-rf-noise/thermal-johnson-nyquist-basics.php

[14] Young H, Freedman R. University Physics with Modern Physics. 14th Edition. Harlow: Pearson Education Ltd; 2015.

[15] Cheol-Woo K, Jae-Ik C, Se-Weon C, Young-Chan K. The effect of alloying elements on thermal conductivity of Aluminium alloys in high pressure die casting. Advanced Materials Research. 2013;813(1):175-178.

[16] Kroschwitz J, ed. Encyclopedia of Polymer Science and Technology. Third Edition. Hoboken: John Wiley & Sons Ltd; 2004.

[17] Pietrak K, Wisniewski T. A review of models for effective thermal conductivity of composite materials. Journal of Power Technologies. 2015;95(1):14-24.

[18] Naslain R. Ceramic Matrix Composites: Matrices and Processing. Encyclopaedia of Materials. 2001;2(1):1060-1066

[19] Xia Z, Curtin W. Tough-to-brittle transitions in ceramic-matrix composites with increasing interfacial shear stress. Division of Engineering. 2000;48(20):4879-4892.

[20] Fang L, Wu C, Qian R, Xie L, Yang K, Jian P. Nano–micro structure of functionalized boron nitride and aluminium oxide for epoxy composites with enhanced thermal conductivity and breakdown strength. RSC Adv. 2014;4(1):21010-21017

[21] Dawson D. M., Briggs A. Prediction of the thermal conductivity of insulation materials. Journal of Materials Science. 1981;16(1):3346–3356

[22] Morrell R. 4.01 Matrix Materials. Reference Module in Materials Science and Materials Engineering. 2000;4(1):1-24

[23] Thermtest Inc. HISTORY.2 – THE GUARDED HOT PLATE METHOD (Internet). New Brunswick: Thermtest Inc; 23rd June 2015 [Updated 23rd June 2015; retrieval date 5th April 2019]. Available from: https://thermtest.com/history-2-the-guarded-hot-plate-method

[24] Skogstad H, Bergheim E. Håndbok for varmelaboraotiret. 3.4 ed. Trondheim: SINTEF Byggforsk;2007.

[25] Sunram A, Velraj R. Thermal management of electronics: A review of literature. Thermal Science - THERM SCI. 2008;12(1):2-26

[26] Fesharaki V, Dehghani M, Fesharaki J. The Effect of Temperature on Photovoltaic Cell Efficiency. 2011;1(1):1-21

[27] Nemec P. Porous Structures in Heat Pipes. 2017; DOI: 10.5772/intechopen.71763.

[28] Parker Hannifin Corporation. Thermal Interface Materials for Electronics Cooling (Internet). Woburn: Parker Chomerics; 1st January 2018 [Updated 1st January 2018; retrieval date 31st March 2019]. Available from: https://www.parker.com/literature/Chomerics/Parker%20Chomerics%20Thermal%20Catalog.pdf

[29] Vincotech. THERMAL INTERFACE MATERIAL (Internet). Mississauga: Vincotech; 14th December 2014 [Updated 14th December 2014; retrieval date 31st March 2019]. Available from: https://www.vincotech.com/news/videos/thermal-interface-material-thermal-grease.html

[30] Blazej D, Thermal Interface Materials. (Internet) 2013;9(1) Available from: https://www.electronics-cooling.com/2003/11/thermal-interface-materials/

[31] Luque A, ed. Handbook of Photovoltaic Science and Engineering. Chichester: John Wiley & Sons Ltd; 2002.

[32] Gupta A, Energy and material constraints concerning the rapid deployment of photovoltaic energy in the twenty-first century [Master thesis]. Rochester: State University of New York College;2012.

[33] Energy Education. Photovoltaic cell (Internet). Calgary: University of Calgary; 25th June 2018 [Updated 25th June 2018; retrieval date 3rd April 2019]. Available from: https://energyeducation.ca/encyclopedia/Photovoltaic_cell

[34] NASA Science. How do Photovoltaics Work? (Internet). Washington: NASA; 6th August 2008 [Updated 1st April 2019; retrieval date 3rd April 2019]. Available from: https://science.nasa.gov/science-news/science-at-nasa/2002/solarcells

[35] Couderc R, Amara M, Degoulange J, Madon F, Einhaus R. Encapsualnt for glass-glass PV modules for minimum optical losses: gas or EVA? Energy Procedia. 2017;124:470-477

[36] Gordon J, ed. Solar energy: The state of the art. London: James & James; 2001.

[37] Alternative Energy tutorials. Solar Dish Collector (Internet). Alternative Energy tutorials; 1st August 2017 [Updated 1st May 2019; retrieval date 10th April 2019]. Available from: http://www.alternative-energy-tutorials.com/solar-hot-water/solar-dish-collector.html

[38] Tiwari G, ed. Solar energy: Fundamentals, Design, Modelling and Applications. New Delhi: Alpha Science International Ltd, 2002.

[39] Alternative Energy tutorials. Flat Plate Collector (Internet). Alternative Energy tutorials; 1st January 2018 [Updated 1st May 2019; retrieval date 10th April 2019]. Available from: http://www.alternative-energy-tutorials.com/solar-hot-water/flat-plate-collector.html

[40] Granta Design. Composites (Simple Bounds): Assumptions and calculations (Internet). Cambridge: Granta; 2018 [Updated 2018; retrieval date 21st May 2019]. Available from: http://support.grantadesign.com/resources/cesedupack/2018/help/topic.htm?fbclid=IwAR1NRcHviZ4PvP8MYSZFvtIFqhryAh6Pr7RA4tu1z7AOZRpceFU6Hf1vhYs#t=html%2Fsynthesizer%2Fcomposites_assumptions.htm

Appendix

1. Popular science article
2. SINTEF risk evaluation sheets
3. XRF scan of the copper tape
4. Plastic identification flowchart
5. Measurements from the heat flow apparatus
6. Thermal pads in the market

Attachment 1: Popular science article

A new era in photovoltaics is on the horizon- FUTURE IS NOW

Ali Haider Raja

With enhanced thermal dissipation techniques, Photovoltaic and Thermal (PV/T) systems are set to revolutionize the renewable energy sector.

Figure 1: Future houses might not look as green as these houses, but they will surely utilize green ways for energy production. Roof mounted PV/T system can be seen in this illustration. Source: Thinkstock

"The ingenious thermal management technique has put us at a brink of something special" says SINTEF researcher, Martin Bellman, who along with many other diligent SINTEF engineers are on the verge of a breakthrough in photovoltaic and thermal management industry.

Why thermal management?

Photovoltaics' (PV) performance reduces with an increase in system's temperature. This is because its material is susceptible to overheating of the system. Thus, thermal management is essential to avoid premature degradation. PV/T systems use innovative materials which have been discovered after an exhaustive but fruitful research by SINTEF engineers.

What is a PV/T system?

A PV/T system has a PV module connected to a thermal collector. This hybrid system captures and carries the heat away from the PV module to be used for space/water heating. Thus, enhancing the electrical output and providing free energy for heating purposes. This system is clean, green and can easily be used as building integrated material.

Research

NTNU and SINTEF led research lasted 6 months where different experiments and modelling was conducted in association with PVadapt and SINTEF byggforsk. Different designs were tested using different materials in the custom built SINTEF heat-flow apparatus according to the international standards, ISO 8301. Experiments on copper tape and Polyvinyl chloride (PVC) pads in a PV/T structure were conducted to investigate the best thermal interface material (TIM).

Figure 2: PV/T setup with copper tape as TIM.

To reduce material costs, a PV/T system without the rear glass in the PV module was also investigated.

"Initially, due to its complexities, we weren't even convinced that this design would lead us to the forthcoming glory days" says Kjersti Kleveland, research supervisor from NTNU.

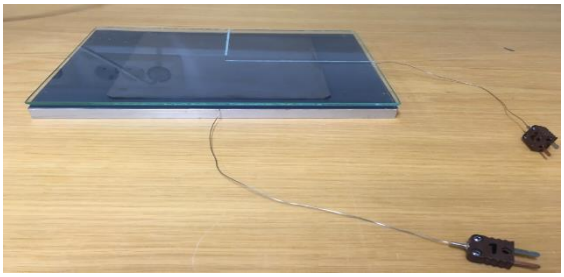

Figure 3: PV/T system with PVC pad as TIM. This unique system-design was void of rear glass in the PV system.

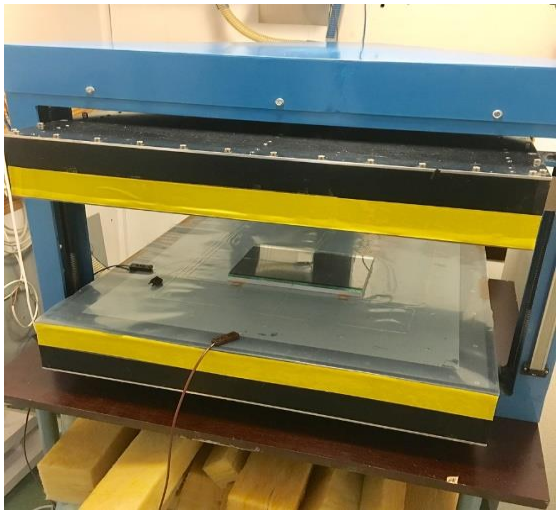

Figure 4: Byggforsk's heat flow apparatus used for experimentation. This apparatus is also referred to as a "box-apparatus".

Thinking outside the box

After some unfulfilling experiments, the researchers thought about modelling their own material. This material would be unorthodox compared to the typical materials in thermal management where it will conduct heat but not electric current. Electrical insulation in a PV/T system is vital for the thermal collector to function without any disturbances. It becomes an absolute necessity in the new design where there is no rear glass. Modelling in Edu Pack was conducted on composites. Technical ceramics were the filler choice in a soft polymer matrix. Hexagonal boron nitride (h-BN) and alumina (Al_2O_3(85)) were chosen as fillers in a polyimide matrix after a profound exploration. Trend in their thermal conductivity and electrical insulation based on filler content (wt %) in the composite was analysed by the experts.

Eureka

h-BN composite exhibited enhanced heat transfer in addition to electrical insulation. They offered better properties than Al_2O_3(85) composite like:

- Better thermal dissipation
- Better electrical insulation
- Lower density

Lighter components are important if the PV/T system is to be used as a building integrated system. This h-BN composite could be inserted between the PV module and the thermal collector for direct plug & play. It is expected that this composite would provide an efficient cooling mechanism for the PV module while providing adequate electrical insulation.

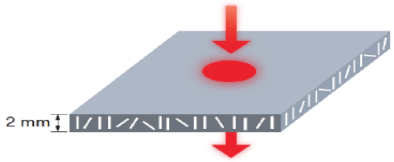

Figure 5: Sketch of the composite modelled with h-BN fillers as white lines in a polyimide matrix. Heat flow is shown in red.
Source: 3M Boron Nitride fillers

Final step

The final step is the experimentation of this composite. Through that, the maximum filler content in the matrix should be determined. This is to avoid the loss of mechanical strength in the composite as it would be exposed to harsh weather conditions throughout its operational time.

Figure 6: Powerhouse Brattørkaia in Trondheim, Norway. Upon completion, this building will utilize building integrated photovoltaics for electricity production.
Source: Snøhetta/MIR

Potential

PV/T system, when incorporated into the building structure, may allow buildings to produce more energy than their actual energy requirements. Courtesy of the improved efficiency of the PV module and reduced energy requirements for heating purposes. The excess energy could then either be saved or sold by transferring to a local grid station. h-BN fillers have paved a way for “smart materials” in electronic industry. Thanks to its enhanced thermal and electrical properties, it has enabled the research on a new generation of electrical components that may offer improved performance and energy savings.

References:

PVadapt. PROJECT. Vision and objectives Available from: http://www.pvadapt.com/vision-and-objectives/

Ali Haider, *Investigation on the best thermal interface material for maximum heat transfer in a building integrated photovoltaic thermal system*, NTNU, 2019

Attachment 2: SINTEF Risk evaluation

RISIKOVURDERING AV HMS-FORHOLD (aktivitet, reise, lab/verksted, felt, utstyr, etc.)

[Obligatoriske* felt kopieres over til skjema]

Organisatorisk enhet * *[Institutt/avdeling/faglag]*	SINTEF
Lokasjon * *[hvor er utstyret plassert? Hvor skal aktiviteten foregå?]*	SINTEF Lab, Gløshaugen Trondheim
Utstyr / Aktivitet * *[navn på utstyr/aktivitet]*	Heat Flow meter
Linjeleder * *[nærmeste ansvarlige linjeleder]*	Martin Bellman
Prosjektnummer/-navn *[skal fylles ut ved prosjekt]*	PVadapt, IMA-B-09-2019
Prosjektleder *[skal fylles ut ved prosjekt]*	Martin Bellman
Dato * *[dato for gjennomføring av risikovurderingen]*	01.02.2019
Deltagere * *[navn på alle deltagere i risikovurderingen]*	Ali Haider Raja, Einar Bergheim, Martin Bellman and Kjersti Kleveland
Beskrivelse av utstyret / aktiviteten *[legg inn mer utfyllende beskrivelse av utstyret / aktiviteten som har betydning for vurdering av risiko. Eventuelt legg ved filer/lenke til filer]*	Heat flow meter. A commercial apparatus used to record thermal conductivity or thermal resistance. This apparatus uses 2 heat plates and the specimen is placed in between them. The sides are insulated using mineral wool. Various thermocouples are used to record the temperature.
Vedlegg *[legg inn lenker til andre relvante dokument]*	

Attachment 2 continues

SINTEF

Organisatorisk enhet: SINTEF
SINTEF Lab, Gløshaugen
Lokasjon: Trondheim
Utstyr / Aktivitet: Heat Flow meter

Dato: 01.02.2019
ALI HAIDER RAJA, EINAR BERGHEIM, MARTIN BELLMAN AND
Deltagere: KJERSTI KLEVELAND
Linjeleder: MARTIN BELLMAN

Delaktivitet	Mulig uønsket hendelse	Eksisterende barrierer	Risikoverdi med eksisterende tiltak					Nye barrierer / risikoreduserende tiltak (handlingsplan)	Risikoverdi med nye tiltak					Ansvarlig	Dato	Status
			Økonomi / materiell	Omdø mme	Ytre miljø	Menneske			Økonomi / materiell	Omdø mme	Ytre miljø	Menneske				
Measuring heat flow in the sandwich sample	Breaking of the front and/or rear glass of the PV module	The mechanical strength of the glass should be adequate enough.	A2	A1	A2	A2								Ali Haider and Einar Bergheim	06.02.2019	
	Ignition of the thermal interface	Non-flammable thermal interfaces are	B2	B2	B2	B2								Ali Haider and Einar Bergheim	06.02.2019	
	Overheating of the heat flow apparatus	Cryostat functions without any fault	B1	B1	B1	B1								Ali Haider and Einar Bergheim	06.02.2019	
	Nose Irritation by smelling the adhesive from close range	Wear face mask	A2	A1	A2	A1								Ali Haider and Einar Bergheim	06.02.2019	
	Skin irritation by direct contact with the adhesive	Use nitrile gloves	A1	A1	A2	A1								Ali Haider and Einar Bergheim	06.02.2019	
	Non-uniform thermal expansion of the different layers in the PV/T sandwich system	Use thermal interface of about the same thermal expansion coefficient as the PV's glass	A2	A2	A2	A3								Ali Haider and Einar Bergheim	06.02.2019	
	Eye irritation in case of ignition of the specimen	Use safety glasses	A2	A3	A2	A3								Ali Haider and Einar	06.02.2019	

Attachment 2 continues

Utstyr/aktivitet	Heat Flow meter
Dato	01.02.2019

MED EKSISTERENDE TILTAK

Menneske	Ytre miljø	Omdømme	Økonomi / materiell
1 1	1 1	1 1	1 1
1 4	3 1 1	5	2 1 2

ETTER NYE TILTAK

Menneske	Ytre miljø	Omdømme	Økonomi / materiell

Attachment 3: XRF scan of the copper tape

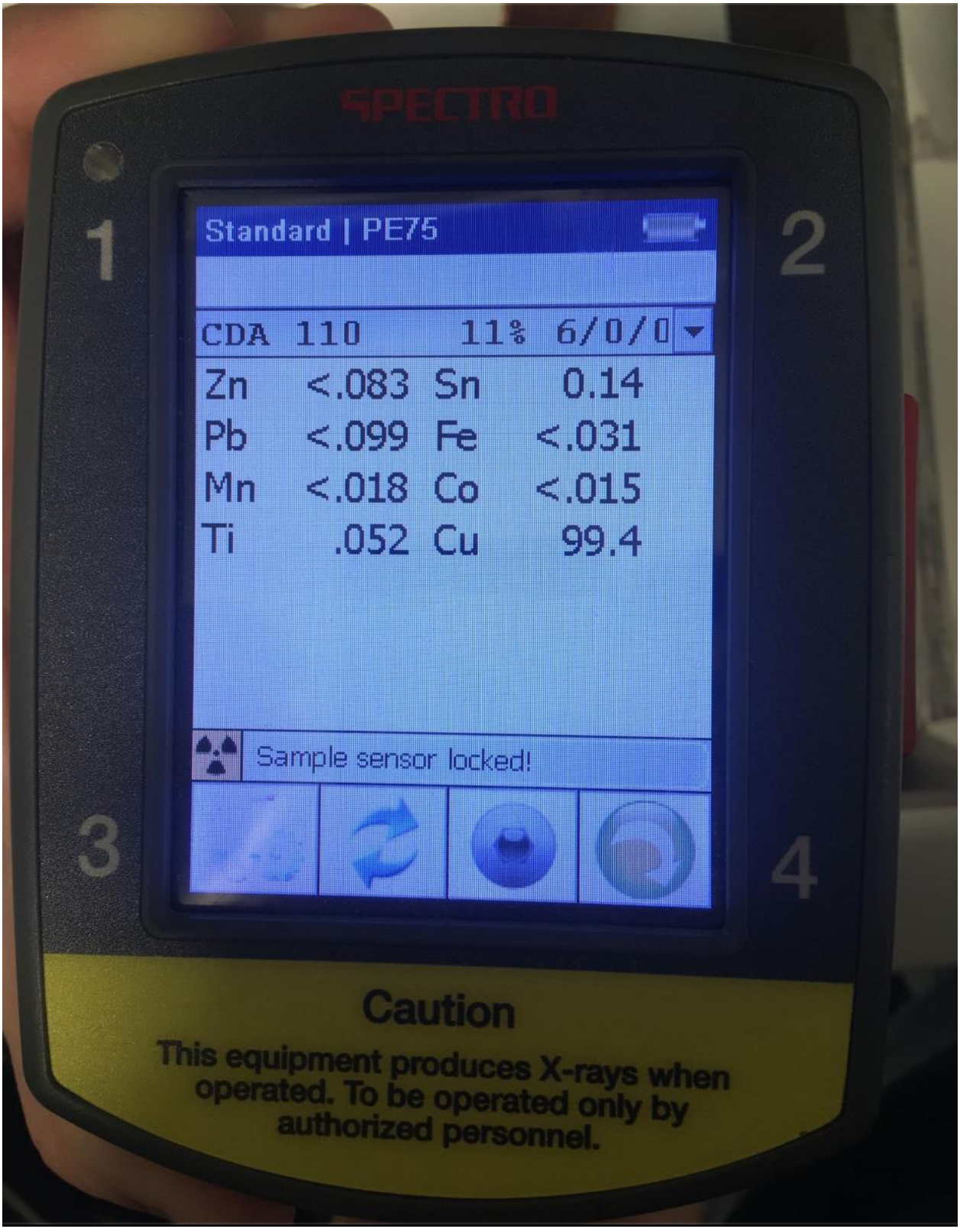

Attachment 4: Plastic identification flowchart

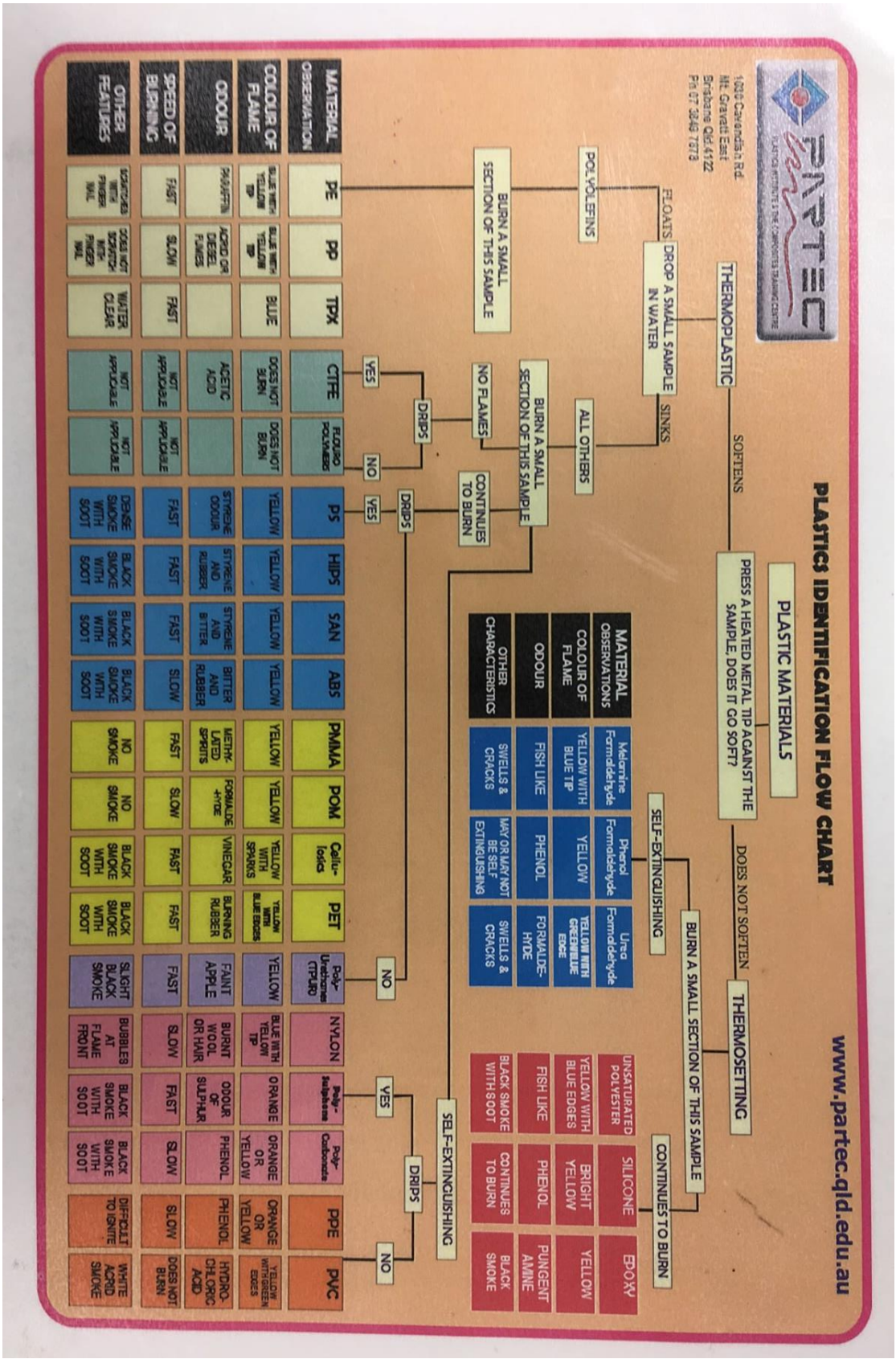

Attachment 5: Measurements from the heat flow apparatus

Internrapport
Varmemotstand og varmekonduktivitet

Rom 1	Kalibreringsfaktorer:	Øvre	0,00355180	+	-0,00000439	x Tmø
		Nedre	0,00361665	+	-0,00000548	x Tmn
	Temperaturdifferanse	Termoserie	0,00516675	+	-0,00001003	x Tm

Produsent:	Produktnavn:	Produkttype:
102019326 SINTEF INDUSTRI	Prosjekt H2020 Pvadapt	SOLCELLER

	Prøve 1	Prøve 2	Prøve 3	Prøve 4
lengde				
bredde				
tykkelse ved måling				
densitet kg/m³	0,0	0,0	0,0	0,0
fuktinnhold kg/kg	0,00	0,00	0,00	0,00

	Prøve 1	Prøve 2	Prøve 3	Prøve 4
masse før måling (g)				
masse etter måling (g)				
masse etter tørking (g)				
tara	-	-	-	-
masseendring under prøving (%)	-	-	-	-

Prøve 1

	µVø	µVn	µVΔ	Tø	Tn	Tr	RF	R
Middelverdier AVG	36667,8	35074	2205	15,5	4,84	10	20	0,09

Måleperiode: START TIME : 05.05.2019 06:43:00 STOP TIME : 05.05.2019 19:26:36

Stabilitetskontroll

Temperatur øvre plate	15,50	°C		Heat flow upper plate	127,74	W/m²
Temperatur nedre plate	4,84	°C		Heat flow lower plate	125,92	W/m²
Temperatur rom	10,01	°C		Mean Heat flow	126,83	W/m²
Middeltemperatur prøve	10,17	°C		Varmemotstand R =	0,09	m²K/W
Temperatur differanse	11,17	°C	OK	**Varmekonduktivitet λ =**	**0,00000**	**W/mK**

Stabilitetskontroll: OK, OK

Prøve 2 — **Copper tape experiment**

	µVø	µVn	µVΔ	Tø	Tn	Tr	RF	R
Middelverdier AVG	27822,5	26886	2595	15,5	3,95	9,99	16,6	0,14

Måleperiode: START TIME : 07.05.2019 00:28:34 STOP TIME : 07.05.2019 08:33:46

Stabilitetskontroll

Temperatur øvre plate	15,53	°C		Heat flow upper plate	96,92	W/m²
Temperatur nedre plate	3,95	°C		Heat flow lower plate	96,65	W/m²
Temperatur rom	9,99	°C		Mean Heat flow	96,79	W/m²
Middeltemperatur prøve	9,74	°C		Varmemotstand R =	0,14	m²K/W
Temperatur differanse	13,15	°C	OK	**Varmekonduktivitet λ =**	**0,00000**	**W/mK**

Stabilitetskontroll: OK, OK

Prøve 3 — **Reference experiment**

	µVø	µVn	µVΔ	Tø	Tn	Tr	RF	R
Middelverdier AVG	25920,8	25082	2745	15,7	3,55	9,8	14,4	#N/A

Måleperiode: START TIME : 07.05.2019 13:30:17 STOP TIME : 07.05.2019 13:51:21

Stabilitetskontroll

Temperatur øvre plate	15,72	°C		Heat flow upper plate	90,28	W/m²
Temperatur nedre plate	3,55	°C		Heat flow lower plate	90,22	W/m²
Temperatur rom	9,80	°C		Mean Heat flow	90,25	W/m²
Middeltemperatur prøve	9,64	°C		Varmemotstand R =	0,15	m²K/W
Temperatur differanse	13,92	°C	OK	**Varmekonduktivitet λ =**	**0,00000**	**W/mK**

Stabilitetskontroll: OK, OK

Prøve 4 — **PVC pad experiment**

	µVø	µVn	µVΔ	Tø	Tn	Tr	RF	R
Middelverdier AVG	18935,5	18289	3148	17,8	2,41	9,96	12,1	0,24

Måleperiode: START TIME : 08.05.2019 04:02:09 STOP TIME : 08.05.2019 08:43:12

Stabilitetskontroll

Temperatur øvre plate	17,80	°C		Heat flow upper plate	65,78	W/m²
Temperatur nedre plate	2,41	°C		Heat flow lower plate	65,90	W/m²
Temperatur rom	9,96	°C		Mean Heat flow	65,84	W/m²
Middeltemperatur prøve	10,11	°C		Varmemotstand R =	0,24	m²K/W
Temperatur differanse	15,95	°C	OK	**Varmekonduktivitet λ =**	**0,00000**	**W/mK**

Stabilitetskontroll: OK, OK

Attachment 6: Thermal pads in the market

Thermally conductive and electircally insulating pads

Product Name	Thermal Conductivity (W/mK)	Electrical Resistance (Ohm•m)	Dielectric constant (1000 Hz)	Flammability rating	Price (NOK/kg)
Silicon polymer thermal pad (3M 5595)	1.6	5.0 x 10^15	3.9	V-0	1142
Arcylic Interface Pad (3M 5578H)	3.5	1.7 x 10^10	...	V-0	781
Silicone fiberglass thermal pad (Sil-Pad A1500)	2.0	1.0 x 10^11	7.0	V-0	3900
Silicone rubber and fiberglass pad (Sil-Pad 400)	0.9	1.0 x 10^11	5.5	V-0	1460
Hi-Flow Polyimide pad (HF300P)	1.6	1.0 x 10^12	4.5	V-0	1510
Silicone elastomer (SSP-1850C)	1.5	2.8 x 10^16	...	...	after contact

Test methods:
Thermal conductivity- ASTM D5470
Electrical resistance- ASTM D257
Dielectric Constant- ASTM D150
Flammability rating- UL 94